

Mathilde Ruud

Experimental study on the effect of ventilation airflow rate and separation distance on the risk of airborne COVID-19 infection

Master's thesis in Energy and Environmental Engineering

Supervisor: Guangyu Cao

Co-supervisor: Amar Aganovic

June 2022

Mathilde Ruud

Experimental study on the effect of ventilation airflow rate and separation distance on the risk of airborne COVID-19 infection

Master's thesis in Energy and Environmental Engineering
Supervisor: Guangyu Cao
Co-supervisor: Amar Aganovic
June 2022

Norwegian University of Science and Technology
Faculty of Engineering
Department of Energy and Process Engineering

Preface

This master thesis was written at department for Energy and Process engineering at NTNU. The thesis compounds 30 STP and is the final work of the master degree in Energy and Environmental Engineering.

The master thesis often extends the project work from the first semester of the master year. However, this was not the case for me. My topic changed to the master thesis. However, parts of the literature review regarding ventilation systems are the same as in my project work.

I would like to thank my supervisor professor Guangyu Cao from NTNU for helpful insights, good support and rewarding discussions during the work. I would also thank my co-supervisor associate professor Amar Aganovic from the University in Tromsø for good input on the theoretical modelling and discussions. A huge thank you to PhD-candidates Tomáš Fečer and Yang Bi for the help in the laboratory. Thank you to Inge Håvard Rekstad and Tore Kristian Eliassen for the help on the experimental set-up.

Thank you to friends and family for the support and motivation during the writing of this Master thesis.

June 2022

Mathilde Ruud

Abstract

The corona pandemic has now lasted for nearly three years, affecting people's lives by imposing intrusive measures to reduce infection risk. Even though precautions have been taken and vaccines have been distributed, the coronavirus has continued to evolve. Experts from around the world have discovered reasons to suspect that the airborne transmission route is crucial, and that ventilation plays a key role in diluting the virus indoors. Together with other infection-prevention measures like social distancing and face masks, this can lower the risk of infection. The goal of the thesis was to quantify exposure, probability of infection and propose ventilation recommendations to reduce the probability of infection.

Exposure and probability of infection by airborne coronavirus were investigated with three ventilation airflow rates (2.7, 5.1 and 9.6 ACH) and four distances between a sitting exposed and a standing infected person (0.7, 1.0, 1.5 and 2.0 meters). Tracer-gas measurements were used to quantify exposure. A personal exposure index/local air quality index was used in a new modification of the Wells-Riley equation to calculate the probability of infection. Smoke visualizations were conducted to gain a better understanding of the airflow pattern and the behavior of aerosols.

The tracer-gas measurements showed that 2.7 ACH gave the highest exposure, while 9.6 ACH gave the lowest. The probability of infection showed the same trend and was overall low for all scenarios. Two meters of separation distance gave the highest exposure. The lowest airflow rate had both highest aerosol concentration in the inhalation zone and the highest local air quality index. Even though the probability of infection was low for every scenario, infection-preventive measures were discussed. It was investigated if improved local air quality index or increased ventilation airflow rate contributed the most to reduce the risk of exposure.

It was concluded that a separation distance of two meters may be insufficient against high exposure of airborne coronavirus if located close to the exhaust or in a place where the airflow pushes aerosols towards this location. For 2.7 and 5.1 ACH, the exposure could be reduced by increasing the airflow rate by 1 ACH. For the highest airflow rate, improvement of the local air quality index is more appropriate in an energy-effective perspective. Improvement of the local air quality index in the inhalation zone of exposed persons is promoted as an infection-preventive measure.

Sammendrag

Koronapandemien har vart i nærmere tre år og påvirket menneskers liv med inngripende tiltak for å redusere smitte. Viruset har fortsatt å utvikle seg, selv med forholdsregler og distribusjon av vaksiner. Ekspertter fra hele verden har funnet grunner til å tro at den luftbårne smitten er dominerende og at ventilasjon spiller en viktig rolle i å fortenne viruset innendørs. Ventilasjon sammen med andre tiltak som sosial distansering og masker kan redusere smitten. Målet med masteroppgaven er å kvantifisere eksponering mot luftbårent koronavirus, smittesannsynlighet og gi ventilasjonsanbefaling for å redusere smittesannsynligheten.

Eksponering og smittesannsynlighet ble undersøkt med tre luftmengder (2.7, 5.1 og 9.6 luftvekslinger per time) og fire avstander mellom en sittende eksponert og en stående smittet person (0.7, 1.0, 1.5 og 2.0 meter). Sporingsgassmålinger ble benyttet for å kvantifisere eksponering. En personlig eksponeringsindeks/lokal luftkvalitetsindeks i inhalasjonssonen til den eksponerte ble brukt i en ny modifikasjon av Wells-Riley likningen for å regne ut smittesannsynlighet. Røykvisualiseringer ble utført for å få en forståelse for luftstrømmen og oppførselen til viruset i rommet.

Sporingsgassmålingene viste at 2.7 ACH gav høyest eksponering og 9.6 ACH lavest. Smittesannsynligheten viste den samme trenden, og var lav for alle scenarioer. Den høyeste eksponeringen ble observert ved to meter avstand mellom eksponert og smittet. Den laveste luftmengden hadde både den høyeste eksponeringen i inhalasjonssonen og den høyeste lokale luftkvalitetsindeksen. Selv om smittesannsynligheten var lav for hvert scenario ble smittevernstiltak diskutert. Det ble undersøkt om forbedret lokal luftkvalitetsindeks eller økt ventilasjonsmengde bidro mest til å redusere sannsynligheten.

To meter mellom en eksponert og en smittet kan være utilstrekkelig mot høy eksponering av luftbårent koronavirus om den eksponerte er plassert nært et avtrekk eller hvor luftstrømmen dytter viruspartikler mot denne lokasjonen. For å redusere smittesannsynligheten for 2.7 og 5.1 ACH bør økt ventilasjonsmengde på 1 ACH innføres som et tiltak. I et energi-effektivt perspektiv bør den lokale luftkvalitetsindeksen forbedres for den høyeste luftmengden, ettersom forskjellen i å innføre de to tiltakene er liten. Forbedring av lokal luftkvalitetsindeks i inhalasjonssonen til eksponerte personer fremmes som et mulig viktig tiltak.

Contents

1	Introduction	1
1.1	Background	1
1.2	Objective	1
1.3	Structure	2
1.4	Sources	2
1.5	Limitations	3
2	Literature review and theory	4
2.1	Coronavirus: Routes of transmission	4
2.1.1	Airborne transmission and inhalation	5
2.2	Ventilation	6
2.2.1	Ventilation airflow rate	6
2.2.2	Non-steady state mass-balance model	8
2.2.3	Air distribution patterns	8
2.2.4	Interaction of ventilation and human: Human Thermal Plume (HTP), breathing and exhaled jet	10
2.2.5	Location of exhaust	12
2.3	Other airborne removal factors	12
2.3.1	Virus inactivation by biological decay	12
2.3.2	Deposition by gravitational settling	13
2.3.3	Temperature and relative humidity	14
2.4	Assessing airborne exposure	15
2.4.1	Simulation/mimic of airborne exposure	15
2.4.2	Contaminant exposure indices	16
2.4.3	Infection risk models	19
3	Method	24
3.1	Introduction	24
3.2	Experimental measurement	24
3.2.1	Scenarios	25
3.2.2	Experimental set-up	25
3.2.3	Measurement equipment	35

3.2.4	Preparation	38
3.2.5	Tracer-gas measurements	40
3.2.6	Temperature and relative humidity	42
3.2.7	Smoke visualizations	42
3.3	Theoretical modelling	43
3.3.1	Personal exposure index/local air quality index	43
3.3.2	Probability of infection from COVID-19 by a modified Wells-Riley equation	43
4	Results	49
4.1	Exposure: N ₂ O tracer gas concentration	49
4.1.1	Scenario 1: 2.7 ACH	49
4.1.2	Scenario 2: 5.1 ACH	53
4.1.3	Scenario 3: 9.6 ACH	58
4.1.4	Summary of tracer-gas concentration for all scenarios	62
4.2	Relative humidity and temperature	63
4.2.1	Scenario 1: 2.7 ACH	63
4.2.2	Scenario 2: 5.1 ACH	66
4.2.3	Scenario 3: 9.6 ACH	68
4.3	Smoke visualizations	70
4.4	Personal exposure index/local air quality index	70
4.5	Probability of infection by a modified Wells-Riley equation	71
5	Discussion	73
5.1	Ventilation airflow rate and exposure	73
5.2	Social distancing and location of exhaust	74
5.3	Increased ventilation airflow rate or improved local air quality index as infection-preventive measures	76
5.4	Modified Wells-Riley model: advantages and disadvantages	81
6	Conclusion	83
7	Further work	85
	References	86

A Risk assessment	93
B Deposition and contact/fomites	114
C Tracer-gas characteristics	114
D Additional equipment	115
D.1 Smoke visualization tools	115
D.2 Heating element	115
E Deposition rate values	117

List of figures

2.1	Virus particles emitted from an infected person (Jayaweera <i>et al.</i> , 2020).	4
2.2	Air distribution pattern with mixing ventilation (Price engineering, 2016).	9
2.3	Air distribution pattern with displacement ventilation (Price engineering, 2016).	9
2.4	Virus inactivation rate (k) dependency on relative humidity (Aganovic <i>et al.</i> , 2021).	13
2.5	Tracer-gas measurement techniques (Han, 2012).	15
2.6	Chain of processes from emission of contaminants to inhalation and health effects (Marshall and Nazaroff, 2006).	18
3.1	Overview of the method chapter.	24
3.2	A model of the HVAC-laboratory at NTNU, Gløshaugen. Made in SketchUp.	26
3.3	Air handling unit from Covent at the HVAC-lab at Gløshaugen, NTNU.	27
3.4	BEMS interface on the computer outside the laboratory. The used parameters are marked in red.	27
3.5	Duct system in the HVAC-laboratory at NTNU, Gløshaugen.	28
3.6	A model of the HVAC-laboratory at NTNU, Gløshaugen. EX_x are exhaust and SU_x are supply inlets.	29
3.7	Air supply diffuser with swirl pattern.	30
3.8	Characteristics of the infected manikin.	31
3.9	Model of breathing box. Made in SketchUp.	32
3.10	The experimental facility with location of the breathing box.	32
3.11	Manikin simulating a sitting exposed person.	33
3.12	Equipment to heat up the exposed manikin to skin surface temperature.	34
3.13	Location of the exposed and the infected manikin.	35
3.14	Autozeroing micromanometer model TT470S to measure the pressure difference in the supply air diffusers.	36
3.15	TinyTag Plus 2 TGP-4500 characteristics.	36
3.16	Memory HiLogger to monitor temperature.	37
3.17	Tracer-gas equipment in the laboratory.	37
3.18	SensoAnemo 5100LSF to measure velocity of the exhaled jet from the infected manikin.	38

3.19	Lindab UltraLink to measure the total ventilation airflow rate.	38
3.20	Plastic-sealed rotating heat exchanger to avoid unnecessary re-transmission of tracer gas from exhaust to supply air.	39
3.21	Exhaled velocity from the infected manikin, M_{inf}	40
3.22	Location of S_2 and S_4 - S_6 . 20 cm from the mouth at both sides and one 35 cm at the left side (outside breathing zone).	41
3.23	Mass-balance in a single-zone model.	44
4.1	Measured tracer-gas concentration for scenario 1A at the sampling channels and the calculated fully-mixed concentration.	50
4.2	Measured tracer-gas concentration for scenario 1B at the sampling channels and the calculated fully-mixed concentration.	51
4.3	Measured tracer-gas concentration for scenario 1C at the sampling channels and the calculated fully-mixed concentration.	52
4.4	Measured tracer-gas concentration for scenario 1D at the sampling channels and the calculated fully-mixed concentration.	53
4.5	Measured tracer-gas concentration for scenario 2A at the sampling channels and the calculated fully-mixed concentration.	54
4.6	Measured tracer-gas concentration for scenario 2B at the sampling channels and the calculated fully-mixed concentration.	55
4.7	Measured tracer-gas concentration for scenario 2C at the sampling channels and the calculated fully-mixed concentration.	56
4.8	Measured tracer-gas concentration for scenario 2D at the sampling channels and the calculated fully-mixed concentration.	57
4.9	Measured tracer-gas concentration for scenario 3A at the sampling channels and the calculated fully-mixed concentration.	58
4.10	Measured tracer-gas concentration for scenario 3B at the sampling channels and the calculated fully-mixed concentration.	59
4.11	Measured tracer-gas concentration for scenario 3C at the sampling channels and the calculated fully-mixed concentration.	60
4.12	Measured tracer-gas concentration for scenario 3D at the sampling channels and the calculated fully-mixed concentration.	61
4.13	Measured temperature for scenario 1 (2.7 ACH) at four separation distances.	64

4.14 Measured relative humidity for scenario 1 (2.7 ACH) at four separation distances.	65
4.15 Measured temperature for scenario 2 (5.1 ACH) at four separation distances.	66
4.16 Measured relative humidity for scenario 2 (5.1 ACH) at four separation distances.	67
4.17 Measured temperature for scenario 3 (9.6 ACH) at four separation distances.	68
4.18 Measured relative humidity for scenario 3 (9.6 ACH) at four separation distances.	69
4.19 Smoke visualization of the exhaled jet of infected manikin and the exposure of the exposed manikin.	70
4.20 Smoke visualization of the ventilation airflow pattern in the HVAC-laboratory.	70
4.21 Personal exposure index for scenario 1, 2 and 3.	71
4.22 Probability of infection based on the modified Wells-Riley model for scenario 1, 2 and 3.	72
5.1 Supply air from SU_1 partly short-circuited to EX_2 and partly descended towards M_{exp} . Red dots represents exhaled aerosols from M_{inf}	74
5.2 Correlation between ACH and local ventilation efficiency for all scenarios. Numbers below each data point shows separation distance.	76
5.3 Comparison of the probability of infection for the measured ϵ_e at 2.7 ACH, fully-mixed conditions at 2.7 ACH and 3.7 ACH at fully mixed conditions.	78
5.4 Comparison of the probability of infection for the measured ϵ_e at 5.1 ACH, fully-mixed conditions at 5.1 ACH and 6.1 ACH at fully mixed conditions.	79
5.5 Comparison of the probability of infection for the measured ϵ_e at 9.6 ACH, fully-mixed conditions at 9.6 ACH and 10.6 ACH at fully mixed conditions.	80
D.1 Drager Air-Flow Tester kit for smoke visualization of exhaled jet.	115
D.2 Manual EasySmoker to visualize the airflow pattern in the laboratory. . . .	115
D.3 5 W heating element to heat up exhaled air from the infected manikin. . .	116

List of tables

2.1	Minimum ACH recommendations for common building types (Robertson, 2021).	7
2.2	Recommendations for relative humidity levels to reduce the risk of infection from airborne coronavirus.	14
2.3	Models from literature used to predict the possibility of infection for the coronavirus.	23
3.1	Scenario set-up for the experimental measurements.	25
3.2	Location of exhaust and supply air units in the HVAC-laboratory.	29
3.3	Air supply diffuser characteristics.	29
3.4	Percentage of the total airflow rate that each supply air diffuser delivered.	30
3.5	Location of exposed person and infected person at different distances. Z_{br} means inhalation zone height.	34
3.6	Location of sampling and dosing tubes during the experiments.	41
3.7	Location of TinyTag loggers during the experiments.	42
3.8	Location of thermocouples during the experiments.	42
3.9	Variables inserted into the differential equation solving for the tracer gas concentration $n(t)$ in a target point.	48
4.1	Properties of tracer-gas measurements for scenario 1A inside the stable area.	50
4.2	Properties of tracer-gas measurements for scenario 1B inside the stable area.	51
4.3	Properties of tracer-gas measurements for scenario 1C inside the stable area.	52
4.4	Properties of tracer-gas measurements for scenario 1D inside the stable area.	53
4.5	Properties of tracer-gas measurements for scenario 2A inside the stable area.	54
4.6	Properties of tracer-gas measurements for scenario 2B inside the stable area.	55
4.7	Properties of tracer-gas measurements for scenario 2C inside the stable area.	56
4.8	Properties of tracer-gas measurements for scenario 2D inside the stable area.	57
4.9	Properties of tracer-gas measurements for scenario 3A inside the stable area.	59
4.10	Properties of tracer-gas measurements for scenario 3B inside the stable area.	60
4.11	Properties of tracer-gas measurements for scenario 3C inside the stable area.	61
4.12	Properties of tracer-gas measurements for scenario 3D inside the stable area.	62

4.13	Summary of the tracer-gas concentration for all scenarios at the exhaust and at the exposed manikin. A, B, C and D is separation distance 0.7, 1.0, 1.5 and 2.0 meters respectively.	63
C.1	Key properties about N ₂ O as tracer gas. Modified from Grieve (1989). . .	115
E.1	Droplet diameter, mean mass diameter and droplet number concentration to calculate the deposition rate for size ranges from 0 to 8 μm (Aganovic <i>et al.</i> , 2021).	117

Abbreviations

WHO World Health Organization

ACH Air Changes per Hour

IAQ Indoor Air Quality

ECDC European Centre for Disease Prevention and Control

FHI/NIPH Folkehelseinstituttet/Norwegian Institute for Public Health

ASHRAE American Society of Heating, Refrigerating and Air-Conditioning Engineers

FOA Fraction of Outdoor Air

HTP Human Thermal plume

RH Relative Humidity

CFD Computational Fluid Dynamics

LAQI Local Air Quality Index

IF Intake Fraction

QER Quanta Emission Rate

ID Infectious Dose

G-N Gammaitoni-Nucci

SDI Social Distancing Index

BEMS Building Energy Management System

HVAC Heating, Ventilation and Air Conditioning

AHU Air Handling Unit

1 Introduction

1.1 Background

The corona pandemic has now lasted nearly three years, affecting people's lives by imposing intrusive measures to reduce infection risk. The primary motivation was to keep the health-care system from becoming overburdened, as well as to protect people who are at risk of developing serious sickness if infected. Despite the fact that precautions have been taken and vaccines have been distributed, the coronavirus has continued to evolve (WHO, 2021). As a result, the risk of infection persists far into the pandemic.

The importance of airborne transmission of the virus was not initially recognized (Noorimotlagh *et al.*, 2021). However, experts from all around the world have discovered reasons to suspect that the airborne transmission route is crucial and that ventilation plays a key role in diluting the virus indoors (Greenhalgh *et al.*, 2021). Together with other key precautions like social distancing and face masks, this can lower the risk of infection (WHO, 2021).

The highest risk of infection occurs indoors as people are sharing the same indoor environment and are often in close contact (Ai, Z., Hashimoto, K. and Melikov, A., 2019). In everyday life, ventilation systems are crucial for dispersing contaminants, but they are considerably more important during a pandemic (Greenhalgh *et al.*, 2021). As a result, it is critical to look into the risk of infection and exposure in ventilated spaces indoors. In previous sickness outbreaks, important mathematical methods to evaluate and predict infection risk were applied. Dose-response and Wells-Riley models are examples (Sze and Chao, 2010). The coronavirus infection risk has now been quantified using these approaches. This can provide crucial information to government and operating personnel on how to use indoor spaces effectively during a pandemic to limit the risk of infection for building occupants.

1.2 Objective

The goal of this thesis is to investigate the exposure and the probability of infection for the coronavirus under different ventilation solutions in a case study with a sitting exposed and a standing infected person. Ventilation airflow rate is varied within three values

(2.7, 5.1 and 9.6 ACH) and the separation distance between the infected person and the exposed person (0.7 meter, 1.0 meter, 1.5 meter and 2.0 meter). This can give important information on what combination of the scenarios gives higher or lower probability of infection.

The tasks that were planned to do under the specific conditions mentioned was:

- Literature review regarding ventilation solutions, indoor air quality (IAQ) and models to predict infection risk during the COVID-19 pandemic
- Selection of theoretical models and relevant indoor air parameters to calculate infection risk
- Establish a measurement procedure to measure real ventilation rate and relevant indoor air parameters under different ventilation solutions
- Perform experimental measurements with tracer gas under different ventilation conditions
- Calculate infection risk with the selected model using experimental measurement results from the laboratory
- Develop ventilation recommendations for reducing infection risk of occupants during a pandemic.

1.3 Structure

Relevant literature and theory is presented in section 2, the experimental method is presented in 3, the results are shown in 4 and further discussed in 5. 6 gives the conclusion of the thesis.

1.4 Sources

The sources in the literature search was mostly found from Science Direct and Wiley. The key words that was searched was "airborne coronavirus", "probability of infection corona", "model infection risk corona", "ventilation corona" and "coronavirus".

1.5 Limitations

The limitations of this master thesis was:

- The exposed manikin did not have a breathing function, which may influence the results
- Only airborne transmission was investigated
- The tracer-gas measurements could not catch the dynamic exhalation process from the infected manikin
- The findings are limited to the details in the experimental set-up
- A protocol was developed to keep parameters constant for every investigated scenario. The protocol was followed, but outside weather conditions were out of control for the author

2 Literature review and theory

2.1 Coronavirus: Routes of transmission

The routes of transmission for the coronavirus have been under discussion since the beginning of the pandemic. WHO stated early that the virus only transmitted by droplets (Noorimotlagh *et al.*, 2021). Later in 2020, WHO stated that the virus could additionally be airborne (WHO, 2020). Firstly, the routes were strictly separated into droplet transmission and airborne transmission (FHI, 2020*a*). Far into the pandemic, ECDC and US ECDC did no longer distinguish between the two, as they often overlap (FHI, 2020*a*). Currently, the European Centre for Disease prevention (ECDC) and US ECDC (United States) categorize the routes of transmission by inhalation, deposition and contact/fomites (FHI, 2020*a*). Although deposition and contact/fomites are not the investigated routes of transmission in this thesis, they are included in Appendix B to provide a broader understanding if necessary. To understand the routes of transmission, the virus-laden particles are explained in the following section and the definition of inhalation.

When an infector talks, breath, coughs or sings, virus-laden particles are emitted (Jayaweera *et al.*, 2020). The particles are both droplets and droplet nuclei/aerosols, as shown in Figure 2.1. Initially, large droplets fall to the ground or at other surfaces before they evaporate. Some particles are smaller droplets that evaporate in the air, before they gravitate towards the floor or may travel long distances along with the indoor air stream.

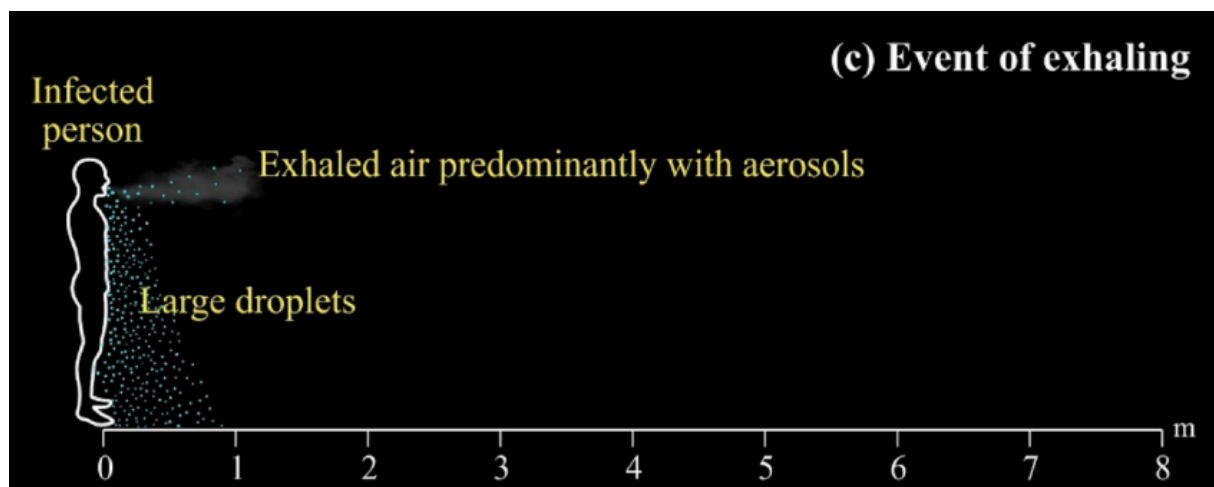


Figure 2.1: Virus particles emitted from an infected person (Jayaweera *et al.*, 2020).

2.1.1 Airborne transmission and inhalation

Airborne transmission is defined by that bacteria or virus is contained in smaller droplets (Jayaweera *et al.*, 2020). WHO defines “smaller droplets” as particles with diameter $< 5 \mu\text{m}$ (2014, as cited in Jayaweera *et al.*, 2020). Others state that particle sizes with diameter $< 10\text{-}20 \mu\text{m}$ characterizes as smaller droplets (Jayaweera *et al.*, 2020). These particles are referred to as droplet nuclei or aerosols. From here, the particles are called aerosols. It is proven that aerosols can travel long distances together with the airflow stream in a room. It is therefore in research stated that airborne transmission is dependent on the ventilation system in a room, as this thesis is highlighting (Ai, Z., Hashimoto, K. and Melikov, A., 2019).

Research have investigated how far aerosols can travel under different conditions. Somsen *et. al* found that aerosols with a diameter of $5 \mu\text{m}$ can linger in the air for around 9 minutes until they fall to the ground (2020, as cited in Ahlawat, A., Mishra, S. and Wiedensohler, A., 2020). van Doremalen *et al.* (2020) also investigated the survival of the virus in aerosols and found that the virus can survive up to 3 hours. This can prove that the long-range airborne route is of significance indoors. Noorimotlagh *et al.* (2021) found the same. Other situations that prove the long-range airborne route are super-spreading events (Greenhalgh *et al.*, 2021). These events cannot be caused by droplet transmission alone. This is because super-spreading events happen with big crowds, and there is a low chance that the super-spreader is in close contact with every person at the event.

Ai, Z., Hashimoto, K. and Melikov, A. (2019) states that the airborne cross-infection risk can be divided into two categories: direct and indirect transmission. Direct transmission refers to when an infector is emitting aerosols that penetrates the breathing zone of a healthy person and inhalation of the virus occur. Direct transmission is dependent on air distribution in a room, distance between infector and susceptible, positioning, orientation, breathing mode, activity level and movement. Indirect transmission refers to when aerosols are emitted from an infector and the aerosols travels with the air stream before it enters the breathing zone of a healthy person that inhales the virus. Indirect transmission is dependent on the supply airflow rate and the volume of the room.

The Norwegian Institute of Public Health (NIPH/FHI) states that the probability to get infected by inhalation from small or medium sized droplets is largest with short distances between an infector and a susceptible (FHI, 2020a). Within short distances of 0.5 meters,

the human micro-environment is of significance (Ai, Z., Hashimoto, K. and Melikov, A., 2019). This is further examined in 2.2.4.

2.2 Ventilation

The key factor of a ventilation system in reducing the risk of exposure to contaminants/viruses, is to dilute the concentration with adequate ventilation rates (Xu *et al.*, 2022). A ventilation system can consequently affect the route from the virus is exhaled until an exposed person inhales the virus. In this section, ventilation systems role in reducing the exposure risk in indoor spaces is reviewed.

2.2.1 Ventilation airflow rate

The minimum requirements for ventilation airflow rates are in Norway given in §13 in TEK-17. §13-3 concerns ventilation in public buildings (Norwegian Building Authority, 2017). The minimum requirement is based on pollutants from occupants (A), materials, installations and products (B) and processes and activities (C). The required airflow rate in category A is minimum $26 \text{ m}^3/\text{h} \cdot \text{person}$. For category B it is minimum $2.5 \text{ m}^3/\text{h} \cdot \text{m}^2$ when the room is occupied, and $0.7 \text{ m}^3/\text{h} \cdot \text{m}^2$ when not occupied. In category C it is varying for what process or activity takes place in a room. The minimum required ventilation airflow rate is $A + B$ if $(A + B) > C$, or C if the opposite is true.

Table 2.1 shows the recommended Air Changes per Hour (ACH) by building category, made by the American Society of Heat, Refrigerating and Airconditions Engineers (ASHRAE). ACH is defined by the total ventilation rate in m^3/h divided by the volume of a confined space (Nilsson, 2003).

Table 2.1: Minimum ACH recommendations for common building types (Robertson, 2021).

Building type	ACH recommendation
Office	2-3
Home	0.35-1
Shop	2-3
School	5-6
Sports facility	4-8
Restaurant	6-8
Airborne Infection Isolation Room	12
Examination room	6

There has been raised questions during the pandemic if increased ventilation airflow rates are beneficial to reduce the infection risk for the coronavirus. FHI (2020*b*) states that increased ventilation airflow rates are beneficial when they are originally is too low. Rocha-Melogno *et al.* (2021) supports this statement with their findings. They found that where people do not wear a mask and the ventilation is inadequate, the risk of infection increases with 424-488%. Li *et al.* (2021) also found that higher airflow rate gave lower concentration of small aerosols.

Increased ventilation airflow rate and exposure time have been found to be connected. Rocha-Melogno *et al.* (2021) found that increased airflow rate has low effect when the exposure time is lower than 30 minutes. A ventilation rate of 5 ACH for 1-4 hour events may reduce the risk of infection by 40-60%, while the benefit of increasing ventilation rates is low above 5 ACH. Dai and Zhao (2020) also found that exposure time was important for the same purpose. They investigated the required ventilation rate to keep the probability of infection below 1%. The required airflow rate for an event of 0.25 hours was found to be significantly lower than for an event of 3 hours.

Cotman *et al.* (2021) studied the effect of different ventilation solutions on transmission of virus and the risk of infection from airborne coronavirus. The investigated parameters were Air Changes per Hour (ACH), Fraction of Outdoor Air (FOA) and UVC-filtration. The most effective measure was to increase ACH, even with low virus emission rates. However, none of the simulated scenarios gave zero-risk of infection. They stated that higher ventilation rates cannot remove the risk of infection where the susceptible and infector are in close contact. However, Li, Y., Cheng, P. and Jia, W. (2021) found that

ventilation plays an important role in reducing the risk of infection in both the short-range and long-range airborne route.

2.2.2 Non-steady state mass-balance model

The concentration of a pollutant inside a room can be calculated by a non-steady state mass-balance model (Nilsson, 2003). This is shown in Equation 2.1.

$$\dot{V} \cdot c_s + \dot{M} = \dot{V} \cdot c_r + V \cdot \frac{dc_r}{dt}, \quad (2.1)$$

where

- \dot{V} is ventilation airflow rate [$\frac{m^3}{h}$]
- c_s is the supply air concentration [$\frac{mg}{m^3}$]
- \dot{M} is the source pollutant concentration [$\frac{mg}{h}$]
- c_r is the exhaust concentration [$\frac{mg}{m^3}$]
- V is the volume of the room [m^3]

The solution of the differential equation is shown in Equation 2.2.

$$c_{r(\tau)} = c_s + \frac{\dot{M}}{\dot{V}} - (c_s + \frac{\dot{M}}{\dot{V}} - c_{r(o)})e^{-n\tau}, \quad (2.2)$$

where

- $n = \frac{\dot{V}}{V}$ [h^{-1}]
- τ , time [h]

If the room air is fully mixed, the concentration of the pollutant in the whole room equals to the exhaust concentration and consequently can be calculated by Equation 2.2.

2.2.3 Air distribution patterns

Mixing ventilation

Mixing ventilation is an air distribution design that supply air outside the occupied zone, typically in the ceiling. The driving force is the high momentum from the supply air with

high velocity. The goal is to obtain a uniformly distributed temperature and contaminant concentration, which is described as a fully mixed condition. A typical air distribution pattern in a room with mixing ventilation is shown Figure 2.2.

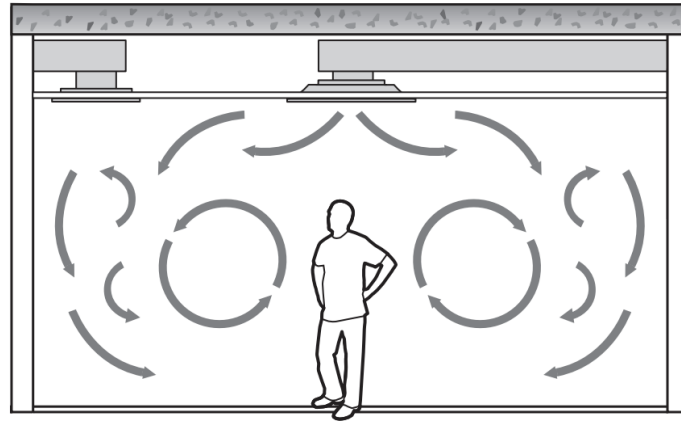


Figure 2.2: Air distribution pattern with mixing ventilation (Price engineering, 2016).

Displacement ventilation

Displacement ventilation is an air distribution design that supply air in the occupied zone, usually close to the floor. Air is supplied with low velocity and lower temperature than the indoor temperature. The driving force is thermal plumes generated from heat sources in the room. Thermal plumes are generated from amongst other computers and people. This phenomenon will force the air to raise and lead contaminated air to the exhaust, typically located in the ceiling. A typical air distribution pattern for displacement ventilation is shown in Figure 2.3.

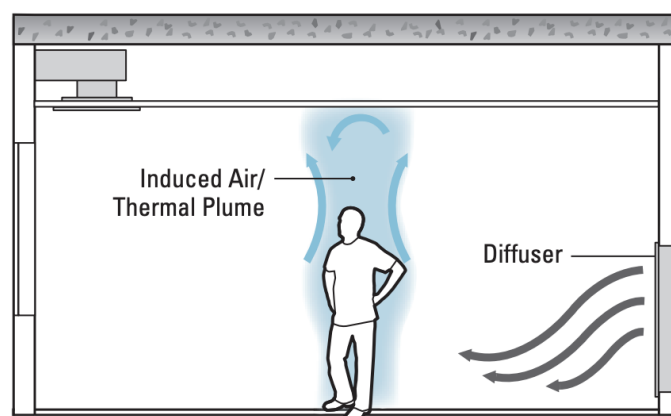


Figure 2.3: Air distribution pattern with displacement ventilation (Price engineering, 2016).

Distribution of airborne pathogens in a room are dependent on ventilation, specifically

air patterns and dilution (Sze and Chao, 2010). Jurelionis *et al.* (2015) found that a mixing ventilation strategy performed better than displacement ventilation regarding risk of infection of airborne viruses. Similar results was found by Olmedo *et al.* (2012). However, Xu *et al.* (2022) highlights that for a mixing ventilation strategy to effectively diluting airborne viruses, the ventilation airflow rate needs to be sufficient.

2.2.4 Interaction of ventilation and human: Human Thermal Plume (HTP), breathing and exhaled jet

The human micro-environment is important to consider regarding the risk of corona-infection, and is the "last inch" of infection. This section is exploring the human-micro environment, thermal plumes, exhaled jets generated by breathing and human interaction.

Human Thermal Plume (HTP)

The Human Thermal Plume (HTP) is generated because of the constant heat exchange between the human body and the surroundings (Sun, S., Li, J. and Han, J., 2020). The human body generates a Free Convection Flow (FCF) and creates the Convective Boundary Layer (CBL) that interacts with the surrounding environment. Recommendations on indoor temperature often ranges 20-27 °C, consequently giving a temperature difference of 7-13 °C from human body temperature. The HTP develops from the feet as a laminar flow, to a thicker and higher velocity turbulent flow moving towards the head because of buoyancy forces.

One research gap regarding the coronavirus and the HTP is how the thermal plume can influence "the last inch" of infection by the coronavirus (Sun, S., Li, J. and Han, J., 2020). "The last inch" refers to that a virus-laden particle has successfully travelled into the breathing zone of a susceptible and the remaining penetration zone for infection is the HTP. The author illustrates how pathogens carrying the coronavirus may be transported from floor level and into the breathing zone. This was argued by that most inhaled air comes from the boundary layer of the human body.

Human breathing

Human breathing can be approximated with a sinusoidal function, where exhalation and inhalation have approximately the same time period (Gupta *et. al* (2010), as cited in Olmedo *et al.* (2011)). The exhalation phase is a compound flow that consist of a vortex ring and a turbulent flow (Olmedo *et al.*, 2011). The exhaled jet behaves as a free jet

at maximum velocity. A healthy human being have 10-15 breathing cycles per minute (Ivanov, 2019). The breathing zone is defined as 0.3m radius around the mouth of a human (Ojima, 2012).

Breathing thermal manikins

Breathing thermal manikins have been commonly used to simulate a human being and the exposure to contaminants in indoor environments (Qian and Li, 2010; Olmedo *et al.*, 2011; Olmedo *et al.*, 2012; Liu *et al.*, 2016; Villafruela, J., Olmedo, I. and San José, J., 2016; Aganovic and Cao, 2019; Ai, Z., Hashimoto, K. and Melikov, A., 2019; Zhang *et al.*, 2020; Cheng *et al.*, 2021).

To successfully simulate a real human being, a thermal plume needs to be generated around the manikin. This may be fulfilled by a power supply and heating wires inside the manikin. The required power is dependent on the surface body area. Shuter and Aslani (2000) proposed an equation based on weight and height, to calculate the surface body area and is shown in Equation 2.3.

$$A_{bs} = 0.00949m^{0.441}h^{0.655} \quad (2.3)$$

where

- A_{bs} , body surface area [m²]
- m , weight [kg]
- h , height [cm]

Orientation and distance

One of the introduced measures early in the pandemic was to keep distance from others to reduce the exposure risk (WHO, 2021). WHO recommended to keep at least 1 meter of distance to other people.

The orientation between an infector and a susceptible may affect the exposure risk. Olmedo *et al.* (2012) investigated four different orientations: face to face, face to side, face to back and the infected person seated and the susceptible standing. With displacement ventilation, they found that the exposure risk is highest with face to face and face to side orientations, while face to back orientation gave zero exposure risk. With mixing ventilation, the authors highlight the significance of the relative height difference of an

infector and a susceptible.

2.2.5 Location of exhaust

The location of the exhaust may be important considering risk of infection. This is because the circulating air in a room flow towards this location. Occupants should not be located or have working stations close to the exhaust, to minimize the exposure to high contaminant- or virus concentrations (FHI, 2020b). Su *et al.* (2022) found that location of the exhaust was important to influence the risk of infection. However, the author requires more research to find the significance.

2.3 Other airborne removal factors

There are several removal factors to dilute the coronavirus, where ventilation parameters was reviewed in 2.2. In this chapter, additional biological factors that serves as removal factors for airborne pathogens are described.

2.3.1 Virus inactivation by biological decay

Biological decay describes how biological factors can affect the viability of a virus inside droplets and aerosols. This has been researched for the coronavirus since the beginning of the pandemic. Beggs and Avital (2021) investigated the biological decay constant k for the coronavirus. A psychrometric model was used to find the k -value, as well as influencing factors for biological decay. Psychrometric parameters as temperature, relative humidity and enthalpy have an impact of the biological decay of the virus (Beggs and Avital, 2021). The virus inactivation by biological decay k and it's dependency on relative humidity is shown in Figure 2.4.

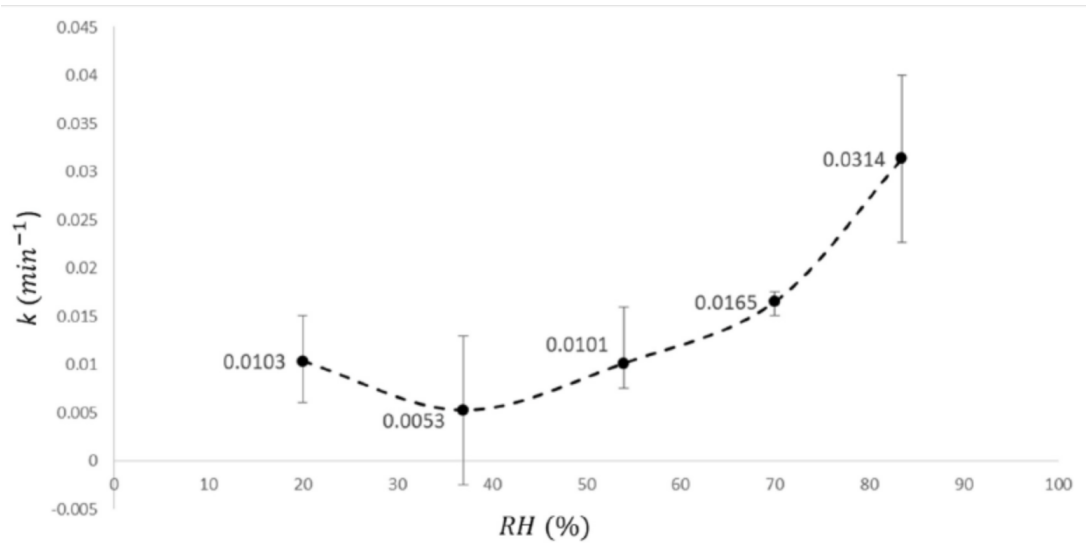


Figure 2.4: Virus inactivation rate (k) dependency on relative humidity (Aganovic *et al.*, 2021).

2.3.2 Deposition by gravitational settling

The deposition of viruses that is contained in aerosols is affected by gravitation (Aganovic *et al.*, 2021). It is amongst others influenced by the size of aerosols (Sze and Chao, 2010). The deposition by gravitational settling, D , is defined by Equation 2.4 (Aganovic *et al.*, 2021).

$$D = \frac{v_s}{H_{person}}, \quad (2.4)$$

where

- H_{person} , height of infected person [m]
- v_s , velocity of gravitational settling [$\frac{m}{s}$]

Velocity of gravitational settling is determined by Equation 2.5 (Aganovic *et al.*, 2021).

$$v_s = \sqrt{\frac{4 \cdot \rho_d \cdot g \cdot D_{eq}}{3 \cdot \rho_a \cdot C_{d,s}}}, \quad (2.5)$$

where

- ρ_d , droplet density [$\frac{kg}{m^3}$]
- ρ_a , air density [$\frac{kg}{m^3}$]

- D_{eq} , droplet diameter [m]
- g , gravitational settling [$\frac{m}{s^2}$]
- $C_{d,s}$, drag coefficient at sedimentation [-]

2.3.3 Temperature and relative humidity

Studies have shown that the coronavirus have long survival time with low air temperature and dry air (FHI, 2020*b*). FHI highlights that WHO and ECDC’s recommendations on room air temperature and relative humidity are challenging in practice in cold climates, as in Norway. Relative humidity and temperature are closely connected and further discussed in the next section about relative humidity.

Dry indoor environments has been proved to prolong the survival time of coronavirus (Ahlawat, A., Mishra, S. and Wiedensohler, A., 2020; FHI, 2020*b*; Rocha-Melogno *et al.*, 2021; Berry *et al.*, 2022; Harvard School of Public Health, 2020). People are more susceptible for infection as the human mucous membranes are more susceptible in this state. Ahlawat, A., Mishra, S. and Wiedensohler, A. (2020) stated that relative humidity lower than 40% could increase the risk of airborne transmission, while FHI (2020*b*) stated that RH lower than 20% should be avoided to reduce the risk. Berry *et al.* (2022) found that the range 40-70% is the best environment to reduce risk of infection. Rocha-Melogno *et al.* (2021) found that a 4-hour event with 70% RH decreased the risk of infection with 40% compared to a drier environment of 25% RH. With relative humidity around 60%, the viability of the microorganisms inside a droplet is lower than at other levels (Lin and Marr (2020), as cited in Ahlawat, A., Mishra, S. and Wiedensohler, A., 2020). Harvard School of Public Health (2020) raised a similar point. Table 2.2 summarizes the recommendations for RH levels to reduce the risk of infection from the coronavirus in indoor environments.

Table 2.2: Recommendations for relative humidity levels to reduce the risk of infection from airborne coronavirus.

Source	Recommendation of RH [%]
Ahlawat, A., Mishra, S. and Wiedensohler, A. (2020)	40-60
Berry <i>et al.</i> (2022)	40-70
FHI (2020 <i>b</i>)	>20

2.4 Assessing airborne exposure

The previous chapters, 2.2 and 2.3, have shown the removal factors of the coronavirus and airborne pathogens in general. In this chapter, technical approaches, exposure indices and models to calculate probability of infection are introduced in 2.4.1, 2.4.2 and 2.4.3, respectively.

2.4.1 Simulation/mimic of airborne exposure

Three approaches have been used to examine personal exposure to airborne particles: tracer-gas measurements, Computer Fluid Dynamics (CFD) and a trained panel (Brohus, 1997). In research, the first two methods are most frequently used. This section discusses tracer-gas techniques and CFD simulations.

Tracer-gas techniques

Tracer-gas techniques are commonly used to experimentally quantify ventilation rates and ventilation efficiency (Grieve, 1989). Gases used in the technique are colorless, odorless and should not be present in the analyzed indoor environment. The chosen gas should have similar density to air, be non-flammable and non-toxic. The most used tracer-gases are CO_2 , N_2O and SF_6 . The commonly used tracer-gas measurement techniques are step-down method, step-up method and pulse method (Han, 2012), as shown in Figure 2.5.

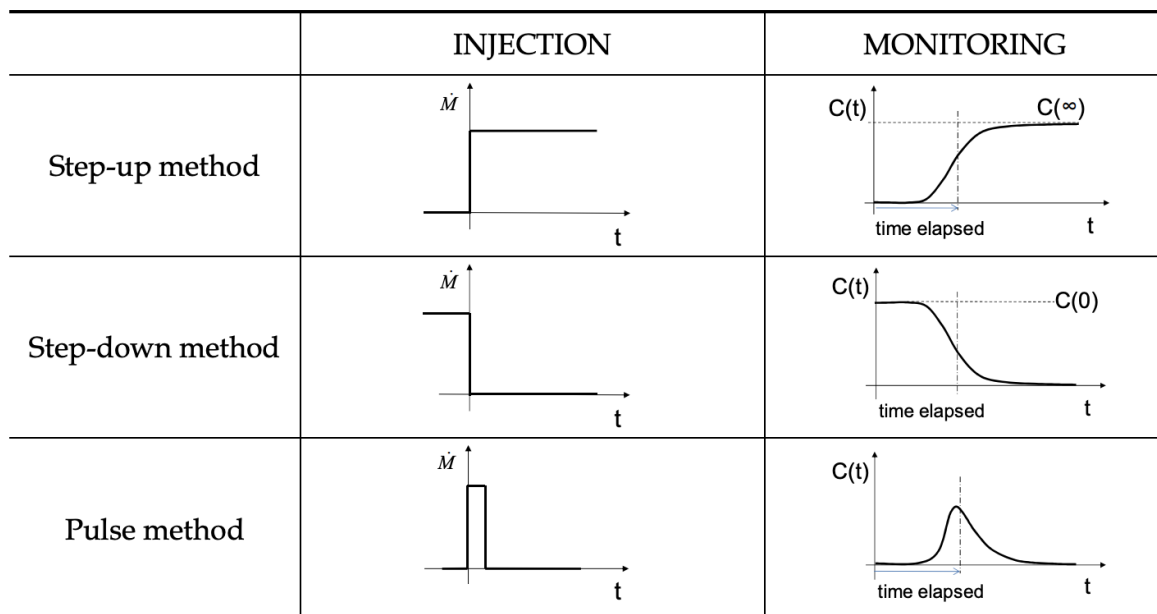


Figure 2.5: Tracer-gas measurement techniques (Han, 2012).

The step-up method are used in this thesis and therefore further explained. A constant amount of tracer- gas is injected to a room until it reaches a steady-state concentration (Han, 2012). This concentration can be used to determine ventilation efficiency/personal exposure index to contaminants. This is further described in 2.4.2.

Tracer-gas experiments have been used to quantify the risk of infection and how virus concentration spreads in a room. To simulate aerosols with diameter $< 5 \mu\text{m}$ containing coronavirus in human exhaled breath, tracer gases CO_2 , SF_6 and N_2O have been used (Liu *et al.*, 2016; Ai, Z., Hashimoto, K. and Melikov, A., 2019; Aganovic and Cao, 2019; Ai *et al.*, 2020; Zhang and Lin, 2021; Rencken *et al.*, 2021).

Computational Fluid Dynamics (CFD)

CFD simulations are used to numerically calculate air flow patterns, and point sources in the software can mimic airborne particles (Brohus, 1997). The numerical solutions are based on fluid mechanic equations like Navier-Stokes equation, conservation of mass, energy balances etc. CFD can clarify air flow patterns in an indoor environment, and consequently calculate the risk of infection. CFD have been used to confirm and compare results with experimental measurements regarding infection risk (Qian and Li, 2010; Villafruela, J., Olmedo, I. and San José, J., 2016; Cheng *et al.*, 2021).

2.4.2 Contaminant exposure indices

There are several indices to estimate the exposure of contaminants in an indoor environment. This section reviews the personal exposure index, the susceptible exposure index, the intake fraction index and the local air quality index.

Personal exposure index

Brohus (1997) proposed an exposure index to express the ventilation effectiveness that a person experience. The index is defined by Equation 2.6 (Brohus, 1997, p. 13)

$$\epsilon_e = \frac{c_R}{c_e}, \quad (2.6)$$

where,

- c_R , contaminant concentration in the exhaust
- c_e , contaminant concentration in the inhaled air for an exposed person

The author assumed that the supply concentration of the contaminant was zero. A high personal exposure index means a low concentration of pollutants in the inhalation zone compared to the exhaust, and the opposite for a low index (Qian *et al.*, 2006). The index can be calculated by measuring tracer-gas concentration at the inhalation zone of a person and in the exhaust.

Susceptible exposure index

The susceptible exposure index was proposed by Qian and Li (2010), and is shown in Equation 2.7. Aganovic and Cao (2019) used a similar index, named the *local relative contaminant index*.

$$\epsilon = \frac{C_i - C_s}{C_r - C_s}, \quad (2.7)$$

where,

- C_s , supply concentration
- C_r , exhaust concentration
- C_i , inhaled concentration

If the contaminant concentration in the supply is zero or low compared to the other variables, Equation 2.7 become Equation 2.8.

$$\epsilon = \frac{C_i}{C_r} \quad (2.8)$$

A high value of ϵ indicate high concentration of airborne particles in the breathing zone of a susceptible, and the opposite for a low value of ϵ . This index is the opposite of the one proposed by Brohus (1997).

Intake fraction index

Intake Fraction (IF) indices have been used to determine the exposure risk for airborne contaminants (Cheng *et al.*, 2021). The process from emission of a contaminant to inhalation by a susceptible consist of several steps as shown in Figure 2.6. The IF index consider the whole chain of an exposure process into one single value (Marshall and Nazaroff, 2006).

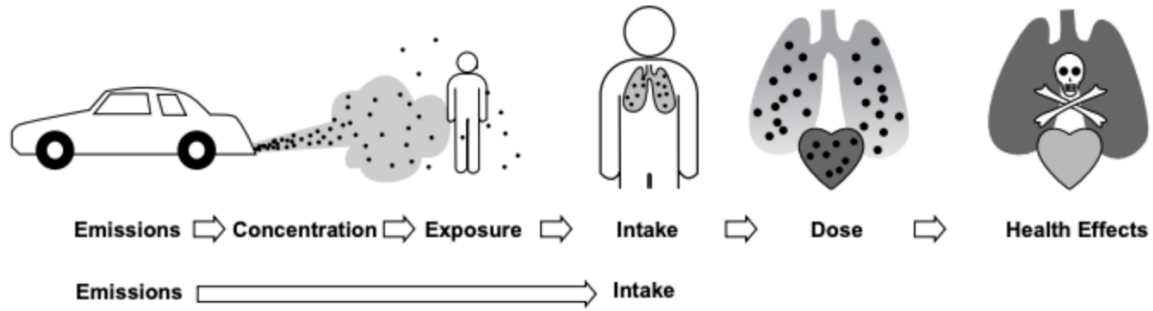


Figure 2.6: Chain of processes from emission of contaminants to inhalation and health effects (Marshall and Nazaroff, 2006).

IF is defined by the mass of the contaminant inhaled by exposed persons and the mass of exhaled contaminant, as shown in Equation 2.9 (Marshall and Nazaroff, 2006). It can be decided by experimental measurements or modelling.

$$IF = \frac{\text{inhaled mass}}{\text{emitted mass}} \quad (2.9)$$

Local Air Quality Index

The Local Air Quality Index (LAQI), ϵ_p^c , is a measure on how fast a contaminant is removed by the supply air at a specific point in a room (Brouns and Waters, 1991). It is defined by Equation 2.10 (Brouns and Waters, 1991, p. 4)

$$\epsilon_p^c = \frac{C_e(\infty)}{C_p(\infty)}, \quad (2.10)$$

where

- C_e , steady-state concentration of contaminant in the exhaust
- C_p , steady-state concentration of contaminant in a point

The index describe how much cleaner the air is in the investigated point compared to the exhaust air. The desired value for the index is $\epsilon_p^c \geq 1$, which indicate efficient removal of contaminants in the point. $\epsilon_p^c < 1$ should not be accepted.

2.4.3 Infection risk models

The probability to get infected by an airborne virus is important to investigate and quantify, especially when facing a pandemic where the airborne transmission route is of significance. Models for predicting the risk of infection on airborne viruses can give important input if buildings are safe to use for occupants. Several models have been developed with varying precision, and the state-of-the art on the field are presented in this section.

As previously presented in 2.1, there are several routes of transmission for the coronavirus. The presented models in this section applies for airborne transmission and serves the purpose of this thesis.

Dose-response models and Wells-Riley equation have commonly been used to calculate the risk of infection on airborne viruses (Sze and Chao, 2010). The Wells-Riley equation is the most used model because of its' simplicity, while dose-response models are less common as they require more detailed information of the analyzed disease (Sze and Chao, 2010). The Wells-Riley equation, dose-response models and modified versions of the Wells-Riley equation are reviewed in this section.

Wells-Riley equation

The Wells-Riley equation, as shown in Equation 2.11, is the most commonly used model to predict the probability to get infected by an airborne virus. The model was first used and presented by Wells and Riley when investigating an outbreak of measles at a school in Rochester, US (Riley, 1982).

The parameter *quanta* was introduced to form the Wells-Riley equation (Buonanno, G., Stabile, L. and Morawska, L., 2020). It was defined as "the dose of airborne droplet nuclei required to cause infection in 63% of susceptible persons". The Quanta Emission Rate (QER), i.e. the amount of virus needed to infect a susceptible person, differs from different mutants of the coronavirus (Wang *et al.*, 2022). QER is hard to estimate, as the variable is dependent on activity level, scenario, viral load and virus variant (Zhang and Lin, 2021). Buonanno, G., Stabile, L. and Morawska, L. (2020) established an approach to estimate QER, that can be applied for various mutants of the coronavirus. The approach is based on the assumption that aerosols emitted from an infected person is the same as the viral load in sputum.

Together with the parameter *quanta*, it was assumed that the airborne pathogens was

randomly distributed in the air and could be described with a Poisson distribution (Sze and Chao, 2010). Two important assumptions for the equation are fully-mixed air in the considered space and the only sink source for the virus' viability is ventilation.

$$P = 1 - e^{-\frac{Iqpt}{Q}}, \quad (2.11)$$

where

- P: probability to get infected
- I: number of infectors [–]
- q: quanta produced per hour [*quanta/h*]
- p: breathing rate per susceptible per hour [m^3/h]
- t: occupation time [*h*]
- Q: ventilation rate [m^3/h]

The Wells-Riley model is very simplified and may lead to vague conclusions on risk of infection. The fully-mixed air assumption does not apply to every situation and may lead to misinterpretation of the probability P. Also, other sink sources than ventilation influence the viability of the virus and the possibility to get infected, as described in 2.3. Consequently, many researchers have used the Wells-Riley equation as the foundation to develop models with more sink variables and non-fully mixed conditions. These models are presented in 2.4.3.

Dose-response models

Dose-response models are using a dose-response relationship to calculate the probability to get infected (Sze and Chao, 2010). Dose-response relationships describes how living organisms are affected by different *doses*. *Doses* may refer to substances as drugs, chemicals or biological matter. The term *dose* is defined as a certain dose of a pathogen, and can be found from experimental measurements.

There are two main categories of dose-response models: deterministic and stochastic models (Sze and Chao, 2010). The deterministic models are empirical, while the stochastic models are semi-empirical. Deterministic models are threshold models, that gives an

output defined by an Infection Dose (ID) value. This could be ID_{30} . ID_{30} indicate that if the whole susceptible population exhales this dose, 30% would get infected. Examples of deterministic models are the log-normal model, log-logistic model and Weibull model.

Stochastic models are built on if a susceptible breath in a pathogen dose, there is a certain probability that the susceptible gets infected (Sze and Chao, 2010). The authors state that stochastic models are most suitable for evaluating the risk of infection for airborne transmitted viruses. Examples of stochastic dose-response models are exponential models and Beta-Poisson models. The main difference between the two models, is that the exponential model does not consider that different susceptibles have different sensitivity to the virus.

Dose-response models have been used to calculate the risk of infection for COVID-19 (Buonanno *et al.*, 2020; Mittal, R., Meneveau, C. and Wu, W., 2020). Both articles used stochastic dose-response models.

Other models for risk of airborne infection of SARS-COV-2

So far in the pandemic, several models have been used to investigate the probability to get infected by the coronavirus in the airborne transmission route. This section presents scientific research using different approaches. 2.4.3 discussed the two most used models: Wells-Riley equation and dose-response models. This section presents other models that have also been used and an overview is presented in Table 2.3.

One research paper modified the Wells-Riley equation to consider more removal factors than ventilation (Aganovic *et al.*, 2021). These were deposition by gravitational settling and biological decay. The authors investigated if relative humidity had a significant impact on infection risk from the coronavirus and found that it did not. The model assumed fully mixed conditions and was highlighted as a weakness in the research paper. This is the same weakness as in the traditional Wells-Riley equation. This method was a purely theoretical approach.

Gammaitoni-Nucci (G-N) equation has also been used to calculate infection risk (Xu *et al.*, 2021). The model is a variant of the traditional Wells-Riley equation. The significant difference between the G-N equation and the traditional Wells-Riley equation is that the former considers a variable quanta concentration. The researchers investigated infection risk at schools in the US with a scenario-based theoretical approach with historical data.

A dilution-based modification of the Wells-Riley equation was proposed by Zhang and Lin (2021). The authors used an experimental approach based on dilution. The model fits well with experimental approaches and is relying on ventilation's role in diluting contaminants in indoor spaces. The ratio of contaminant concentration at the source and at a target position is the most important factor in the model. This model is not based on the assumption of well-mixed conditions and can be used for both spatial and temporal conditions. The model was tested and validated experimentally.

A modified Wells-Riley equation considering social distance specifically was proposed by Shang *et al.* (2022). This model included an index called Social Distancing Index (SDI). The model was tested with CFD.

In contrast to the former mentioned authors using several modifications of Wells-Riley models, Buonanno *et al.* (2020) and Cotman *et al.* (2021) used dose-response models to quantify the probability of infection from the coronavirus. As discussed in previously, these models require more detailed information about the virus and is therefore a more thorough approach to calculate the probability of infection. Early in the pandemic, this might have been a problem as there was undiscovered information about the virus. This could also be a problem when new virus variants and mutants appeared later (omicron, delta etc.).

As discussed in this chapter, several models have been used to calculate the risk of infection. Dose-response models, Wells-Riley models and modified Wells-Riley models has been used with different approaches. Some authors used purely theoretical approach that was scenario-based, others used CFD or tracer gas measurements. This shows that there is a development in research in how to calculate the risk of infection in a correct and precise manner. The analyzed situation needs to fit with the chosen model, and therefore it seems to be different approaches.

Table 2.3: Models from literature used to predict the possibility of infection for the coronavirus.

Source	Model
<i>Aganovic et al.</i> (2021)	Modified Wells-Riley
<i>Xu et al.</i> (2021)	Gammaitoni-Nucci (modified Wells-Riley)
<i>Buonanno et al.</i> (2020)	Dose-response model
Zhang and Lin (2021)	Dilution-based Wells-Riley model
<i>Cotman et al.</i> (2021)	Dose-response model
<i>Shang et al.</i> (2022)	Modified Wells-Riley model
<i>Wang et al.</i> (2022)	Coupled Wells-Riley and CFD
<i>Su et al.</i> (2022)	Coupled Wells-Riley and CFD
<i>Berry et al.</i> (2022)	Dose-response model
Cammarata and Cammarata (2021)	Modified Rudnick and Milton model
Li and Tang (2021)	Modified Wells-Riley

3 Method

3.1 Introduction

The method to explore the probability of infection under different ventilation solutions is separated into two main parts. Experimental measurements were used to measure exposure and were the basis to calculate the personal exposure index for a healthy person exposed to a corona-infected person. The theoretical modelling was used to calculate the probability of infection. The experimental measurements are described in 3.2 and the theoretical modelling is described in 3.3. An overview of the method is shown in Figure 3.1.

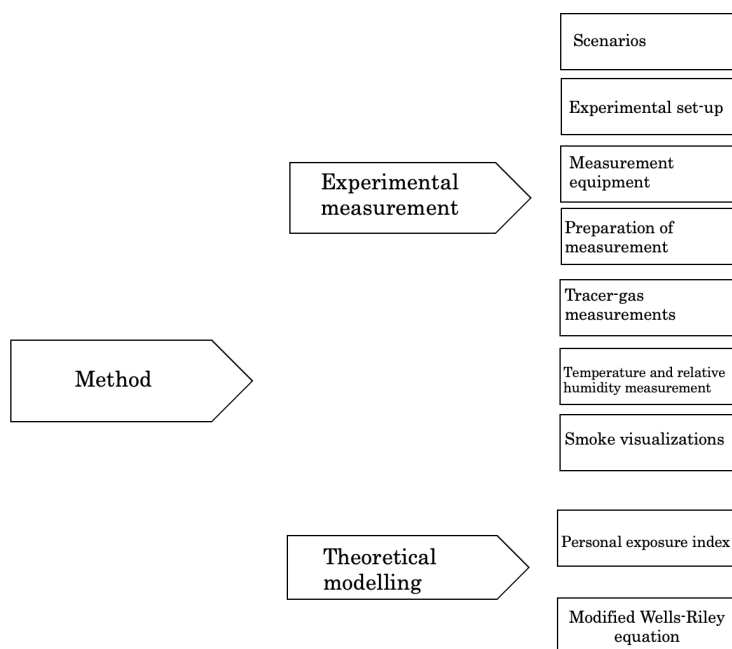


Figure 3.1: Overview of the method chapter.

3.2 Experimental measurement

The purpose of the experimental measurements was to quantify exposure under various scenarios presented in 3.2.1. The risk assessment for the experimental measurement is shown in Appendix A.

3.2.1 Scenarios

The varied parameters in the experiments was Air Changes per Hour (ACH) and separation distance between the exposed and the infected person. As shown in 2.1, 3 ACH corresponds to recommendation for offices and shops, 6 ACH to schools, restaurants and examination rooms and 12 ACH to airborne isolation infection rooms. The separation distance between the exposed person and the infected person was 0.7, 1.0, 1.5 and 2.0 meters. The desired indoor air temperature in the occupied zone, T_{room} , was 22-23 °C.

The scenario set-up needed to be changed because of deviations from the input values to the BEMS-system and the measured ventilation airflow rates. When 3, 6 and 12 ACH were used as input to the BEMS-system, the actual airflow rates were 2.7, 5.1 and 9.6 ACH. The set-up is shown in Table 3.1.

Table 3.1: Scenario set-up for the experimental measurements.

Scenario	Separation distance [m]	ACH	Airflow rate [m ³ /h]
1A	0.7	2.7	226
1B	1.0		
1C	1.5		
1D	2.0		
2A	0.7	5.1	430
2B	1.0		
2C	1.5		
2D	2.0		
3A	0.7	9.6	810
3B	1.0		
3C	1.5		
3D	2.0		

3.2.2 Experimental set-up

The HVAC-laboratory at Gløshaugen, NTNU was used as facility for the experimental measurements. The case study was a corona-infected standing person with an exposed person sitting in front. The experimental set-up consisted of four main elements: ventilation system, a breathing thermal manikin (infected person), a breathing box and a thermal manikin (exposed person).

HVAC laboratory

A model of the HVAC-laboratory is shown in Figure 3.2. The laboratory was of size 3.05 meters (H), 6.17 meters (L) and 4.46 meters (W). This resulted in a volume of 84 m^3 . Figure 3.2 serves as a basis for the description of scenarios in the method section. The left corner is the reference point $(0,0,0)$.

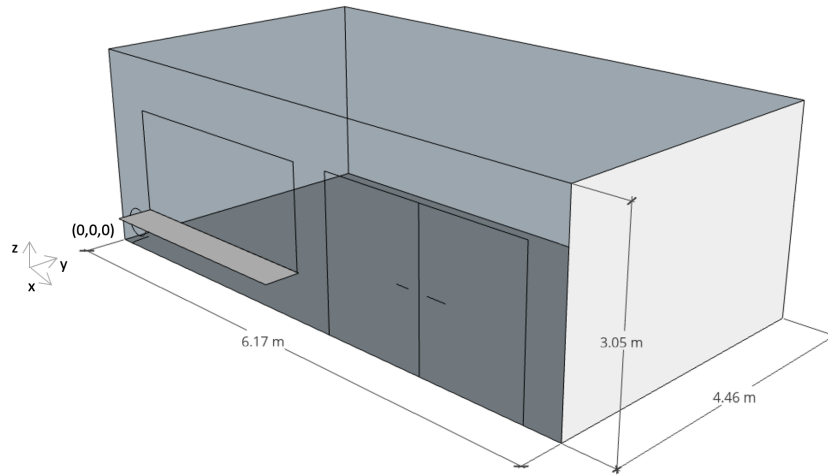


Figure 3.2: A model of the HVAC-laboratory at NTNU, Gløshaugen. Made in SketchUp.

Ventilation system

The ventilation system in the laboratory room was equipped with an Air Handling Unit (AHU) from Covent, as shown in Figure 3.3. The AHU consisted of a rotary wheel heat exchanger, heating- and cooling coils and filters for intake and exhaust air. The maximum capacity was $2000 \frac{\text{m}^3}{\text{h}}$.



Figure 3.3: Air handling unit from Covent at the HVAC-lab at Gløshaugen, NTNU.

The AHU was controlled by the Building Energy Management System (BEMS). A computer outside the laboratory controlled this remotely. The system's interface is shown in Figure 3.4. The controlling parameters used in this thesis were LR501 (exhaust airflow rate settings), LR401 (supply airflow rate settings), RT410 (supply air temperature settings), SB421 (heating coil settings) and LX411 (rotating heat exchanger settings).

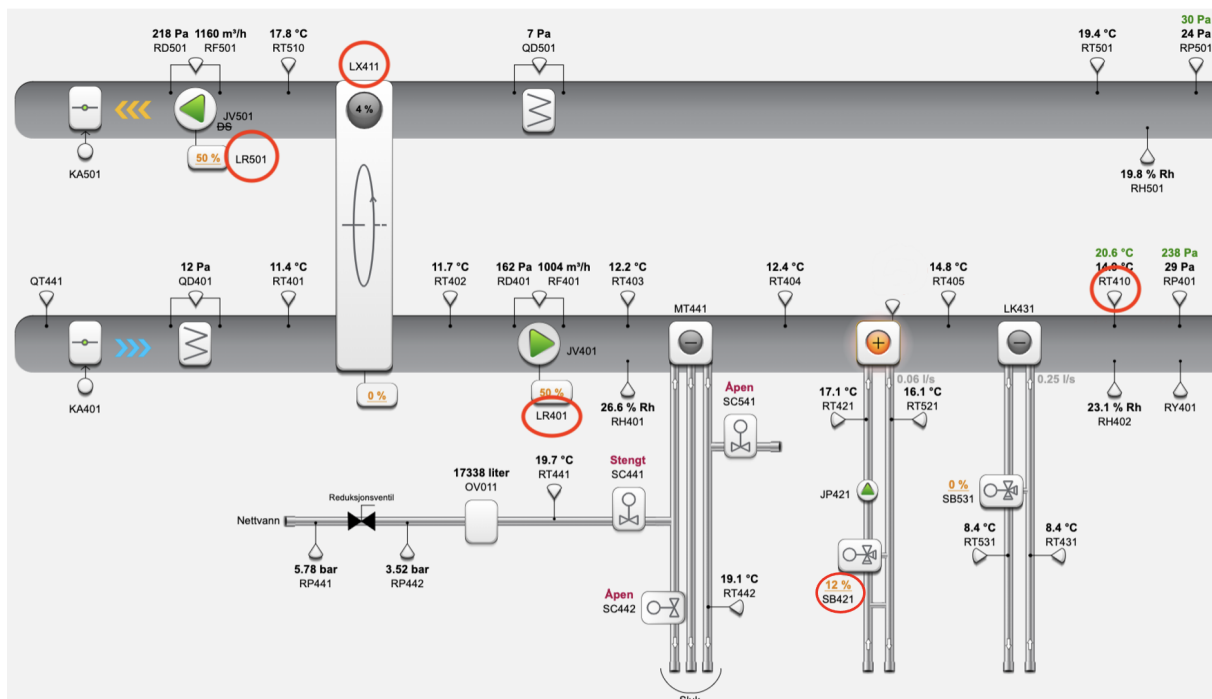


Figure 3.4: BEMS interface on the computer outside the laboratory. The used parameters are marked in red.

A sketch of the duct system is shown in Figure 3.5. The supply air duct-system consisted of one main branch that split into three branches. Branch duct 1 (right-most in Figure 3.5) could be used with a displacement ventilation strategy, while Branch duct 2 and 3 (middle and left-most in Figure 3.5) could be used with a mixing ventilation strategy. Branch duct 1 was shut off by turning off a valve, as a mixing ventilation strategy was used in this thesis. Branch duct 2 was connected to three supply air diffusers, while Branch duct 3 was connected to two supply air diffusers. The duct-system for exhaust air had one main branch with two local ducts connected to one exhaust air unit each.

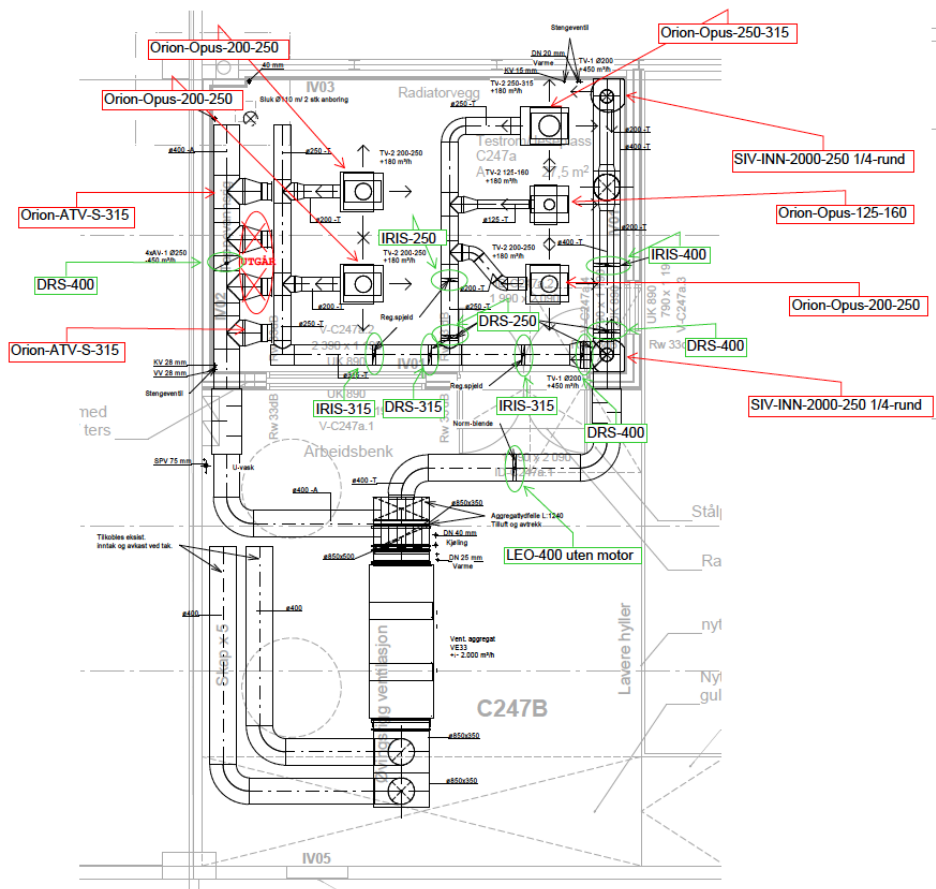


Figure 3.5: Duct system in the HVAC-laboratory at NTNU, Gløshaugen.

The location of the supply air diffusers and exhaust air units is shown in a simplified model in Figure 3.6. Table 3.2 shows the location according to the coordinate system.

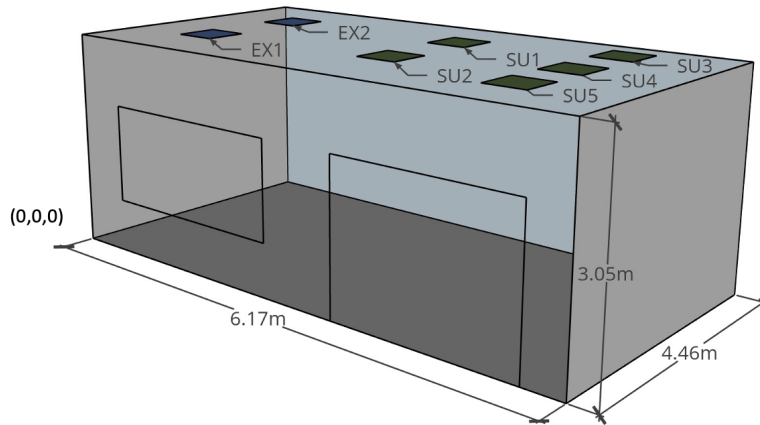


Figure 3.6: A model of the HVAC-laboratory at NTNU, Gløshaugen. EX_x are exhaust and SU_x are supply inlets.

Table 3.2: Location of exhaust and supply air units in the HVAC-laboratory.

Type	x [m]	y [m]	z [m]
EX_1	0.75	0.70	2.47
EX_2	0.75	3.7	2.48
SU_1	2.33	2.64	2.49
SU_2	2.31	1.24	2.49
SU_3	5.11	3.39	2.49
SU_4	5.17	2.36	2.49
SU_5	5.14	1.4	2.49

Table 3.3 shows name, type and k-factor for the supply air diffusers. The diffusers had pressure outlets, where the pressure drop could be measured.

Table 3.3: Air supply diffuser characteristics.

Name of unit	Type	k-factor
Orion-Opus 200-250	Supply units (SU_1 , SU_2 , SU_5)	26.8
Orion-Opus 125-160	Supply unit (SU_4)	12.4
Orion-Opus 250-315	Supply unit (SU_3)	36.7

The supply air diffusers were balanced to deliver the same airflow rate. The pressure drop was measured by the pressure tubes with a *Autozeroing micromanometer model TT470S* (3.2.3). The airflow rate was calculated using the square root of the pressure drop multiplied by the k-factor. A *Lindab Ultralink* (3.2.3) placed on the main supply branch

was used to verify the total ventilation airflow rate. The system was manually regulated by wires connected to the plenum boxes in each diffuser. Table 3.4 shows the percentage of total airflow rate delivered by each diffuser after balancing. It shows that the diffusers supplying the lowest and highest airflow rates differed by less than 5%. The diffusers had a swirl pattern, as shown in Figure 3.7.

Table 3.4: Percentage of the total airflow rate that each supply air diffuser delivered.

Supply air diffuser	% of total airflow rate
SU ₁	20.8
SU ₂	17.6
SU ₃	21.5
SU ₄	17.8
SU ₅	22.2

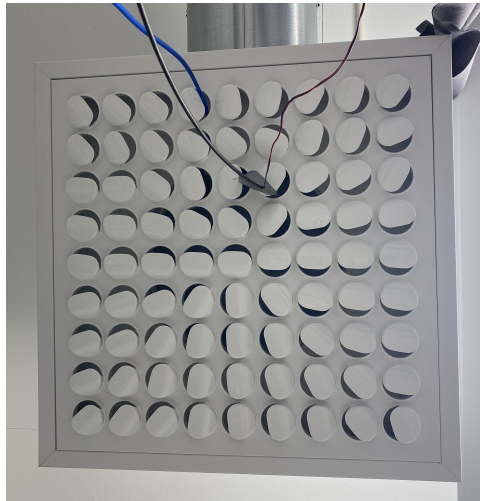


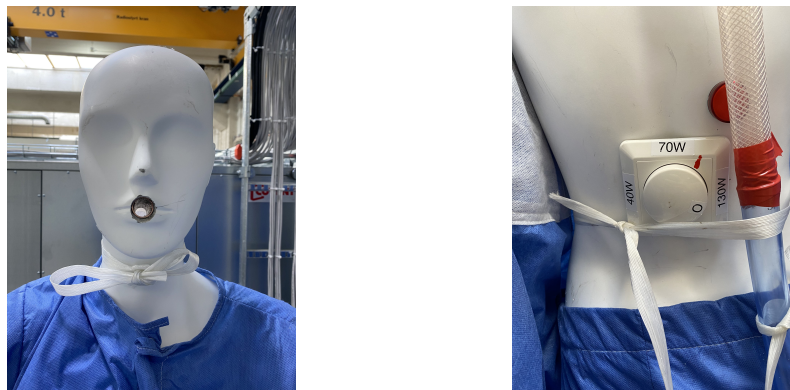
Figure 3.7: Air supply diffuser with swirl pattern.

Thermal breathing manikin: Infected person

A thermal breathing manikin was used to simulate an infected person and is shown in Figure 3.8a. From now called M_{inf} . The manikin was of type *Lo Lzm 09 Ada head (white)* and was produced by Morten Finckenhagen Butikkinnredninger AS. This was the same manikin as previously used in experimental set-ups at NTNU (Aganovic and Cao, 2019). The height of the manikin was 175 cm and an assumed weight of 75 kg. The breathing zone was at 160 cm.

Heating wires inside the manikin were used to heat up the skin surface temperature to 37 °C. The activity level was assumed to be 1.2 met ($=70 \text{ W/m}^2$). The surface area was

1.88 m², calculated by Equation 2.3. This gave a heat output of 130 W. The skin surface temperature got too high when measured at the lab. Therefore, a heat output of 75 W was used. This value is widely used in literature to obtain correct skin surface temperature (Qian and Li, 2010). The heat output was controlled by a dimmer on the back, as shown in Figure 3.8b. This generated a realistic scenario with a rising thermal plume around the manikin.



(a) Hole in the mouth for breathing mechanism. (b) A dimmer located on the back for control of heat output.

Figure 3.8: Characteristics of the infected manikin.

A breathing box was used to simulate breathing. The exhaled air was heated to 34 °C (Bjørn (1999), as cited in Olmedo *et al.* (2012)). 34 °C was used to simulate exhaled air temperature that is saturated with water vapor at 31 °C. A heating element of 5 W was used to obtain the correct temperature and it was controlled by a Variac Variable Controller. The element is described in D.2. The heating element was mounted in a metal tube inside the manikins' mouth. The metal tube and the hole in the mouth is shown in Figure 3.8a, and had dimension Ø16 mm. The metal tube was connected to a plastic tube that was inserted into the breathing box.

The breathing function also consisted of obtaining a realistic exhaled jet velocity. When people do not wear a mask, the exhaled jet can be 1 $\frac{m}{s}$ for breathing and 2 $\frac{m}{s}$ for a stronger exhale (Rencken *et al.*, 2021). The exhaled jet was set up by the breathing box and further explained in the following section.

Breathing box and human exhaled air

A model of the breathing box is shown in Figure 3.9. The location of the box in the experimental facility is shown in Figure 3.10. The box was of size 0.5 meters (L), 0.3 meters (B) and 0.4 meters (H). The box consisted of two controllers (two black buttons),

a fan, two supply inlets (a and b) and one outlet (c).

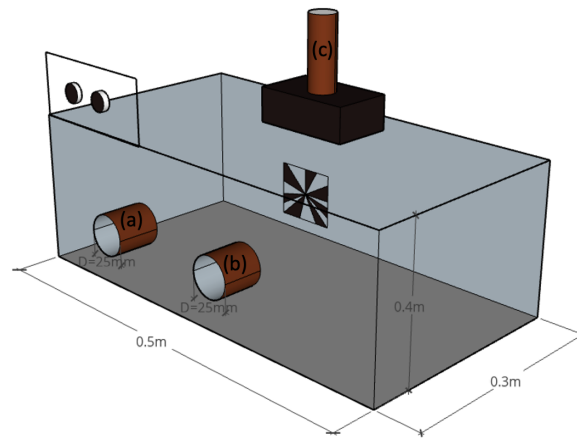


Figure 3.9: Model of breathing box. Made in SketchUp.

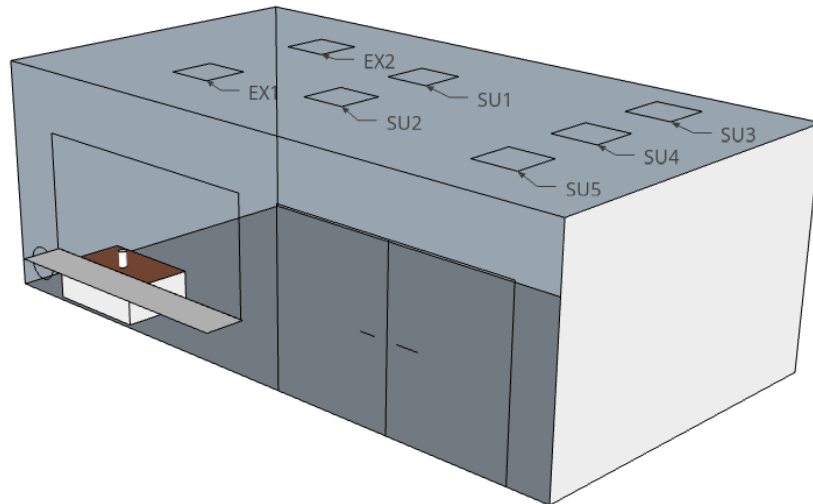


Figure 3.10: The experimental facility with location of the breathing box.

Inlet (a) was supplied with air and inlet (b) with N_2O tracer gas. N_2O tracer gas was used to mimic aerosols with diameter $< 5 \mu m$, as infected by the coronavirus (Ai *et al.*, 2020). The total exhaled and inhaled volumetric flow rate was 11.34 L/min (Villafruela, J., Olmedo, I. and San José, J., 2016). Human adult breathing are normally from 12 breaths per minute, which means 5 second period of one breath (Johns Hopkins Medicine, n.d.). This consists of 2.5 seconds of exhale and 2.5 seconds of inhale. The dosing of fresh air was therefore 22 L/min. N_2O tracer gas was dosed directly from a tracer gas bottle to the breathing box with a mass fraction of $Y_s = 0.027$ (Villafruela, J., Olmedo, I. and San José, J., 2016). This gave a dosed tracer-gas flow rate of 0.594 L/min. A flow meter was

used to control the flow rate of N_2O tracer-gas before entering the breathing box. It is described in 3.2.3.

Air and tracer gas was mixed inside the box. The mix of N_2O and air was led out by the exhaust outlet (c) to obtain a realistic exhaled jet from the manikin. From the box, the mix was connected by the plastic tube in the mouth of M_{inf} . The fan inside the breathing box was simulating a periodic exhaled jet of a human being. The exhaled jet was periodic with 2.5 seconds per exhale. The breathing box provided 12 breathing cycles per minute. The breathing box did not simulate inhalation.

Thermal manikin: Exposed person

The exposed person was simulated by a thermal manikin, as shown in Figure 3.11. From now called M_{exp} . This was the same type of manikin as M_{inf} .



Figure 3.11: Manikin simulating a sitting exposed person.

The height of the manikin was 175 cm and an assumed weight of 75 kg. The breathing zone was at 110 cm. The manikin was sitting with an assumed metabolic rate of 1.2 met ($= 70 \text{ W/m}^2$). The heat output was calculated to be 130 W by Equation 2.3, but because of the same problem as M_{inf} , it was reduced to 75 W. The heat loss was simulated by heating wires inside the manikin. The heat was controlled by a heating device, as shown in Figure 3.12. The temperature on the legs, arms, torso and head was adjusted on the instrument. During the measurements, the skin surface temperature was held constant around 37°C . The manikin did not have a breathing function.



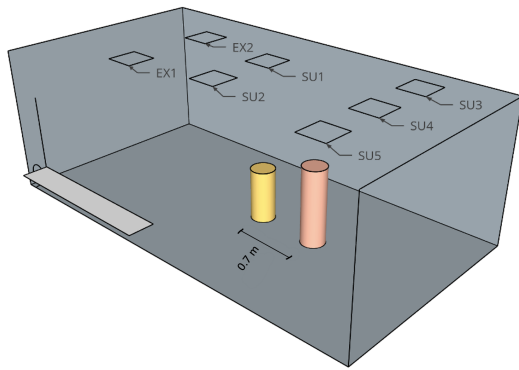
Figure 3.12: Equipment to heat up the exposed manikin to skin surface temperature.

Location of manikins

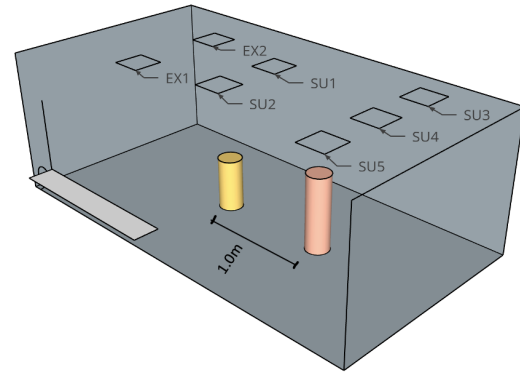
The location of the two manikins during the experiments is shown in Figure 3.13. The location according to the coordinate system is shown in Table 3.5. The pink cylinder represents M_{inf} and the yellow cylinder represent M_{exp} . M_{inf} was placed in a manner where the air jets from the supply air diffusors were not directly penetrating the exhaled jet.

Table 3.5: Location of exposed person and infected person at different distances. Z_{br} means inhalation zone height.

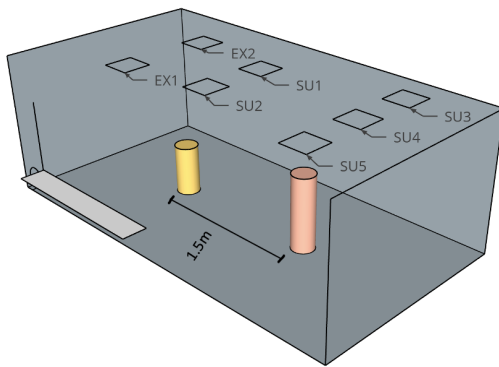
Separation distance [m]	M_{exp}			M_{inf}		
	x [m]	y [m]	z_{br} [m]	x [m]	y [m]	z_{br} [m]
0.7	3.5	2.4	1.1	4	2.4	1.6
1.0	3.0	2.4	1.1	4	2.4	1.6
1.5	2.5	2.4	1.1	4	2.4	1.6
2.0	2.0	2.4	1.1	4	2.4	1.6



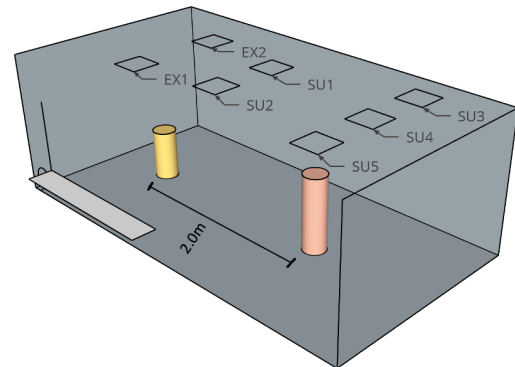
(a) Separation distance of 0.7 meters.



(b) Separation distance of 1.0 meters.



(c) Separation distance of 1.5 meters.



(d) Separation distance of 2.0 meters.

Figure 3.13: Location of the exposed and the infected manikin.

Heat load

The known heat loads in the laboratory room was 150 W from the manikins and lights with unknown heat output. There was a minimum of 150 W of known heat output in the room.

3.2.3 Measurement equipment

This section presents the measurement equipment in the experimental set-up.

Autozeroing micromanometer

The pressure difference to calculate airflow rates was measured with an *Autozeroing micromanometer model TT470S*. The equipment had a measurement accuracy of ± 2 Pa. The equipment is shown in Figure 3.14.



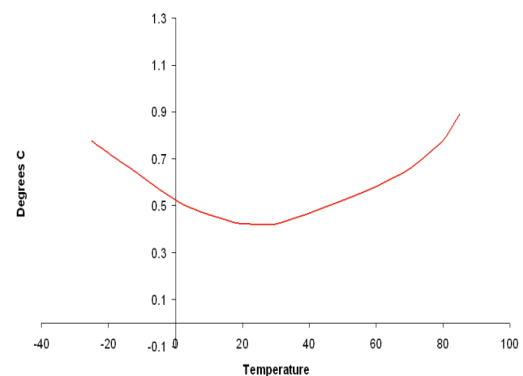
Figure 3.14: Autozeroing micromanometer model TT470S to measure the pressure difference in the supply air diffusers.

TinyTag Plus 2

TinyTag Plus 2 TGP-4500 were used to monitor relative humidity and temperature. The equipment is shown in Figure 3.15a. They were set up with a measurement interval of 20 seconds. The accuracy for was $\pm 3.0\%$ RH at $25\text{ }^{\circ}\text{C}$ and the accuracy for temperature is shown in Figure 3.15b (TinyTag, 2018).



(a) TinyTag Plus 2 TGP-4500.



(b) Accuracy for temperature (TinyTag, 2018).

Figure 3.15: TinyTag Plus 2 TGP-4500 characteristics.

Hioki Memory HiLogger

A Hioki Memory HiLogger was used to measure temperature, and is shown in Figure 3.16. The logger was of type LR8400-20. The logging interval was set to 20 seconds. The accuracy when measuring temperatures at 23 ± 5 °C and a relative humidity of 80% or less was ± 0.6 °C.



Figure 3.16: Memory HiLogger to monitor temperature.

Multipoint Sampler/Doser and Multi-gas Monitor

The equipment for tracer-gas was 1303 Multipoint Sampler and Doser, Multi-gas Monitor Type 1302 and the digital interface Innova AirTech Instruments was used for monitoring. The two equipments are shown in Figure 3.17.

The equipment consist of six dosing and six sampling channels. The sampling channels measured the tracer-gas concentration in ppm and logged in the INNOVA software. The software tracked concentration at each sampling tube every six minutes.



Figure 3.17: Tracer-gas equipment in the laboratory.

Flow meter

A glass flow meter from Platon were used to control the flow rate of tracer-gas. It was of type Platon NG-GTF 0.2-1.9 L/min. The accuracy of the flow meter was $\pm 1.25\%$ in Forecast Standard Deviation (FSD).

Velocity: SensoAnemo

SensoAnemo 5100LSF was used to measure the velocity of the exhaled jet from the infected manikin, and is shown in Figure 3.18. The accuracy of the anemometer was ± 0.02 m/s and $\pm 3\%$ with a range of 0.05-5 m/s.



Figure 3.18: SensoAnemo 5100LSF to measure velocity of the exhaled jet from the infected manikin.

Lindab UltraLink

Lindab UltraLink was used to measure the total supplied ventilation airflow rate and is shown in Figure 3.19. The UltraLink was placed at the main supply duct outside the laboratory. The uncertainty of the equipment was $\pm 5\%$ according to the manufacturer.



Figure 3.19: Lindab UltraLink to measure the total ventilation airflow rate.

3.2.4 Preparation

The rotary wheel heat exchanger in the AHU might cause tracer-gas to be re-transmitted from the exhaust to supply air. It was desired to achieve the lowest possible background

concentration. The heat exchanger was turned off and tested for this purpose. The testing revealed that there was re-transmission, hence it was sealed as shown in Figure 3.20.

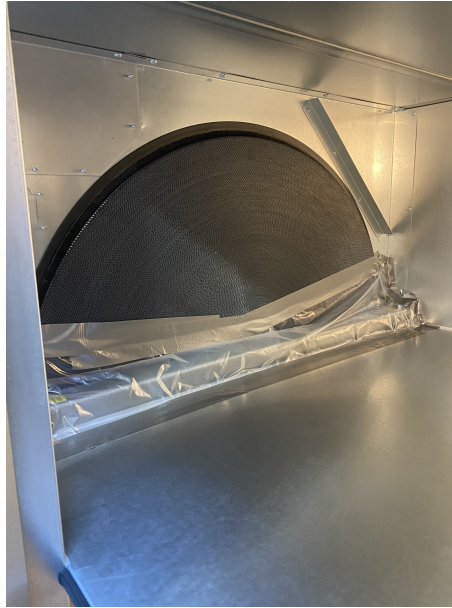


Figure 3.20: Plastic-sealed rotating heat exchanger to avoid unnecessary re-transmission of tracer gas from exhaust to supply air.

The exhaled air jet velocity from M_{inf} was tested with *SenseAnemo anemometer* (3.2.3). This was done to ensure that the heating element in the mouth did not disrupt the airflow pattern. The measured velocity is shown in Figure 3.21. Figure 3.21 shows that the exhaled velocity had extreme values at 2 and 0.25 m/s . Most of the time the exhaled jet was 1.5 m/s . This confirms that the velocity was within the range of a normal human exhaled breath, as reported by Rencken *et al.* (2021), and the set-up represented a realistic scenario.

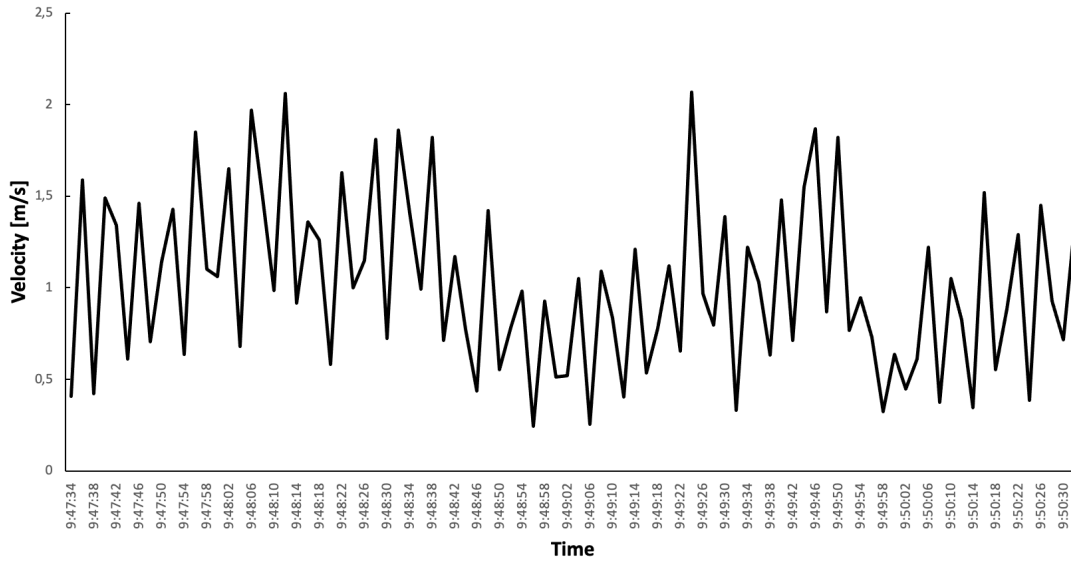


Figure 3.21: Exhaled velocity from the infected manikin, M_{inf} .

3.2.5 Tracer-gas measurements

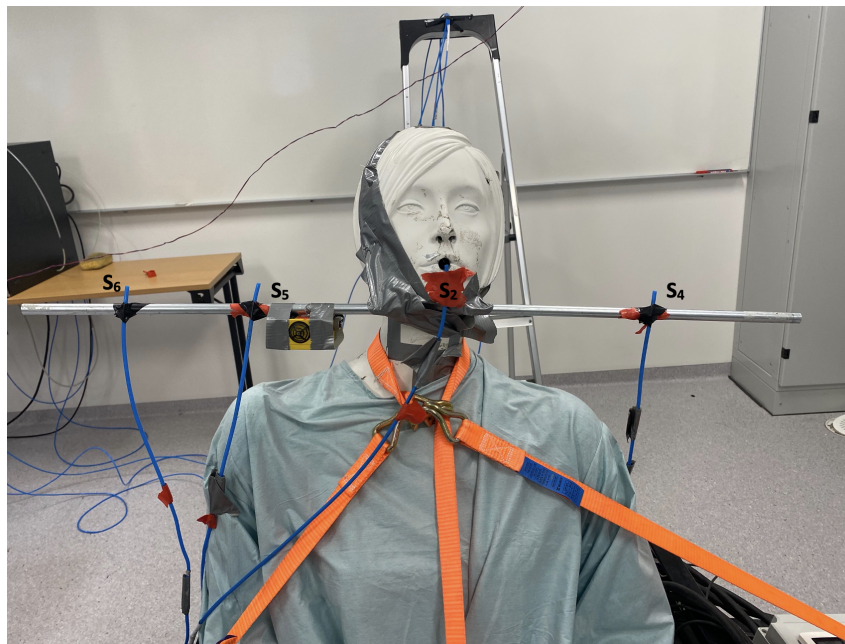
Tracer-gas measurements was conducted for each of the scenarios presented in Table 3.1, to calculate the personal exposure index/local air quality index for the exposed person. N_2O was used as tracer-gas. Detailed information about N_2O is provided in C. The step-up method was used as tracer-gas technique.

To measure the distribution of tracer-gas concentration in the laboratory room, the *Brüel & Kjaer gas equipment* (3.2.3) was used. All six sampling channels were used in the measurements. A tracer-gas bottle with N_2O tracer-gas was directly connected to the breathing box, and therefore the dosing channels were not used.

Table 3.6 shows the location of the sampling and dosing tubes. D refers to the dosing tube and S_1 - S_6 refers to sampling tubes. S_1 was located in the exhaust. The tube was located in the duct where the extracted air from both exhaust units was mixed. This value was further used to calculate the local air quality index/personal exposure index as shown in Equation 3.4. S_2 was mounted in the inhalation zone of the exposed manikin. This value was used together with S_1 to calculate the local air quality index/personal exposure index in Equation 3.4. S_3 was located in the main supply duct to control the background concentration. S_4 and S_5 was located at 20 cm (shoulder width) around the manikin, and S_6 was located at 35 cm from the mouth as shown in Figure 3.22. This was monitored to observe the effect of the thermal plume around M_{exp} , as requested by Sun, S., Li, J. and Han, J. (2020).

Table 3.6: Location of sampling and dosing tubes during the experiments.

Tube	Location
D	Inlet (a) breathing box
S ₁	Exhaust duct
S ₂	M_{exp} inhalation zone
S ₃	Main supply duct
S ₄	20 cm right of mouth, M_{exp}
S ₅	20 cm left of mouth, M_{exp}
S ₆	35 cm left of mouth, M_{exp}

**Figure 3.22:** Location of S₂ and S₄-S₆. 20 cm from the mouth at both sides and one 35 cm at the left side (outside breathing zone).

All electrical equipment was turned on in the morning. The temperature in the room stabilized after 2 hours. After thermal stabilization, the tracer-gas was dosed by the exhaled jet from M_{inf} . The measurements were carried out with 2.7 ACH, 5.1 ACH and 9.6 ACH (scenario 1, 2 and 3), with the manikins initially separated by 2 meters. 10 measurement points were carried out inside the stable concentration area. The stable concentration was decided to be when the concentration in the inhalation zone of M_{exp} and in the exhaust no longer fluctuated significantly. When the tracer gas concentration reduced to ≈ 0.5 ppm, M_{exp} was moved to 1.5 m. The same procedure was repeated for 1.0 m and 0.7 m.

3.2.6 Temperature and relative humidity

Temperature and relative humidity may affect the risk of exposure for the coronavirus, as discussed in 2.3.3. Consequently, temperature and relative humidity were logged at every scenario during the tracer-gas measurements. Temperature was logged with the *Hioki MemoryLogger* (3.2.3) and the *TinyTag loggers* (3.2.3). Relative humidity was measured by the *TinyTag loggers* 3.2.3.

The location of the TinyTag loggers is shown in Table 3.7.

Table 3.7: Location of TinyTag loggers during the experiments.

Logger	Location
1	EX ₁
2	EX ₂
3	M _{exp} breathing zone
4	Occupied zone
5	SU ₅

Thermocouples connected to the Hioki Memorylogger was placed in the exhaust, in the mouth of M_{inf} and in the breathing zone of M_{exp}. The location of the thermocouples connected to the Hioki MemoryLogger is shown in Table 3.8.

Table 3.8: Location of thermocouples during the experiments.

Channel	Location
1-7	EX ₂
1-8	SU ₃
1-9	SU ₁
1-1	M _{inf} exhalation zone

3.2.7 Smoke visualizations

Smoke visualizations were conducted to observe the airflow pattern and the exhaled jet from the infected manikin. This could reveal important information on how the aerosols migrate from the infected person to the exposed person.

A *Drager Air-Flow Tester Kit* was used to conduct a smoke visualization of the exhaled jet containing aerosol particles. A *Manual Easysmoker* was used to conduct a smoke

visualization of the ventilation airflow pattern. The smoke generator was connected to the main supply duct outside the laboratory. This produced smoke that was supplied by all five supply air diffusors. It was conducted for ventilation airflow rate 5.1 ACH. The smoke generators are described in D.1.

3.3 Theoretical modelling

This section is showing the theoretical modelling to calculate the personal exposure index/local air quality index and the probability to get infected by the coronavirus.

3.3.1 Personal exposure index/local air quality index

The personal exposure index was calculated based on the average tracer-gas concentrations at location EX (S_1) and in the inhalation zone of M_{exp} (S_2) from 3.2.5. The index was presented in 2.4.2. The personal exposure index/local air quality index was further used to calculate the probability of infection in 3.3.2.

$$\epsilon_e = \frac{S_{1,mean}}{S_{2,mean}}, \quad (3.1)$$

where $S_{1,mean}$ and $S_{2,mean}$ are the steady-state mean concentrations of tracer-gas in the exhaust and at the inhalation zone of the exposed manikin, respectively.

This index gives the actual ventilation efficiency experienced by the exposed person (Brohus, 1997).

3.3.2 Probability of infection from COVID-19 by a modified Wells-Riley equation

To calculate the probability of infection, a mass-balance equation can describe how the concentration of airborne coronavirus are distributed in the laboratory room. The model was proposed by Aganovic *et al.* (2021). The virus was simulated with N_2O tracer gas. The mass-balance equation Equation 3.2 is based on a single-zone model, as shown in Figure 3.23.

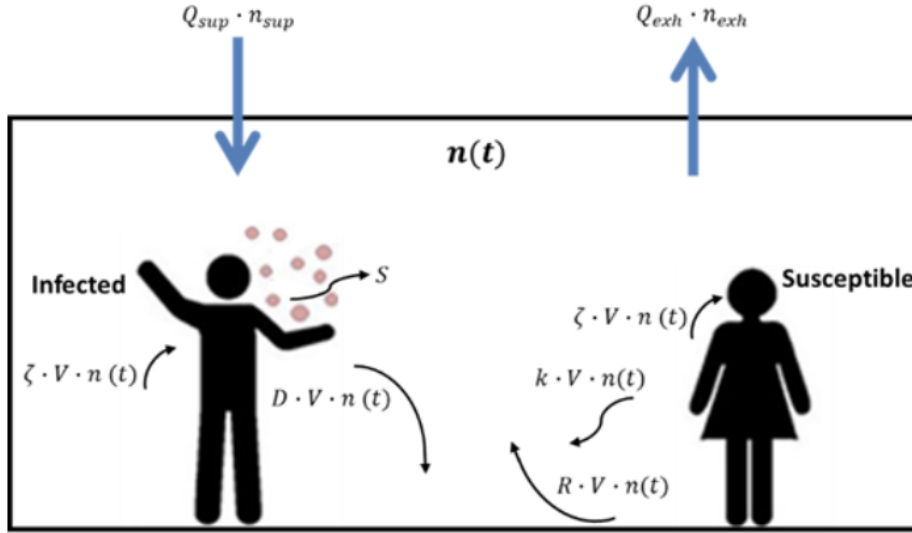


Figure 3.23: Mass-balance in a single-zone model.

$$V \cdot \frac{dn(t)}{dt} = S + Q_{sup} \cdot n_{sup}(t) - Q_{exh} \cdot n_{exh}(t) - k \cdot n(t) \cdot V - D \cdot V \cdot n(t) - R \cdot V \cdot n(t) - 2 \cdot \zeta \cdot V \cdot n(t) \quad (3.2)$$

where

- V , volume of the enclosed space [m^3]
- S , Quanta Emission Rate (QER) from infected person [$\frac{quanta}{h}$]
- Q_{sup} , supply airflow rate [$\frac{m^3}{h}$]
- Q_{exh} , exhaust airflow rate from the enclosed space [$\frac{m^3}{h}$]
- $n(t)$, quanta concentration in a measurement point at time t [$\frac{quanta}{m^3}$]
- $n_{sup}(t)$, quanta concentration in supply at time t [$\frac{quanta}{m^3}$]
- $n_{exh}(t)$, quanta concentration in exhaust at time t [$\frac{quanta}{m^3}$]
- k , virus inactivation rate [$\frac{1}{h}$]
- D , deposition rate [$\frac{1}{h}$]
- R , resuspension rate [$\frac{1}{h}$]
- ζ , respiratory tract absorption rate [$\frac{1}{h}$]

The following assumptions yielded for the model (Aganovic *et al.*, 2021):

- The room air is fully mixed
- No air recirculation by the ventilation system
- The only emission source of SARS-CoV-2 is from the infected individual within the room who emits quanta at a constant rate
- Three removal mechanisms: deposition by gravitational settling, virus inactivation by biological decay and ventilation without recirculation or exhaust to outdoor air
- The volumetric flow rates of outdoor and exhaust air is assumed to be equal and constant for the time interval of analysis
- Infectious respiratory airborne droplets quickly become evenly distributed in the room air
- No virus-laden airborne particles enter from the outside ($n_o u = 0$)
- There is no prior source of quanta in the space
- Filtration of the exhalation droplets was not performed using a face mask
- The viral content of a saliva droplet produced by an infected person is proportional to its initial volume
- The indoor RH does not change due to the vapor generated by human breathing and evaporation processes
- Resuspension rate R is neglected in the model ($R = 0$)
- The removal rate due to absorption in the respiratory tract by the infected person is neglected in this model
- There is no simulated sunlight indoors (ultraviolet B solar irradiance = 0 W/m^2)
- The infection risk calculation does not account for the potential effect of RH on human response in terms of susceptibility to infection

The model proposed by Aganovic *et al.* (2021) considered a fully-mixed scenario. To obtain an equation which is applicable for non-fully mixed conditions, the local air quality index is introduced by Equation 3.3. This is the same as the *personal exposure index* Brohus (1997) proposed to examine exposure.

$$\epsilon_e = \frac{n_{exh} - n_{sup}}{n(t) - n_{sup}}, \quad (3.3)$$

and becomes Equation 3.4 after the assumption that $n_{sup}(t) = 0$.

$$\epsilon_e = \frac{n_{exh}}{n(t)}, \quad (3.4)$$

where n_{exh} is the measured concentration [ppm] at the exhaust (sampling channel S₁) and $n(t)$ is the measured concentration [ppm] at the inhalation zone of M_{exp}, S₂.

The mass-balance model then becomes

$$V \cdot \frac{dn(t)}{dt} = S - \epsilon_e \cdot n(t) \cdot Q_{exh} - k \cdot n(t) \cdot V - D \cdot V \cdot n(t) - R \cdot V \cdot n(t) - 2 \cdot \zeta \cdot V \cdot n(t) \quad (3.5)$$

The solution of the differential equation is shown in Equation 3.6.

$$n(t) = n_0 \cdot e^{-\left(\frac{\epsilon_e \cdot Q}{V} + D + k + 2 \cdot \zeta\right) \cdot t} + \frac{S}{V} \left(\frac{1}{\frac{\epsilon_e \cdot Q}{V} + D + k + 2 \cdot \zeta} - \frac{1}{\frac{\epsilon_e \cdot Q}{V} + D + k + 2 \cdot \zeta} \cdot e^{-\left(\frac{\epsilon_e \cdot Q}{V} + D + k + 2 \cdot \zeta\right) t} \right) \quad (3.6)$$

The respiratory tract absorption rate (ζ) is usually negligible because the impact is very small, and was therefore assumed to be 0. This gave a simpler equation, as shown in Equation 3.7.

$$n(t) = n_0 \cdot e^{-\left(\frac{\epsilon_e \cdot Q}{V} + D + k\right) \cdot t} + \frac{S}{V} \left(\frac{1}{\frac{\epsilon_e \cdot Q}{V} + D + k} - \frac{1}{\frac{\epsilon_e \cdot Q}{V} + D + k} \cdot e^{-\left(\frac{\epsilon_e \cdot Q}{V} + D + k\right) t} \right), \quad (3.7)$$

where n_0 is the initial concentration of tracer gas in the room at $t=0$.

A collected term called *Infectious Virus Removal Rate* (IVRR) was proposed by Aganovic *et al.* (2021) and was defined as Equation 3.8.

$$IVRR = \frac{\epsilon_e \cdot Q}{V} + \frac{\sqrt{\frac{4 \cdot \rho_d \cdot g \cdot D_{eq}}{3 \cdot \rho_a \cdot C_{d,s}}}}{H_{person}} + k \quad (3.8)$$

The final simplified solution of the differential equation is shown in Equation 3.9.

$$n(t) = \sum_{i=1}^4 n_{o,i} \cdot e^{-IVRR_i \cdot t} + \frac{S}{V} \left(\frac{1}{IVRR_i} - \frac{1}{IVRR_i} \cdot e^{-IVRR_i \cdot t} \right) \quad (3.9)$$

Source term (S)

The source term S can be calculated from Equation 3.10.

$$S = I \cdot c_v \cdot c_i \cdot IR \cdot \sum_{i=1}^n (N_i \cdot V_i) \quad (3.10)$$

I is the number of infected persons, c_v is the viral load in sputum, c_i is a conversion factor which is the ratio of infectious quantum and infectious dose, IR is the inhalation rate, N_i is droplet number concentration and V_i is the mean volume of a droplet. Aganovic *et al.* (2021) proposed a viral load in sputum value, $c_v = 10^7 \frac{RNA}{mL}$, corresponding to mild-to-moderate cases of infection. This value was used in this thesis. The conversion factor c_i was set as $6.94 \cdot 10^{-4}$, the same as Aganovic *et al.* (2021). The inhalation rate was assumed to be $0.54 \frac{m^3}{h}$, and is the average inhalation rate for females (Aganovic *et al.*, 2021).

The source term is dominantly dependent on biological factors, that is not the main part of this thesis. If necessary, the whole derivation can be found in Aganovic *et al.* (2021).

Virus inactivation by biological decay (k)

The virus inactivation rate (k) is dependent on amongst others relative humidity (Aganovic *et al.*, 2021). In this thesis, k was assumed to be constant around $0.0101 \text{ m}^{-1} = 0.6 \text{ h}^{-1}$ with RH=53% (Aganovic *et al.*, 2021).

Deposition rate (D)

The deposition rate was shown in 2.3.2 with Equation 2.4. The deposition rate is dependent on several biological factors, and can be derived from amongst others Köhler theory. Additional and detailed material can be found in Aganovic *et al.* (2021). The deposition rate values for this calculation is shown in Appendix E.

A summary of the variables used into Equation 3.9 is shown in Table 3.9.

Table 3.9: Variables inserted into the differential equation solving for the tracer gas concentration $n(t)$ in a target point.

Variable	Value
Inhalation Rate, IR [$\frac{m^3}{h}$]	0.54
Virus inactivation rate, k [h^{-1}]	0.6
Resuspension rate, R [h^{-1}]	≈ 0
Respiratory tract absorption rate, ζ [h^{-1}]	≈ 0
Volume of the enclosed space, V [m^3]	84
Height of infected person, H_{pers} [m]	1.75
Viral load in sputum, c_v [$\frac{RNA}{mL}$]	10^7
Conversion factor, c_i [$\frac{quanta}{RNA}$]	$6.94 \cdot 10^{-4}$

Conclusionary, the infection risk can be calculated based on the Wells-Riley equation:

$$P = \left(1 - e^{-IR \int_0^T n(t) dt} \right) \quad (3.11)$$

where

- IR, inhalation rate for susceptible
- T, exposure time
- $n(t)$, concentration in target point

For clarification, the measured variable in the lab was the personal exposure index/local air quality index. Every other variable in Equation 3.9 and Equation 3.11 was calculated theoretically and based on Aganovic *et al.* (2021).

4 Results

4.1 Exposure: N₂O tracer gas concentration

This chapter shows the N₂O tracer gas concentration measured at the sampling channels for each scenario. Sampling channel 1 and 2 are the most important channels, as they are used to calculate the personal exposure index. The four remaining channels, S₃-S₆, will also be analyzed. Every figure presented in this section have dotted lines for where the stabilization period starts and stops.

4.1.1 Scenario 1: 2.7 ACH

This section presents the tracer-gas concentration from scenario 1. The theoretical fully mixed concentration is shown in every figure. The fully-mixed concentration for 2.7 ACH is $284.3 \frac{mg}{m^3} \approx 158$ ppm at steady state.

1A: 0.7 meter

Figure 4.1 shows the tracer-gas concentration at the six sampling channels and the calculated fully-mixed concentration. The stabilization period was from 3:03 to 4:06. The maximum and average concentrations inside the stable area at the channels as well as the standard deviations are shown in Table 4.1.

The average concentration inside the stable area at the exhaust, 174.5 ppm, was higher than the concentration at the inhalation zone of the exposed manikin, 159.8 ppm. The three channels located around the exposed manikin had average measured concentration close to the same value: 161.3, 160.3 and 164.4 ppm. However, the highest concentration was 5 cm outside the breathing zone of M_{exp} . The average supplied tracer-gas concentration to the laboratory room, 1.7 ppm, was only 0.97% of the extracted tracer-gas concentration, 174.5 ppm.

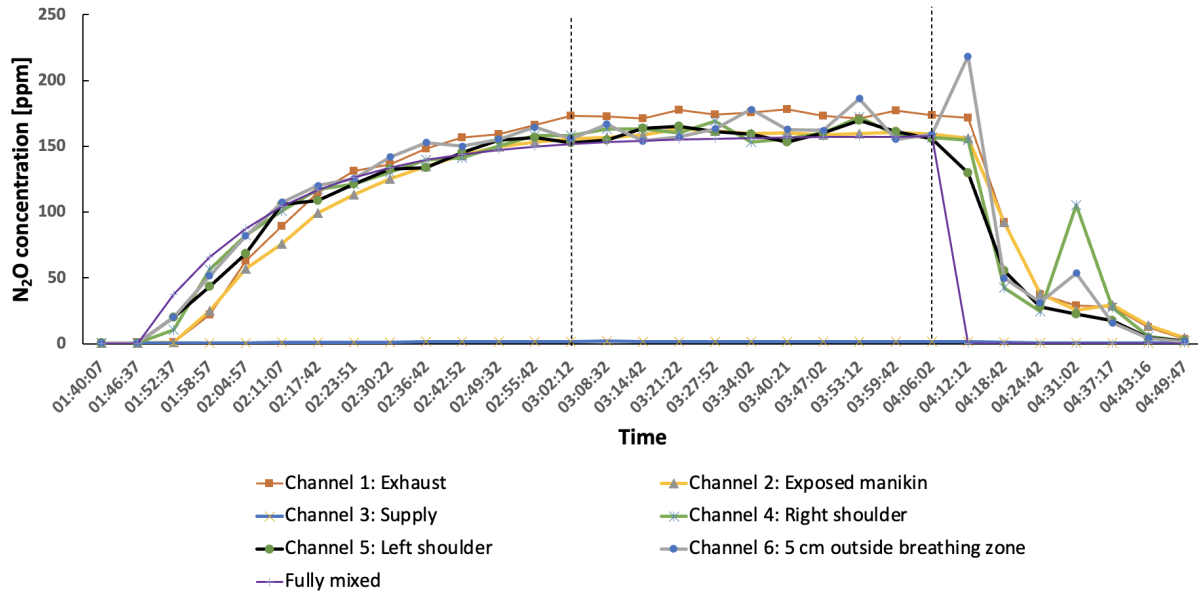


Figure 4.1: Measured tracer-gas concentration for scenario 1A at the sampling channels and the calculated fully-mixed concentration.

Table 4.1: Properties of tracer-gas measurements for scenario 1A inside the stable area.

Sampling tube	Maximum concentration [ppm]	Average concentration [ppm]	Standard deviation [ppm]
Exhaust, S ₁	178.1	174.5	2.6
M _{exp} , S ₂	163.4	159.8	1.8
Supply, S ₃	2.2	1.7	0.2
Right shoulder, S ₄	172.4	161.3	6.0
Left shoulder, S ₅	165.1	160.3	5.0
5 cm outside breathing zone, S ₆	186.2	164.4	10.3

1B: 1.0 meter

Figure 4.2 shows the tracer-gas concentration at the six sampling channels and the calculated fully-mixed concentration. The stabilization period was from 10:45 to 11:45. The maximum and average concentrations inside the stable area at every channel as well as the standard deviations are shown in Table 4.2.

The average concentration inside the stable area at the exhaust, 170.4 ppm, was higher than the concentration at the inhalation zone of the exposed manikin, 161.1 ppm. The three channels located around the exposed manikin had average measured concentration close to the same value: 161.3, 162.1 and 161.1 ppm. The average supplied tracer-gas

concentration to the laboratory room, 1.2 ppm, was only 0.70% of the extracted tracer-gas concentration.

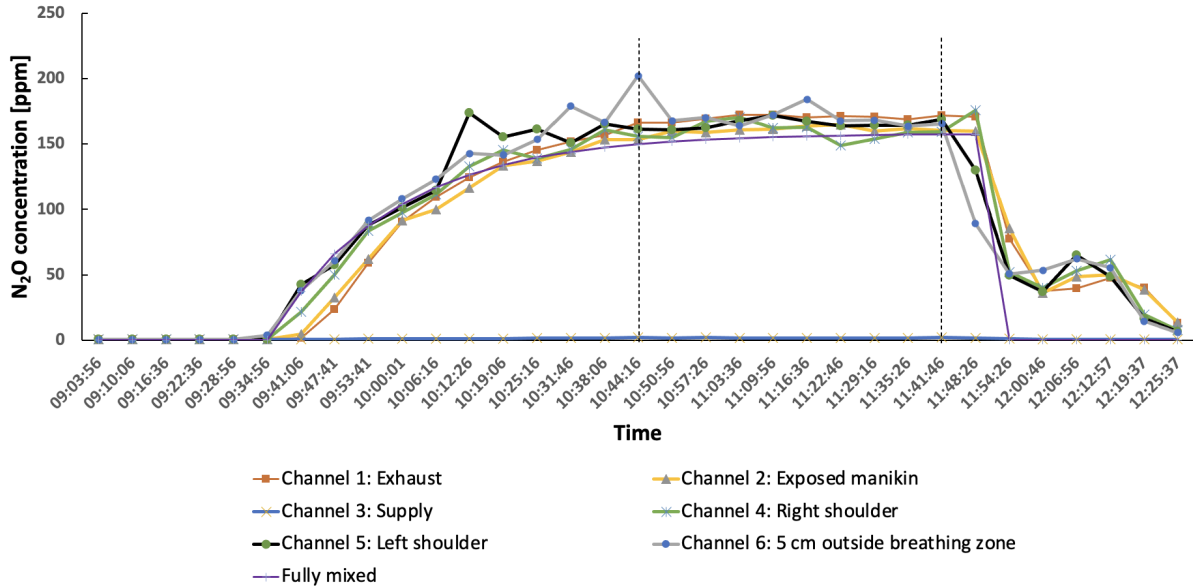


Figure 4.2: Measured tracer-gas concentration for scenario 1B at the sampling channels and the calculated fully-mixed concentration.

Table 4.2: Properties of tracer-gas measurements for scenario 1B inside the stable area.

Sampling tube	Maximum concentration [ppm]	Average concentration [ppm]	Standard deviation [ppm]
Exhaust, S ₁	172.4	170.4	1.9
M _{exp} , S ₂	163.8	161.1	2.0
Supply, S ₃	2.0	1.2	0.2
Right shoulder, S ₄	175.9	161.3	8.2
Left shoulder, S ₅	171.7	162.1	11.8
5 cm outside breathing zone, S ₆	184.0	161.1	26.0

1C: 1.5 meter

Figure 4.3 shows the tracer-gas concentration at the six sampling channels and the calculated fully-mixed concentration. The stabilization period was from 05:29 to 06:27. The maximum and average concentrations inside the stable area at every channel as well as the standard deviations are shown in Table 4.3.

The average concentration inside the stable area at the exhaust, 166.8 ppm, was higher than the concentration at the inhalation zone of the exposed manikin, 160.3 ppm. The

three channels located around the exposed manikin had average measured concentration close to the same value: 156.0, 160.5 and 163.6 ppm. The average supplied tracer-gas concentration to the laboratory room, 1.2 ppm, was only 0.72% of the extracted tracer-gas concentration.

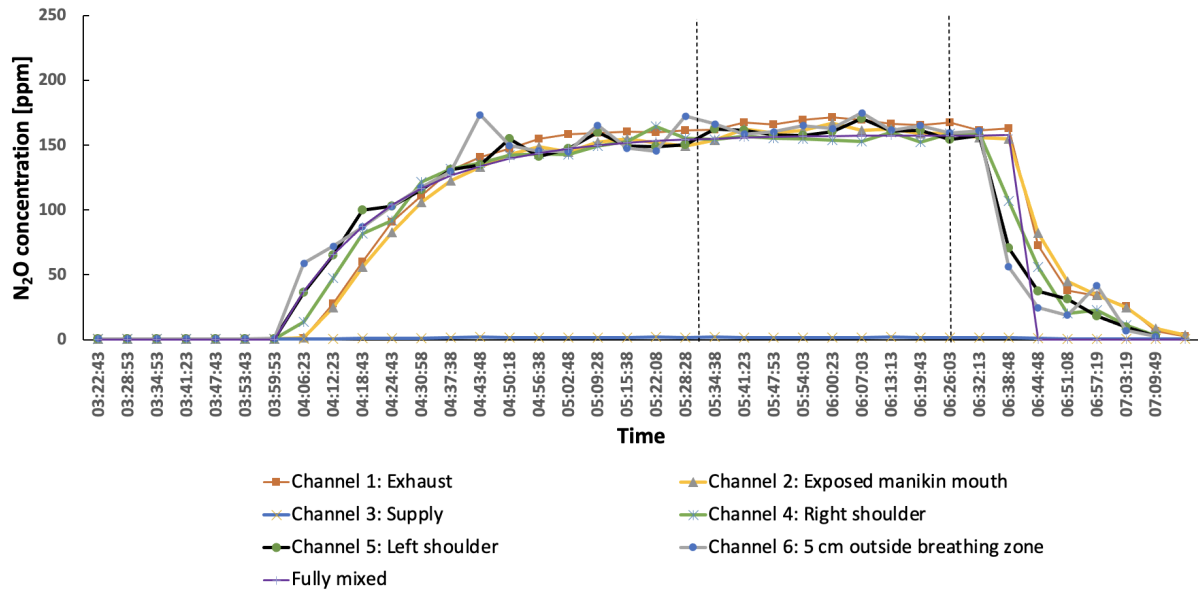


Figure 4.3: Measured tracer-gas concentration for scenario 1C at the sampling channels and the calculated fully-mixed concentration.

Table 4.3: Properties of tracer-gas measurements for scenario 1C inside the stable area.

Sampling tube	Maximum concentration [ppm]	Average concentration [ppm]	Standard deviation [ppm]
Exhaust, S ₁	171.8	166.8	3.3
M _{exp} , S ₂	167.1	160.3	3.7
Supply, S ₃	2.0	1.2	0.1
Right shoulder, S ₄	160.1	156.0	2.7
Left shoulder, S ₅	170.7	160.5	4.4
5 cm outside breathing zone, S ₆	175.1	163.6	4.8

1D: 2.0 meter

Figure 4.4 shows the tracer-gas concentration at the six sampling channels and the calculated fully-mixed concentration. The stabilization period was from 1:10 to 2:08. The maximum and average concentrations inside the stable area at every channel as well as the standard deviations are shown in Table 4.4.

The average concentration inside the stable area at the exhaust, 172.3 ppm, was higher than the concentration at the inhalation zone of the exposed manikin, 161.5 ppm. The three channels located around the exposed manikin had average measured concentration of 177.1, 152.3 and 151.2 ppm. The average supplied tracer-gas concentration to the laboratory room, 1.2 ppm, was only 0.69% of the extracted tracer-gas concentration.

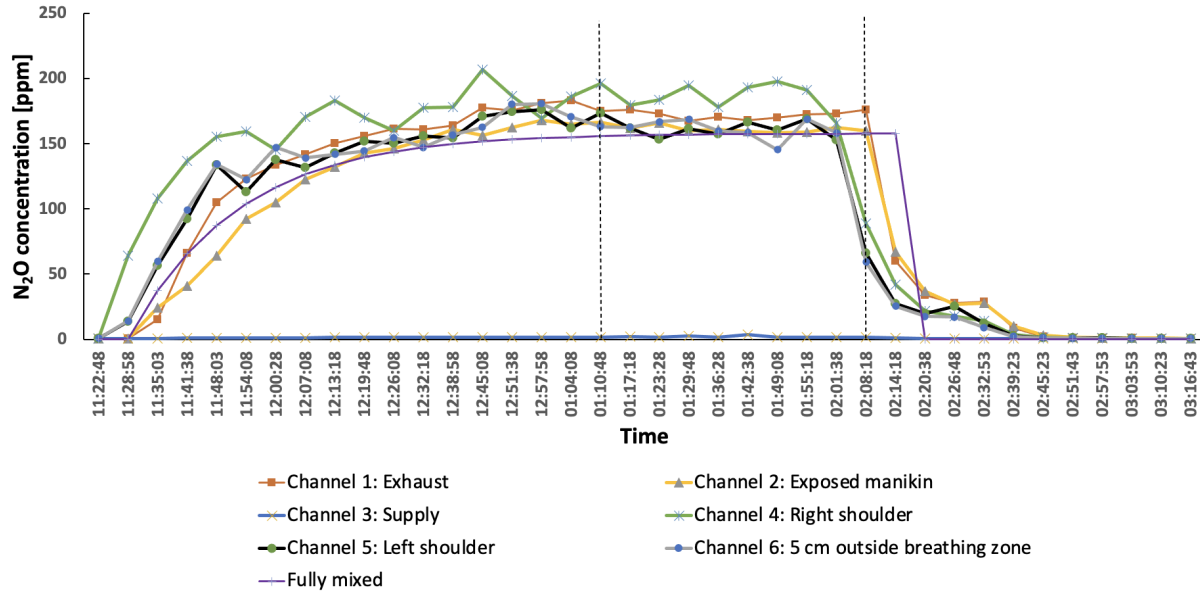


Figure 4.4: Measured tracer-gas concentration for scenario 1D at the sampling channels and the calculated fully-mixed concentration.

Table 4.4: Properties of tracer-gas measurements for scenario 1D inside the stable area.

Sampling tube	Maximum concentration [ppm]	Average concentration [ppm]	Standard deviation [ppm]
Exhaust, S ₁	176.1	172.3	3.1
M _{exp} , S ₂	166.4	161.5	2.8
Supply, S ₃	3.3	1.2	0.6
Right shoulder, S ₄	197.8	177.1	32.5
Left shoulder, S ₅	173.4	152.3	31.0
5 cm outside breathing zone, S ₆	168.9	151.2	33.0

4.1.2 Scenario 2: 5.1 ACH

This section presents the tracer-gas concentration measurements from scenario 2. The fully mixed concentration development is shown in every figure, and the fully-mixed concentration for 5.1 ACH was $149.4 \frac{mg}{m^3} \approx 83$ ppm at steady state.

2A: 0.7 meter

Figure 4.5 shows the tracer-gas concentration at the six sampling channels and the calculated fully-mixed concentration. The stabilization period was from 02:53 to 03:50. The maximum and average concentrations inside the stable area at every channel as well as the standard deviations are shown in Table 4.5.

The average concentration inside the stable area at the exhaust, 99.4 ppm, was higher than the concentration at the inhalation zone of the exposed manikin, 87.9 ppm. The three channels located around the exposed manikin had average measured concentration of 99.9, 81.6 and 88.7 ppm. The average supplied tracer-gas concentration to the laboratory room, 2.4 ppm, was only 2.4% of the extracted tracer-gas concentration.

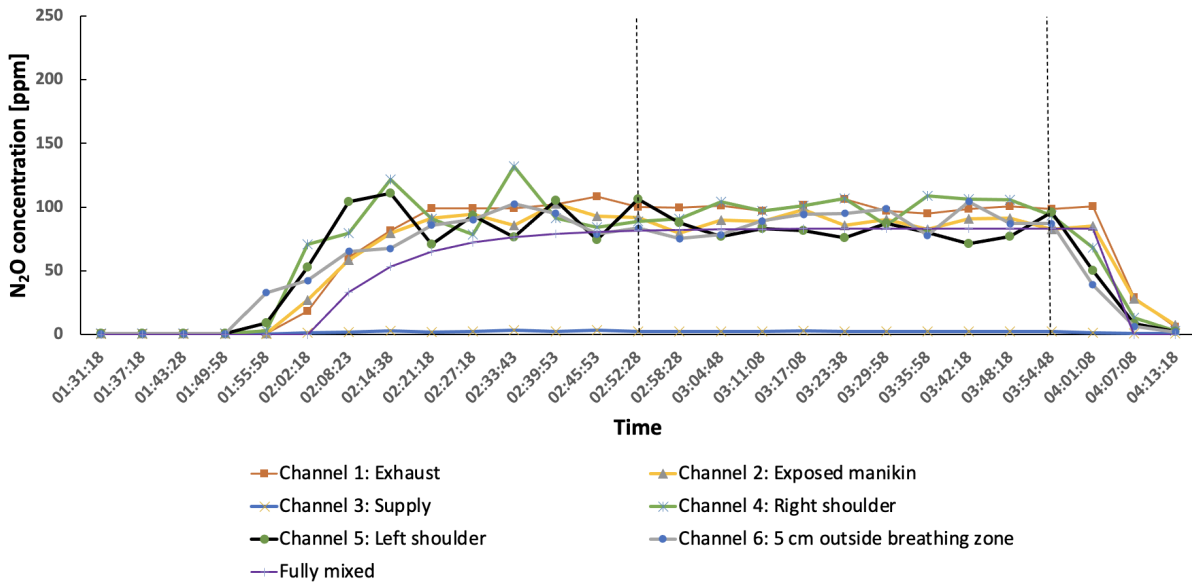


Figure 4.5: Measured tracer-gas concentration for scenario 2A at the sampling channels and the calculated fully-mixed concentration.

Table 4.5: Properties of tracer-gas measurements for scenario 2A inside the stable area.

Sampling tube	Maximum concentration [ppm]	Average concentration [ppm]	Standard deviation [ppm]
Exhaust, S ₁	106.4	99.4	3.2
M _{exp} , S ₂	98.0	87.9	5.4
Supply, S ₃	2.5	2.4	0.2
Right shoulder, S ₄	108.9	99.9	7.9
Left shoulder, S ₅	95.8	81.6	7.1
5 cm outside breathing zone, S ₆	104.2	88.7	9.6

2B: 1.0 meter

Figure 4.6 shows the tracer-gas concentration at the six sampling channels and the calculated fully-mixed concentration. The stabilization period was from 11:15 to 12:17. The maximum and average concentrations inside the stable area at every channel as well as the standard deviations are shown in Table 4.6.

The average concentration inside the stable area at the exhaust, 88.6 ppm, was lower than the concentration at the inhalation zone of the exposed manikin, 102.4 ppm. The three channels located around the exposed manikin had average concentration of 113.9, 104.8 and 119.7 ppm. The average supplied tracer-gas concentration to the laboratory room, 2.2 ppm, was only 2.4% of the extracted tracer-gas concentration.

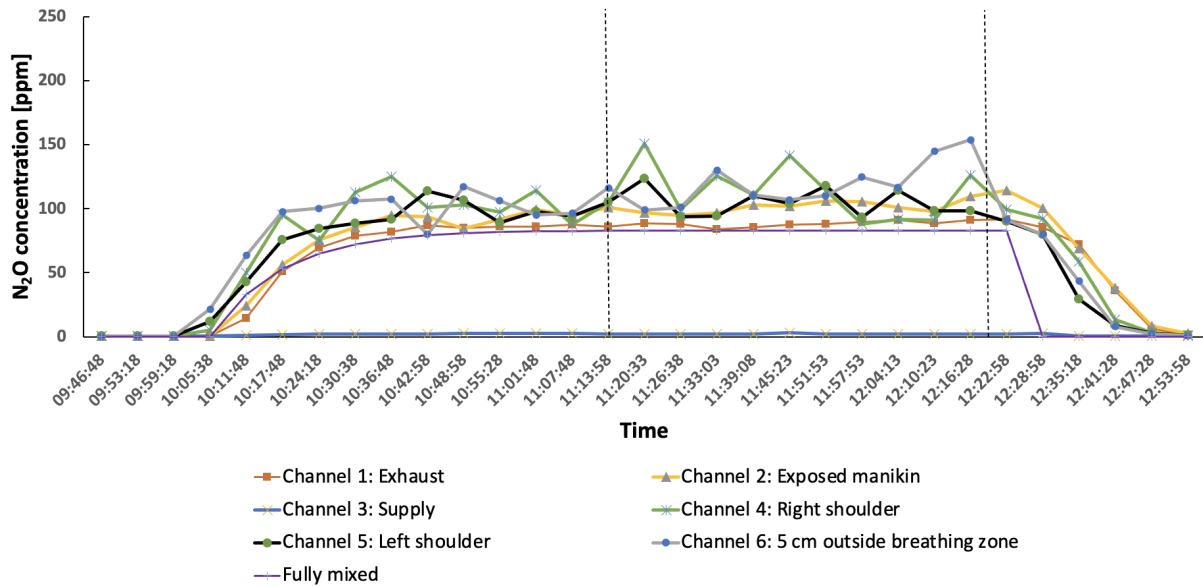


Figure 4.6: Measured tracer-gas concentration for scenario 2B at the sampling channels and the calculated fully-mixed concentration.

Table 4.6: Properties of tracer-gas measurements for scenario 2B inside the stable area.

Sampling tube	Maximum concentration [ppm]	Average concentration [ppm]	Standard deviation [ppm]
Exhaust, S ₁	91.3	88.6	2.4
M _{exp} , S ₂	109.6	102.4	6.0
Supply, S ₃	3.1	2.2	0.3
Right shoulder, S ₄	150.9	113.9	21.2
Left shoulder, S ₅	123.7	104.8	11.4
5 cm outside breathing zone, S ₆	153.7	119.7	19.4

2C: 1.5 meter

Figure 4.7 shows the tracer-gas concentration at the six sampling channels and the calculated fully-mixed concentration. The stabilization period was from 06:23 to 07:23. The maximum and average concentrations inside the stable area at every channel as well as the standard deviations are shown in Table 4.7.

The average concentration inside the stable area at the exhaust, 102.3 ppm, was lower than the concentration at the inhalation zone of the exposed manikin, 108.2 ppm. The three channels located around the exposed manikin had average concentration of 126.1, 93.1 and 133.2 ppm. The average supplied tracer-gas concentration to the laboratory room, 2.3 ppm, was only 2.2% of the extracted tracer-gas concentration.

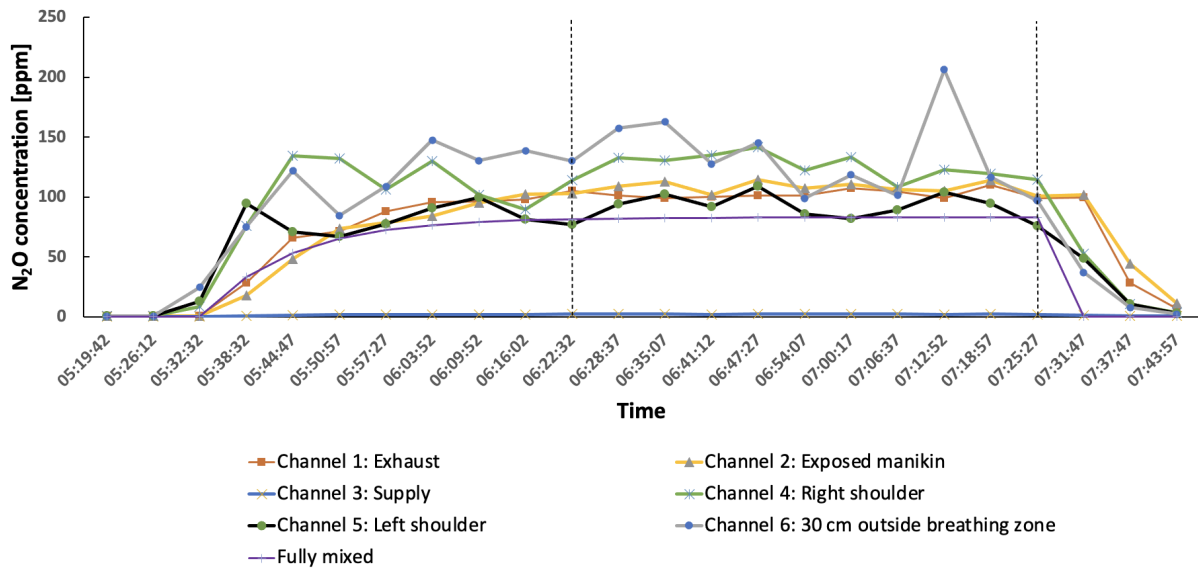


Figure 4.7: Measured tracer-gas concentration for scenario 2C at the sampling channels and the calculated fully-mixed concentration.

Table 4.7: Properties of tracer-gas measurements for scenario 2C inside the stable area.

Sampling tube	Maximum concentration [ppm]	Average concentration [ppm]	Standard deviation [ppm]
Exhaust, S ₁	110.0	102.3	3.8
M _{exp} , S ₂	114.6	108.2	4.9
Supply, S ₃	2.3	2.3	0.1
Right shoulder, S ₄	141.5	126.1	10.2
Left shoulder, S ₅	109.3	93.1	10.4
5 cm outside breathing zone, S ₆	206.3	133.2	34.9

2D: 2.0 meter

Figure 4.8 shows the tracer-gas concentration at the six sampling channels and the calculated fully-mixed concentration. The stabilization period was from 11:20 to 12:20. The maximum and average concentrations inside the stable area at every channel as well as the standard deviations are shown in Table 4.8.

The average concentration inside the stable area at the exhaust, 95.1 ppm, was lower than the concentration at the inhalation zone of the exposed manikin, 118.3 ppm. The three channels located around the exposed manikin had average concentration of 133.6, 129.3 and 140.3 ppm. The average supplied tracer-gas concentration to the laboratory room, 2.3 ppm, was only 2.4% of the extracted tracer-gas concentration.

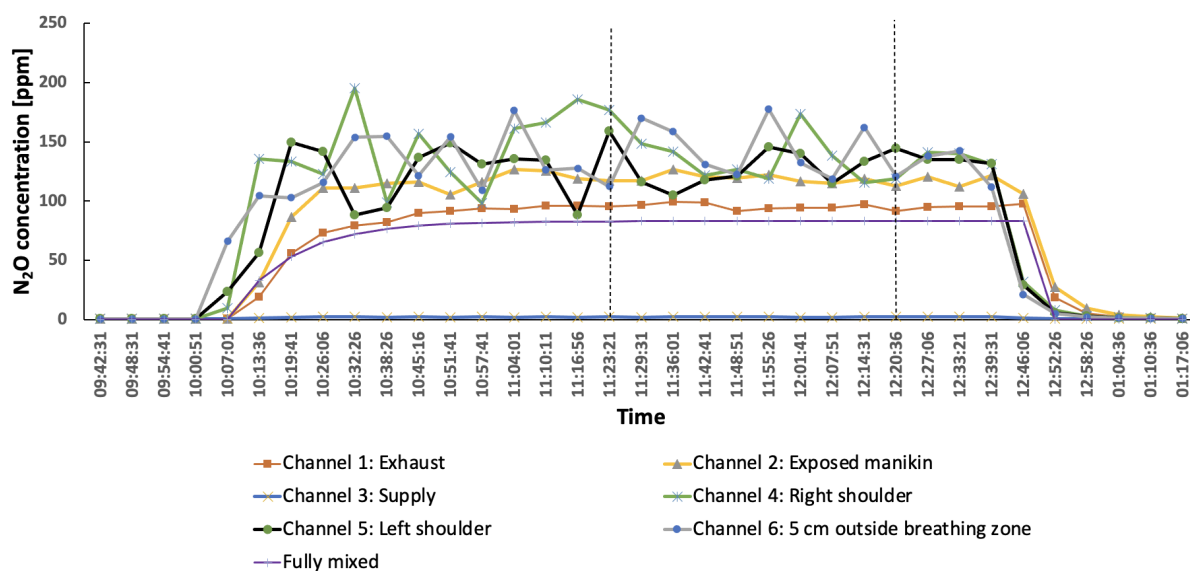


Figure 4.8: Measured tracer-gas concentration for scenario 2D at the sampling channels and the calculated fully-mixed concentration.

Table 4.8: Properties of tracer-gas measurements for scenario 2D inside the stable area.

Sampling tube	Maximum concentration [ppm]	Average concentration [ppm]	Standard deviation [ppm]
Exhaust, S ₁	99.1	95.1	2.6
M _{exp} , S ₂	126.4	118.3	4.5
Supply, S ₃	2.6	2.3	0.2
Right shoulder, S ₄	141.5	133.6	17.5
Left shoulder, S ₅	145.4	129.3	13.6
5 cm outside breathing zone, S ₆	162.1	140.3	19.8

4.1.3 Scenario 3: 9.6 ACH

This section presents the tracer-gas concentration measurements from scenario 3. The fully mixed concentration development is shown in every figure, and the fully-mixed concentration for 9.6 ACH was $79.3 \frac{mg}{m^3} \approx 44.1$ ppm at steady state.

3A: 0.7 meter

Figure 4.9 shows the tracer-gas concentration at the six sampling channels and the calculated fully-mixed concentration. The stabilization period was from 03:04 to 04:04. The maximum and average concentrations inside the stable area at every channel as well as the standard deviations are shown in Table 4.9.

The average concentration inside the stable area at the exhaust, 47.4 ppm, was lower than the concentration at the inhalation zone of the exposed manikin, 51.4. The three channels located around the exposed manikin had average concentration of 46.5, 55.0 and 61.8 ppm. The average supplied tracer-gas concentration to the laboratory room, 1.5 ppm, was only 3.2% of the extracted tracer-gas concentration.

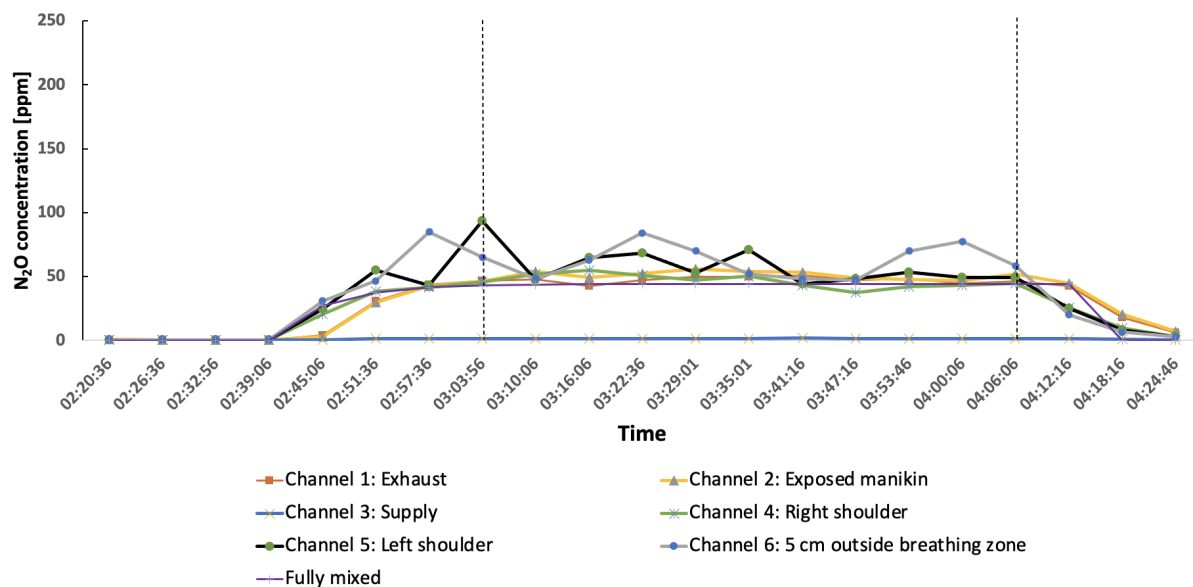


Figure 4.9: Measured tracer-gas concentration for scenario 3A at the sampling channels and the calculated fully-mixed concentration.

Table 4.9: Properties of tracer-gas measurements for scenario 3A inside the stable area.

Sampling tube	Maximum concentration [ppm]	Average concentration [ppm]	Standard deviation [ppm]
Exhaust, S ₁	50.8	47.4	2.5
M _{exp} , S ₂	53.8	51.4	3.1
Supply, S ₃	1.9	1.5	0.2
Right shoulder, S ₄	54.5	46.5	5.4
Left shoulder, S ₅	71.0	55.0	9.5
5 cm outside breathing zone, S ₆	84.0	61.8	13.2

3B: 1.0 meter

Figure 4.10 shows the tracer-gas concentration at the six sampling channels and the calculated fully-mixed concentration. The stabilization period was from 11:39 to 12:41. The maximum and average concentrations inside the stable area at every channel as well as the standard deviations are shown in Table 4.10.

The average concentration inside the stable area at the exhaust, 46.7 ppm, was lower than the concentration at the inhalation zone of the exposed manikin, 48.5. The three channels located around the exposed manikin had average concentration of 55.9, 57.5 and 55.1 ppm. The average supplied tracer-gas concentration to the laboratory room, 1.4 ppm, was only 2.9% of the extracted tracer-gas concentration.

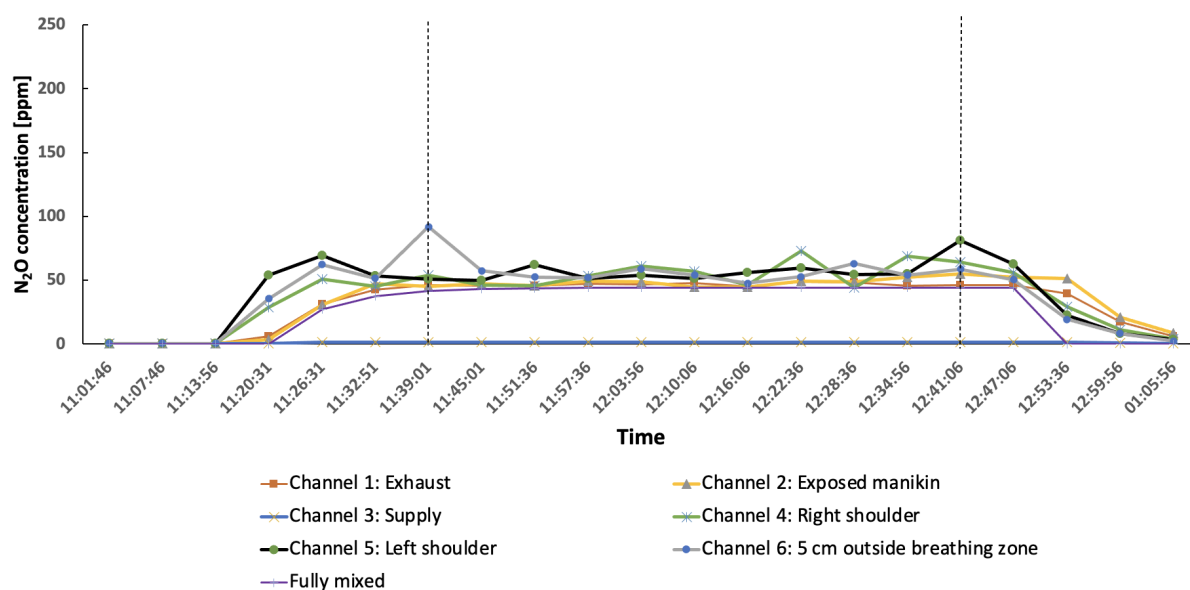
**Figure 4.10:** Measured tracer-gas concentration for scenario 3B at the sampling channels and the calculated fully-mixed concentration.

Table 4.10: Properties of tracer-gas measurements for scenario 3B inside the stable area.

Sampling tube	Maximum concentration [ppm]	Average concentration [ppm]	Standard deviation [ppm]
Exhaust, S ₁	47.7	46.7	1.2
M _{exp} , S ₂	54.7	48.5	3.3
Supply, S ₃	1.7	1.4	0.1
Right shoulder, S ₄	72.7	55.9	10.4
Left shoulder, S ₅	81.1	57.5	9.1
5 cm outside breathing zone, S ₆	62.9	55.1	4.4

3C: 1.5 meter

Figure 4.11 shows the tracer-gas concentration at the six sampling channels and the calculated fully-mixed concentration. The stabilization period was from 03:40 to 04:43. The maximum and average concentrations inside the stable area at every channel as well as the standard deviations are shown in Table 4.11.

The average concentration inside the stable area at the exhaust, 48.9 ppm, was lower than the concentration at the inhalation zone of the exposed manikin, 58.9 ppm. The three channels located around the exposed manikin had average concentration of 65.8, 84.9 and 81.6 ppm. The average supplied tracer-gas concentration to the laboratory room, 1.6 ppm, was only 3.3% of the extracted tracer-gas concentration.

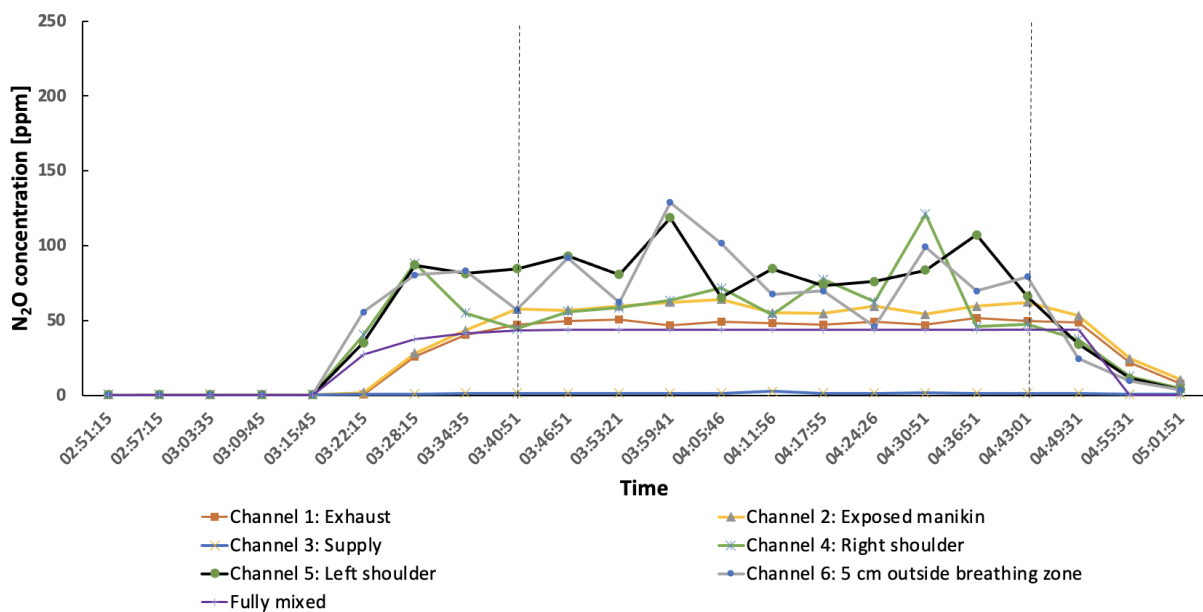
**Figure 4.11:** Measured tracer-gas concentration for scenario 3C at the sampling channels and the calculated fully-mixed concentration.

Table 4.11: Properties of tracer-gas measurements for scenario 3C inside the stable area.

Sampling tube	Maximum concentration [ppm]	Average concentration [ppm]	Standard deviation [ppm]
Exhaust, S ₁	51.5	48.9	1.5
M _{exp} , S ₂	64.2	58.9	3.5
Supply, S ₃	2.7	1.6	0.4
Right shoulder, S ₄	121.1	65.8	21.8
Left shoulder, S ₅	118.6	84.9	17.2
5 cm outside breathing zone, S ₆	128.8	81.6	24.0

3D: 2.0 meter

Figure 4.12 shows the tracer-gas concentration at the six sampling channels and the calculated fully-mixed concentration. The stabilization period was from 12:09 to 01:11. The maximum and average concentrations inside the stable area at every channel as well as the standard deviations are shown in Table 4.12.

The average concentration inside the stable area at the exhaust, 48.4 ppm, was lower than the concentration at the inhalation zone of the exposed manikin, 67.3 ppm. The three channels located around the exposed manikin had average concentration of 67.6, 75.9 and 73.5 ppm. The average supplied tracer-gas concentration to the laboratory room, 1.7 ppm, was only 3.5% of the extracted tracer-gas concentration.

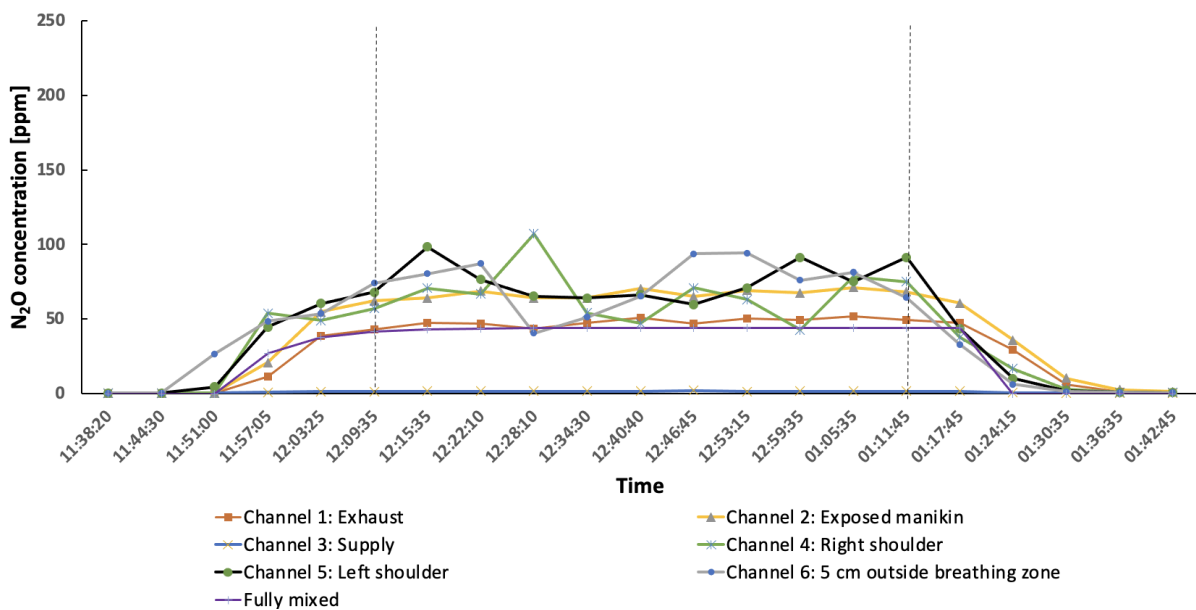
**Figure 4.12:** Measured tracer-gas concentration for scenario 3D at the sampling channels and the calculated fully-mixed concentration.

Table 4.12: Properties of tracer-gas measurements for scenario 3D inside the stable area.

Sampling tube	Maximum concentration [ppm]	Average concentration [ppm]	Standard deviation [ppm]
Exhaust, S ₁	51.7	48.4	2.4
M _{exp} , S ₂	71.1	67.3	2.7
Supply, S ₃	2.1	1.7	0.2
Right shoulder, S ₄	107.1	67.6	18.3
Left shoulder, S ₅	98.3	75.9	13.4
5 cm outside breathing zone, S ₆	94.3	73.5	17.9

4.1.4 Summary of tracer-gas concentration for all scenarios

The measured tracer-gas concentration at the exhaust and at the exposed manikin for all scenarios is shown in Table 4.13. The highest concentration in the inhalation zone of the exposed manikin at each scenario is marked in bold. The highest concentration at the exposed manikin overall scenarios is marked in red, and the lowest marked in blue.

Table 4.13 shows that the highest concentration at the inhalation zone of the exposed manikin, M_{exp}, was at D = 2.0 meters separation distance for every airflow rate. The highest measured concentration overall was measured at D = 2.0 meters at 2.7 ACH as marked in red. The lowest concentrations was measured at 9.6 ACH. The highest concentrations were measured at 2.7 ACH, and gradually reduced further at 5.1 ACH and 9.6 ACH.

The results from scenario 1 shows that the concentration is overall high for all separation distances. The lowest concentration was measured at A = 0.7 meters separation distance, while it was highest at D = 2.0 meters as marked in bold.

The results from scenario 2 shows that the lowest concentration was measured at A = 0.7 meters, while the highest was measured at D = 2.0 meters. The concentration was decreasing from 2.0 to 0.7 meters.

The results from scenario 3 shows that the lowest concentration was measured at B = 1.0 meters separation distance as marked in blue, while the highest concentration was measured at D = 2.0 meters.

Table 4.13: Summary of the tracer-gas concentration for all scenarios at the exhaust and at the exposed manikin. A, B, C and D is separation distance 0.7, 1.0, 1.5 and 2.0 meters respectively.

Scenario	Sampling channel concentration [ppm]	
	Exhaust, S_1	M_{exp} , S_2
1: 2.7 ACH		
1A	174.5	159.8
1B	170.4	161.1
1C	166.8	160.3
1D	172.3	161.5
2: 5.1 ACH		
2A	99.4	87.9
2B	88.6	102.4
2C	102.3	108.2
2D	95.1	118.3
3: 9.6 ACH		
3A	47.4	51.4
3B	46.7	48.5
3C	48.9	58.9
3D	48.4	67.3

4.2 Relative humidity and temperature

The measured relative humidity and temperature for scenario 1, 2 and 3 are shown in this section.

4.2.1 Scenario 1: 2.7 ACH

Figure 4.13 shows the measured temperature and Figure 4.14 shows the measured relative humidity for scenario 1: 2.7 ACH.

Figure 4.13 shows that the temperature in the occupied zone was kept between 22 and 23°C, as desired. The lowest temperature was in the supply air, which was $\approx 21^\circ\text{C}$. The temperature in the two exhausts was very close to the temperature in the occupied zone. The highest temperature occurred inside the thermal plume close to M_{exp} and was between 23°C and 24°C.

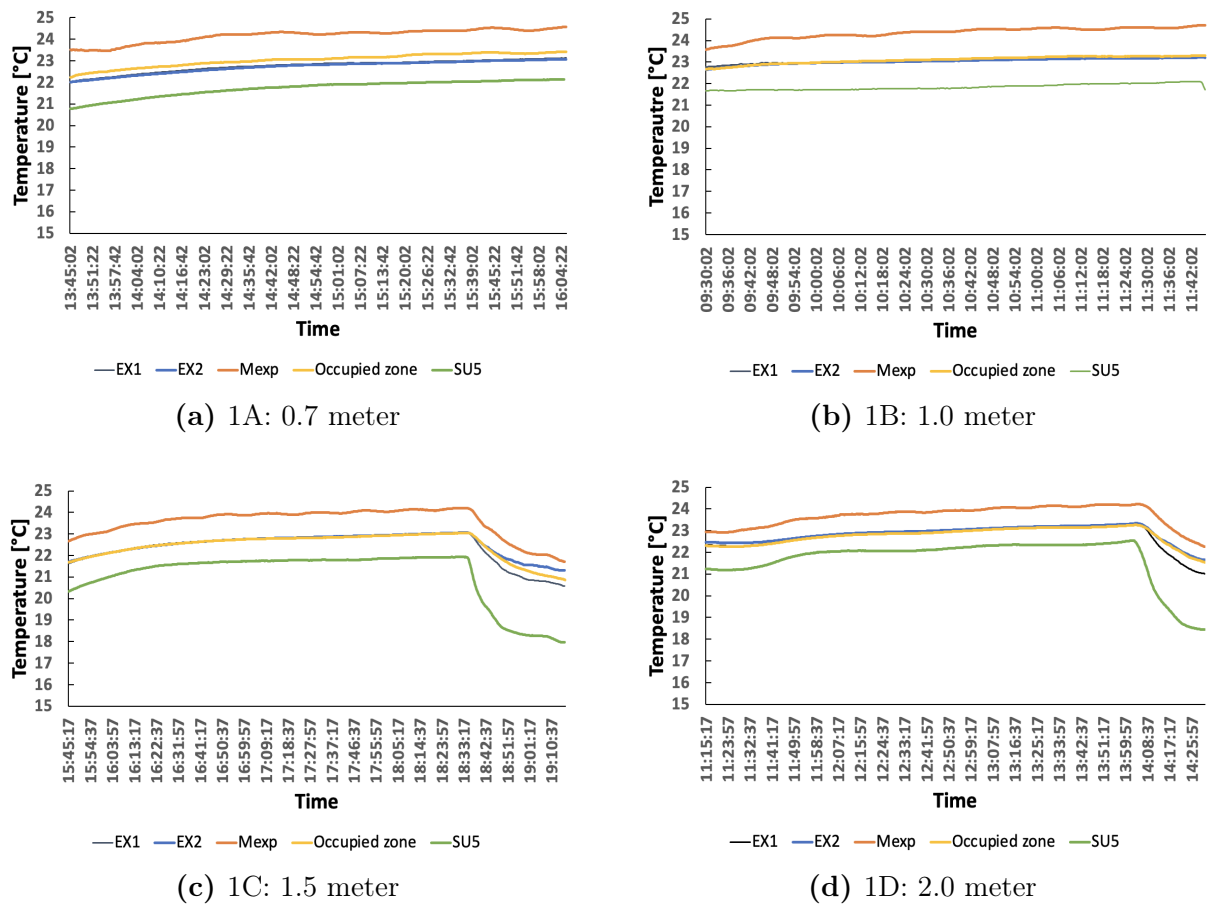


Figure 4.13: Measured temperature for scenario 1 (2.7 ACH) at four separation distances.

Figure 4.14 shows that the relative humidity for all separation distances in scenario 1 was $\approx 15\%$. This yields for all measurement locations. This is below the recommendation of 20% given by FHI.

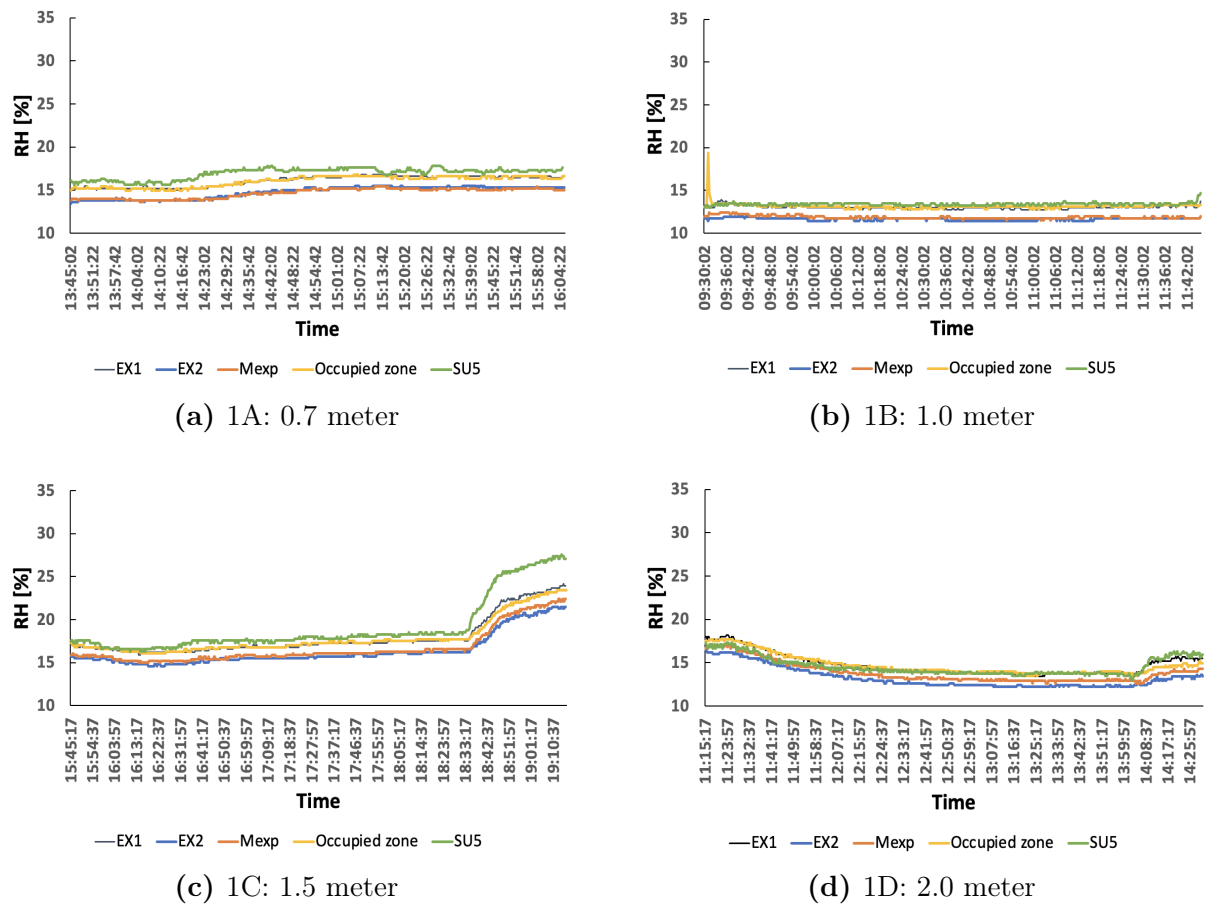


Figure 4.14: Measured relative humidity for scenario 1 (2.7 ACH) at four separation distances.

4.2.2 Scenario 2: 5.1 ACH

Figure 4.15 shows the measured temperature and Figure 4.16 shows the measured relative humidity for scenario 2: 5.1 ACH.

Figure 4.15 shows that the temperature in the occupied zone was kept between 22 and 23°C, as desired. The lowest temperature was in the supply air, which was $\approx 20^\circ\text{C}$. The temperature in the two exhausts was very close to the temperature in the occupied zone. The highest temperature occurred inside the thermal plume close to M_{exp} and was between 23°C and 24°C .

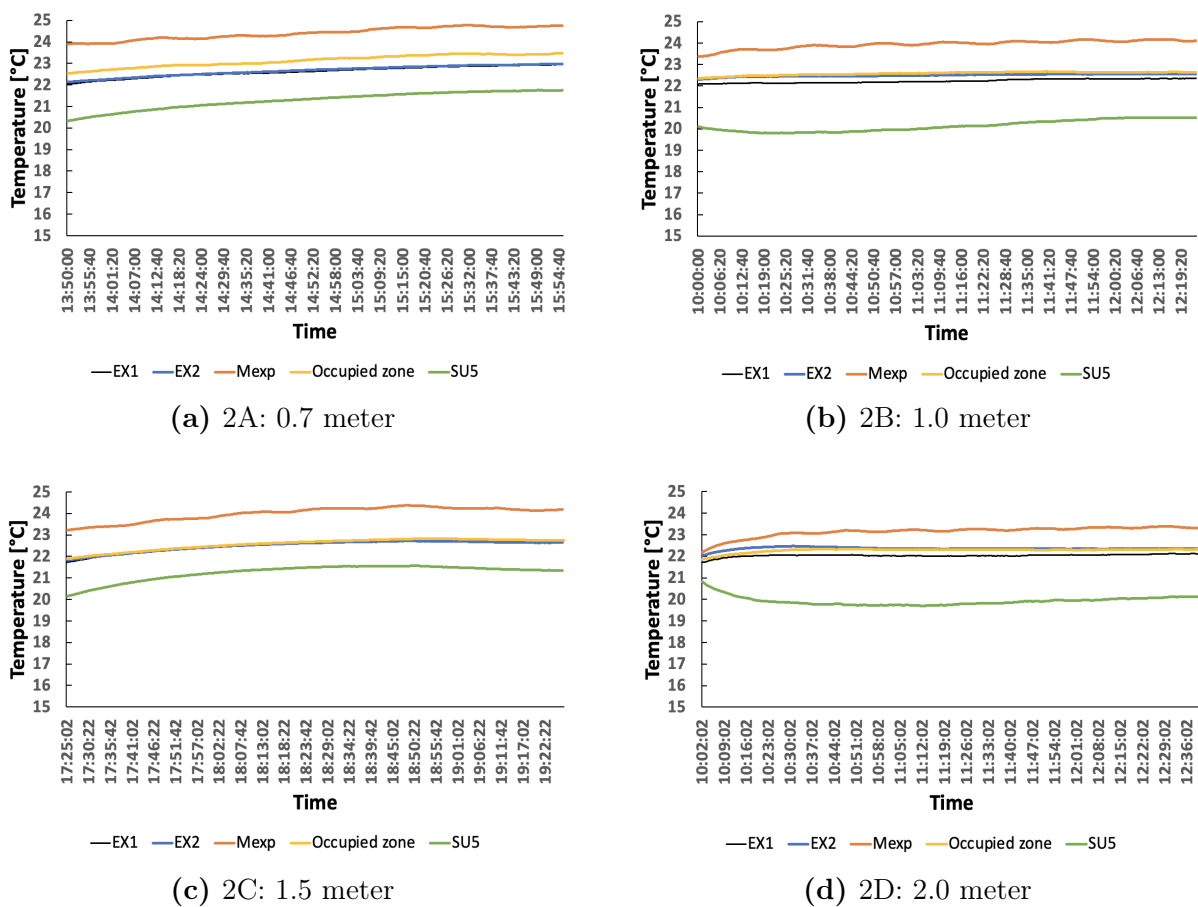


Figure 4.15: Measured temperature for scenario 2 (5.1 ACH) at four separation distances.

Figure 4.16 shows that the relative humidity for scenario 2 was between 20% and 33%. This is inside the recommendation made by FHI to have relative humidity higher than 20%. The highest RH was measured in the supply air, while the lowest was around the exposed manikin M_{exp} .

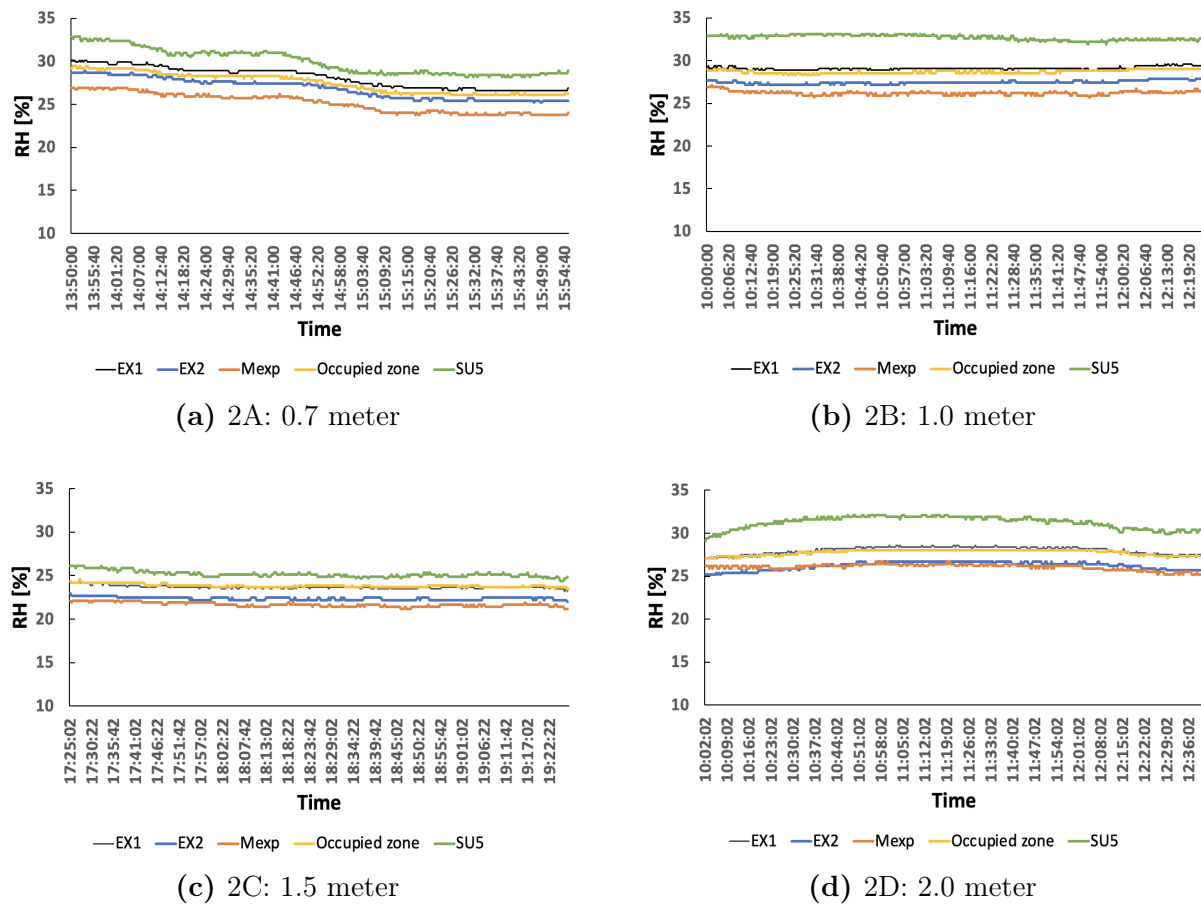
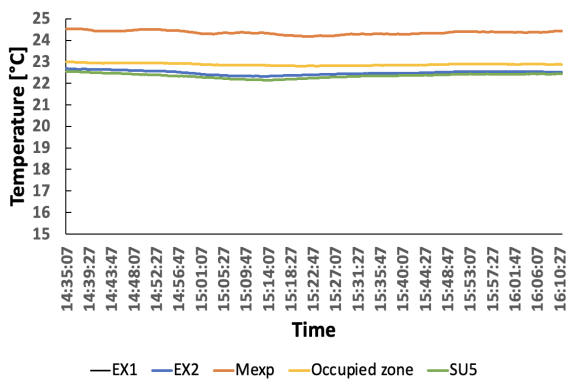


Figure 4.16: Measured relative humidity for scenario 2 (5.1 ACH) at four separation distances.

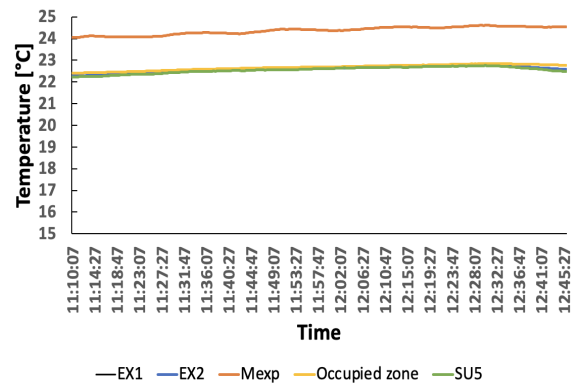
4.2.3 Scenario 3: 9.6 ACH

Figure 4.17 shows the measured temperature and Figure 4.18 shows the measured relative humidity for scenario 3: 9.6 ACH.

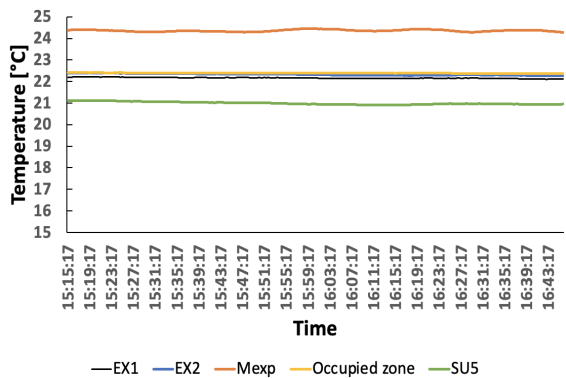
Figure 4.17 shows that the temperature in the occupied zone was kept between 22 and 23°C, as desired. The lowest temperature was in the supply air, which was ≈ 21 -22°C. The temperature in the two exhausts was very close to the temperature in the occupied zone. The highest temperature occurred inside the thermal plume close to M_{exp} and was between 24°C and 25°C.



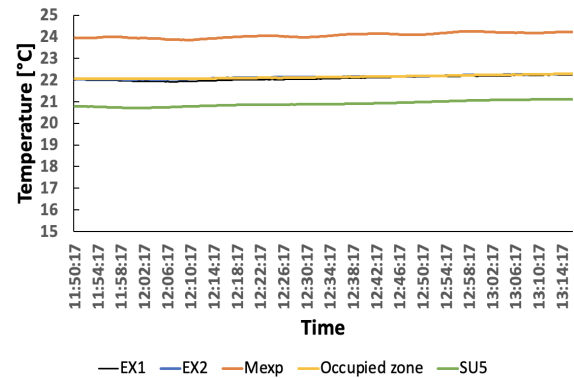
(a) 3A: 0.7 meter



(b) 3B: 1.0 meter



(c) 3C: 1.5 meter



(d) 3D: 2.0 meter

Figure 4.17: Measured temperature for scenario 3 (9.6 ACH) at four separation distances.

Figure 4.18 shows that the relative humidity for scenario 2 was in the range of 15%-35%. Relative humidity should be above 20% to reduce the risk of infection according to FHI, and some time intervals had RH lower than this. The highest measured RH was measured in the supply air, while the lowest was measured around the exposed manikin M_{exp} .

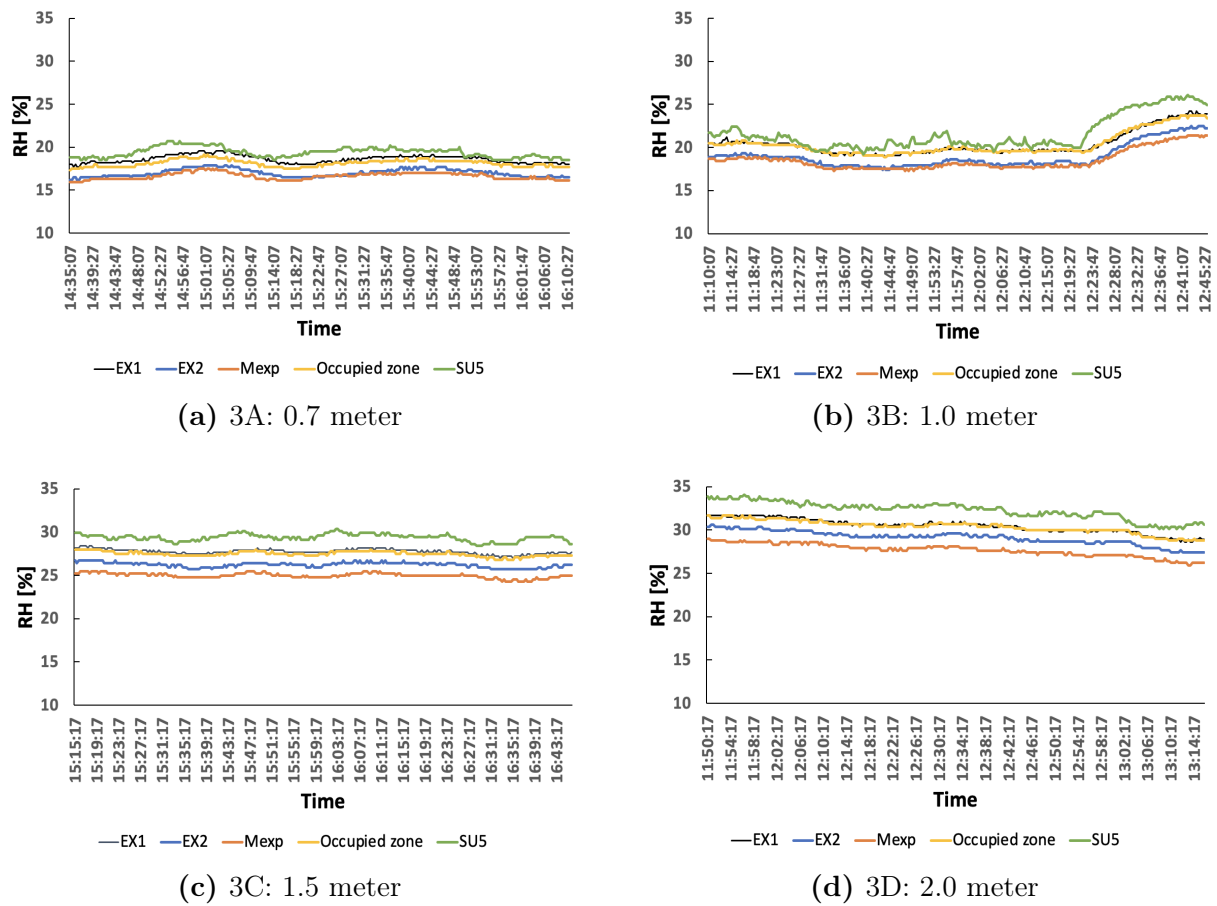


Figure 4.18: Measured relative humidity for scenario 3 (9.6 ACH) at four separation distances.

4.3 Smoke visualizations

The smoke visualization of the exhaled jet from M_{inf} is shown in Figure 4.19. The initial exhaled jet travelled straight forward, as shown in Figure 4.19a. Figure 4.19b depicts the jet elevating upwards towards the ceiling after a short period of time.

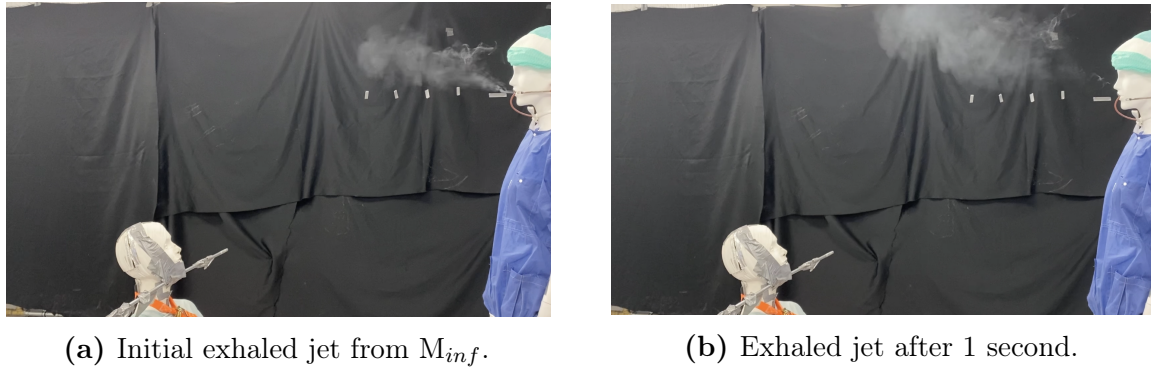


Figure 4.19: Smoke visualization of the exhaled jet of infected manikin and the exposure of the exposed manikin.

The smoke visualization of the airflow pattern in the laboratory is shown in Figure 4.20. The orange arrows indicates that the supply air from diffuser SU_1 partially short-circuited to exhaust EX_1 and partially pushed the air against the location of the exposed manikin at two meters separation distance.



Figure 4.20: Smoke visualization of the ventilation airflow pattern in the HVAC-laboratory.

4.4 Personal exposure index/local air quality index

The calculated personal exposure index/local air quality index for scenario 1, 2 and 3 is shown in Figure 4.21.

Figure 4.21 shows that the overall highest personal exposure index/local air quality index was for 2.7 ACH and 0.7 meters separation distance. The lowest overall index was obtained at 9.6 ACH and 2.0 meters separation distance.

For scenario 1: 2.7 ACH, the personal exposure index was 1.09, 1.06, 1.04 and 1.07 for separation distance 0.7, 1.0, 1.5 and 2.0 meters respectively. The highest index, 1.09, was for the closest distance at 0.7 meters. For scenario 2: 5.1 ACH, the personal exposure index was 1.13, 0.86, 0.95 and 0.8 for separation distance 0.7, 1.0, 1.5 and 2.0 meters respectively. The highest index was obtained for the closest separation distance at 0.7 meters, and the lowest for the longest separation distance. For scenario 3: 9.6 ACH, the personal exposure index was 0.92, 0.96, 0.83 and 0.72 for separation distance 0.7, 1.0, 1.5 and 2.0 meters respectively. The highest index was obtained at 1.0 meters while the lowest at 2.0 meters.

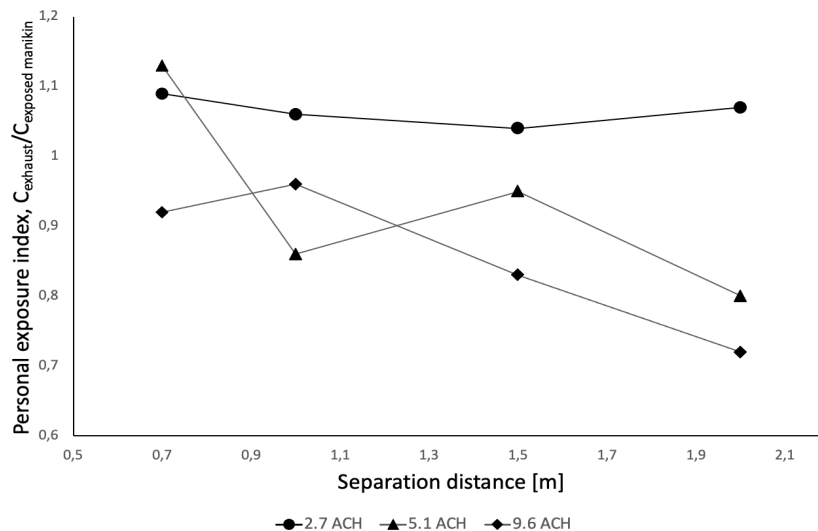


Figure 4.21: Personal exposure index for scenario 1, 2 and 3.

4.5 Probability of infection by a modified Wells-Riley equation

The probability to get infected by airborne coronavirus based on the modified Wells-Riley equation is shown in Figure 4.22. The probability of infection with a theoretically fully-mixed case is also included. Figure 4.22a, Figure 4.22b and Figure 4.22b shows that the probability of infection increased with exposure time.

Figure 4.22a shows that the probability of infection was almost the same for every separation distance for 2.7 ACH. This is because the personal exposure index was around the same

for all positions of the exposed manikin, M_{exp} . The fully mixed scenario gave the highest probability of infection.

Figure 4.22b shows that the probability of infection for 5.1 ACH varied for different separation distances. The probability was highest for scenario D = 2.0 meters and second highest for scenario B = 1.0 meter. The fully mixed scenario gave the second lowest probability of infection.

Figure 4.22c shows that the probability of infection for 9.6 ACH varied for different separation distances. The probability of infection is highest for D = 2.0 meters. The fully mixed scenario gave the lowest probability of infection.

For the maximum exposure time of $t = 50$ minutes, the overall highest probability of infection was 0.004% with 2.7 ACH. The overall lowest was 0.0012% with 9.6 ACH.

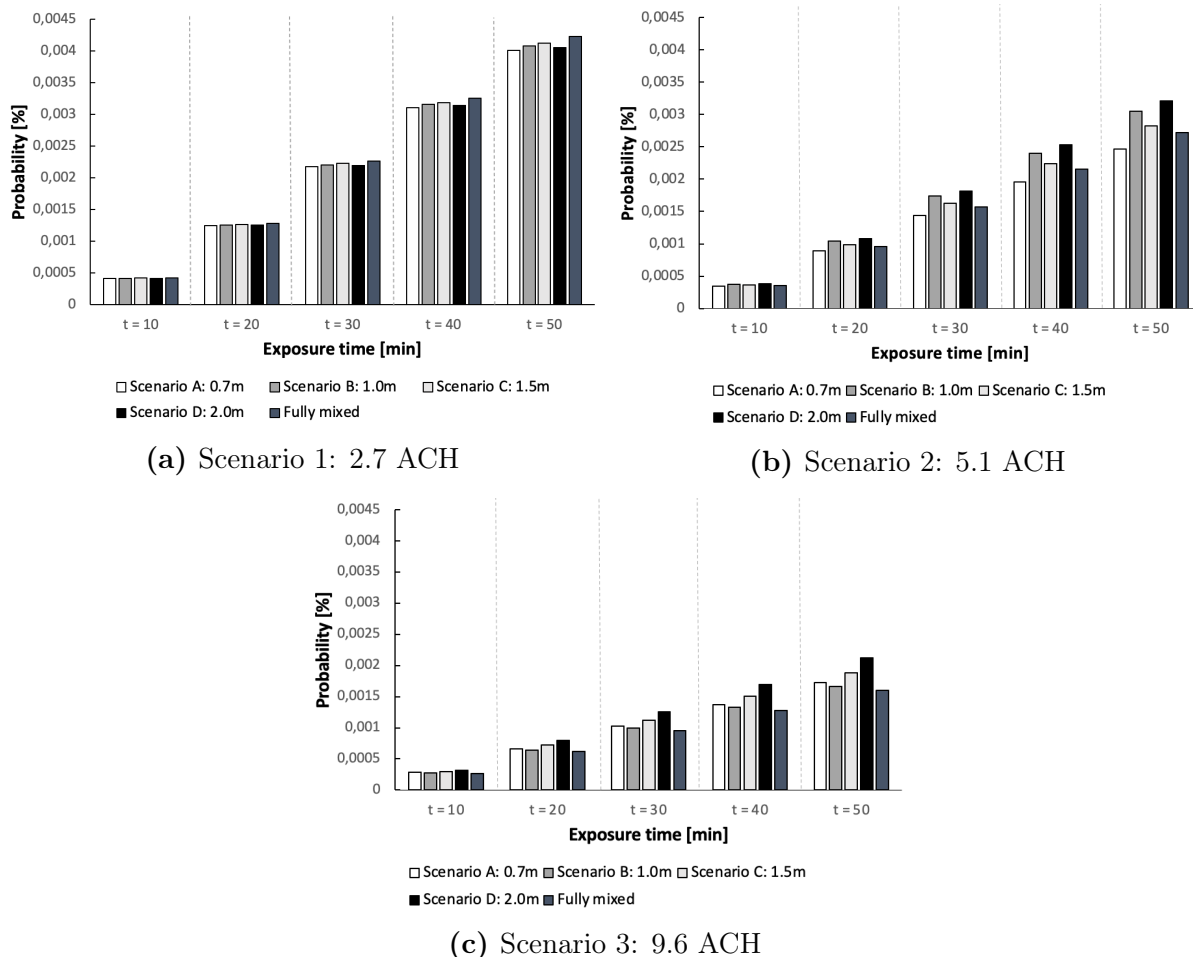


Figure 4.22: Probability of infection based on the modified Wells-Riley model for scenario 1, 2 and 3.

5 Discussion

5.1 Ventilation airflow rate and exposure

The experimental results demonstrated that, as expected, exposure decreased as the ventilation airflow rate increased. This applies for the absolute values measured in the inhalation zone of M_{exp} . Because ventilation is vital in diluting the virus, the findings emphasize the necessity of appropriate ventilation in confined spaces where one infected individual is present. Governments have advocated for this since the beginning of the pandemic (FHI, 2020a), and the results back up this proposal. Li *et al.* (2021) also found that increased ventilation airflow rates resulted in lower concentration of small aerosols.

The results also demonstrated that the short-range airborne transmission caused by direct exposure when the separation distance was short, was lower than the indirect exposure caused by the long-range airborne transmission. This suggests that the indirect exposure is more significant than the direct exposure in this experimental set-up. A hypothesis is presented in 5.2.

The results reflect the risk of exposure in various interior locations as advised by Robertson (2021). It demonstrates that the recommended airflow rate for offices and shops (2.7 ACH) give higher exposure than the recommended airflow rate for examination rooms (5.1 ACH) and between sports facility and airborne isolation infection rooms (9.6 ACH). In this case, this applies for the airflow pattern in the laboratory room, as well as the examined orientation of a sitting exposed and a standing infected with a height difference of 60 cm.

Even though a higher ventilation airflow rate resulted in less exposure, it did not completely eliminate aerosol particle exposure. Cotman *et al.* (2021) discovered the same. During the pandemic period, droplet transmission was highlighted as the main contributor for exposure at short distances (FHI, 2020a). This thesis shows that small aerosols also contribute with exposure at both short and long distances. This was also found by Liu *et al.* (2016). The findings emphasize the necessity of measures protecting against short-range airborne transmission, rather than just infection induced by bigger droplet particles.

5.2 Social distancing and location of exhaust

The results showed that the largest absolute exposure was measured at a separation distance of two meters between the manikins. The lowest ventilation performance was also found at this separation distance, according to the personal exposure index/local air quality index. This is not expected, given that WHO has suggested a social distance of at least 1 meter since the pandemic outbreak (WHO, 2021). FHI has also stated that the risk of exposure from small and medium sized droplets is highest close to an infected person as the droplet concentration is highest in this position (FHI, 2020a). Based on the advice, it was expected that short separation distances would result in the highest exposure.

A hypothesis to explain the results can be formed from the smoke visualizations of the exhaled jet from M_{inf} (Figure 4.19) and the airflow pattern in the laboratory room (Figure 4.20). Figure 5.1 shows a simplified model of the smoke visualizations combined. It indicates that the supply air from SU_1 was split into two paths. One component of the air short-circuited to EX_2 , while the other descended towards the position of M_{exp} at 2.0 meters separation distance. The visualization of the exhaled jet indicated that the aerosols simulated by tracer gas elevated quickly towards the ceiling. This may have been caused because of buoyancy forces and the upward rising thermal plume from the exposed manikin. The simulated aerosols may have travelled with the air stream towards SU_1 and descending towards M_{exp} . As a result, the exposed manikin is more exposed when located close to the exhaust. This may show that a separation distance of 2.0 meters is not safe enough if exposed persons are located close to the exhaust and that the airflow pattern plays an important role. This hypothesis needs to be validated with CFD simulations.

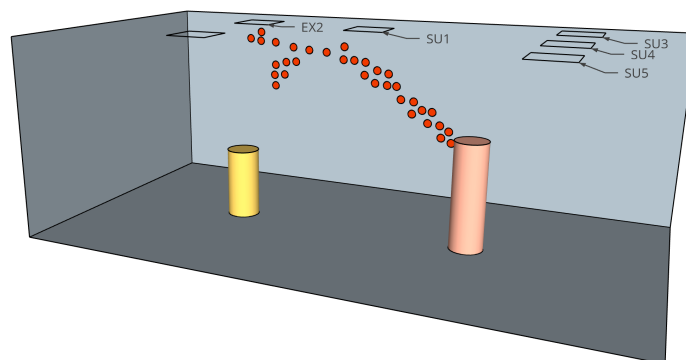


Figure 5.1: Supply air from SU_1 partly short-circuited to EX_2 and partly descended towards M_{exp} . Red dots represents exhaled aerosols from M_{inf} .

One important observation from this hypothesis is the location of the exposed manikin close to the exhaust. This is in line with FHI's guidelines to avoid placing workstations near the exhaust (FHI, 2020b). If CFD simulations validates the airflow pattern, this results shows contradicting statements to the recommended social distancing with the analyzed orientation of a sitting exposed person and a standing infected person.

The smoke visualization may also explain why 2.7 ACH had local air quality indices above 1, while 5.1 and 9.6 ACH had lower than 1. For low ventilation airflow rates, the supply air velocity is low, and more contaminated air may have short-circuited to EX₁ and less descended to the inhalation zone of the exposed manikin. This may have caused higher concentration of tracer-gas in the exhaust than at the exposed manikin. On the other hand, for higher ventilation airflow rates, the supply air velocity is higher and less contaminated air may have short-circuited to EX₁ and more air descended towards the exposed manikin. This may have caused higher concentration of tracer-gas in the inhalation zone of the exposed manikin, and less in the exhaust.

According to Liu *et al.* (2016), closer separation distances give lower exposure if the virus source is taller than the exposed person. This is the same as found in this thesis. According to the authors, the virus source's exhaled jet was directed over the head of the exposed person. This could potentially explain the results found in this thesis. The smoke visualization indicated that the aerosols generated from the mouth breathing by M_{inf} , was directed forward before it elevated rapidly. However, Liu *et al.* (2016) stated that this finding is restricted to when the virus particles is only produced from the mouth. Virus particles can also be generated by nose breathing, and this could cause jets directed slightly downwards and could increase the exposure. Nose breathing was not investigated in this thesis. Additionally, the susceptible person did not have a breathing function. Even though the susceptible did not have a breathing function, the results at close separation distances shows the same. It needs to be validated with CFD how the exhaled jet of the infected manikin is travelling together with the airflow pattern in the room.

Olmedo *et al.* (2012) also investigated personal exposure with different orientations and separation distances between a healthy and an infected person. They found that the exposure index was 1 for every separation distance. This means that they obtained fully mixed conditions. This was not the case in this study. This may be because of different experimental set-up, as the personal exposure is highly dependent on airflow pattern in a

ventilated space (Liu *et al.*, 2016). Olmedo *et al.* (2012) only investigated one airflow rate at 5.6 ACH and had only one air supply diffuser. This highlights that detailed information about a room can be determining factors for the exposure index.

5.3 Increased ventilation airflow rate or improved local air quality index as infection-preventive measures

The personal exposure index is defined in a similar manner as the local air quality index, which means that the index can be interpreted in two different ways.

The personal exposure index is desired to be as high as possible, as described in 2.4.2. The indices obtained at separation distance 0.7, 1.0, 1.5 and 2.0 meter was for 2.7 ACH 1.09, 1.06, 1.04 and 1.07, respectively. These were the highest calculated indices of all scenarios. The lowest and worst index was obtained with 9.6 ACH and 2 meters of separation distance. This means that the experienced ventilation efficiency in the inhalation zone of the exposed manikin was better at the lowest airflow rate.

If the index is interpreted as local air quality index, Figure 5.2 shows that none of the scenarios obtained fully mixed conditions.

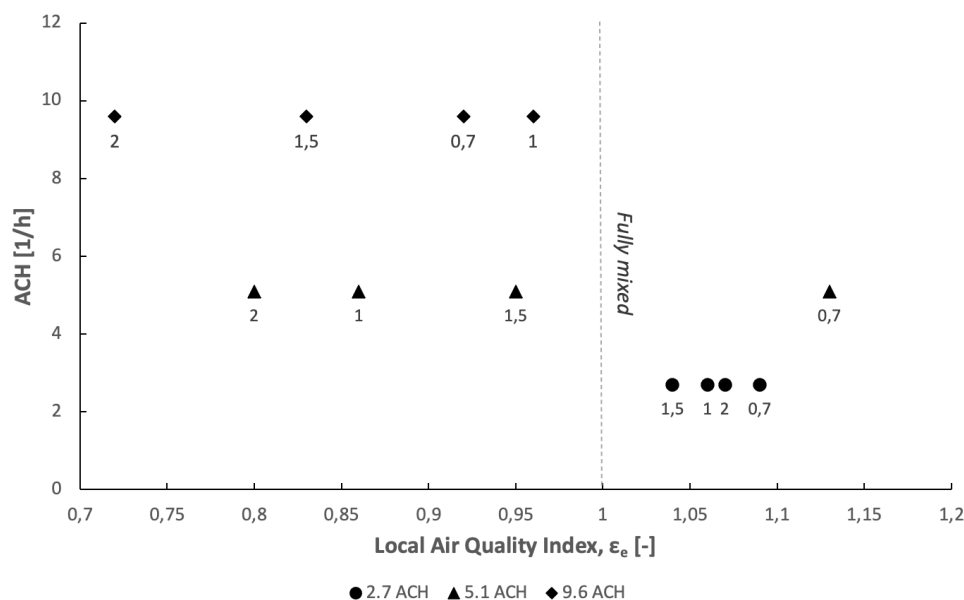


Figure 5.2: Correlation between ACH and local ventilation efficiency for all scenarios. Numbers below each data point shows separation distance.

One interesting observation is the local air quality indices for 2.7 ACH. With the lowest airflow rate, the best ventilation performance was achieved. However, 2.7 ACH also had the

highest absolute exposure and the highest probability of infection based on the modified Wells-Riley model. This brings up an essential point: Which of the parameters *i) local air quality index* or *ii) ventilation airflow rate* contributes more to lowering the risk of infection? This could be a crucial consideration in determining when to implement which infection-prevention measure. A higher airflow rate will dilute the virus more, but it will also require more fan power and consequently increased energy costs. Improving the local air quality index can be a cost-effective approach, as this can be done by moving thermal loads and furniture in the room to adequately distribute the supply of fresh air (Lee and Awbi, 2004).

The probability of infection for three scenarios can be analyzed and compared, to observe the effect of either improved local air quality index or increased ventilation airflow rate: measured local air quality index in the lab with a certain airflow rate (2.7, 5.1 and 9.6 ACH), $\epsilon_e = 1$ (fully mixed case) and increasing ventilation airflow rate by 1 ACH and assume $\epsilon_e = 1$. This assumption is made because the airflow rates between 2.7 and 5.1 ACH and between 5.1 and 9.6 ACH was not measured, hence no index was measured for these airflow rates.

Figure 5.3 shows the probability of infection for three cases: measured local air quality index at 2.7 ACH in the lab, 2.7 ACH and fully-mixed conditions and increase of the airflow rate from 2.7 ACH to 3.7 ACH with fully-mixed conditions. When the airflow rate increases to 3.7 ACH, the probability of infection decreases. When obtaining fully-mixed conditions at 2.7 ACH, the probability of infection increases. This is due to the fact that the ventilation performance was initially superior to fully-mixed conditions.

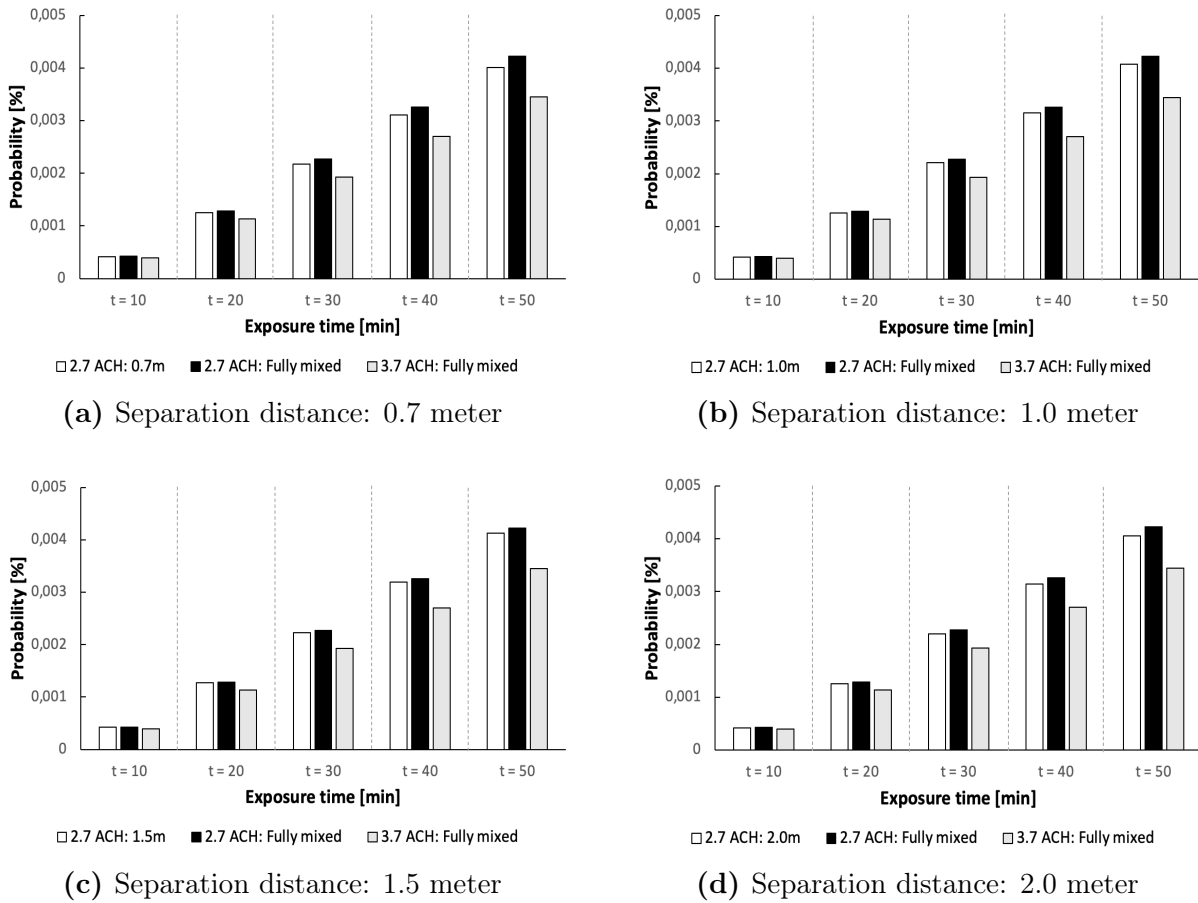


Figure 5.3: Comparison of the probability of infection for the measured ϵ_e at 2.7 ACH, fully-mixed conditions at 2.7 ACH and 3.7 ACH at fully mixed conditions.

Figure 5.4 shows the probability of infection for three cases: 5.1 ACH with the measured local air quality index in the lab, 5.1 ACH with fully-mixed conditions and increasing the airflow rate from 5.1 to 6.1 ACH with fully-mixed conditions. For the separation distances 1.0, 1.5 and 2.0 meters, both options decrease the probability of infection. The biggest reductions are observed when the airflow rate is increased to 6.1 ACH. For separation distance 0.7 meters, there is an increase in the probability of infection when fully mixed conditions are obtained. This is because the measured local air quality index in the lab originally was superior to fully-mixed conditions. When increasing the ventilation airflow rate, a decrease in the probability of infection is observed.

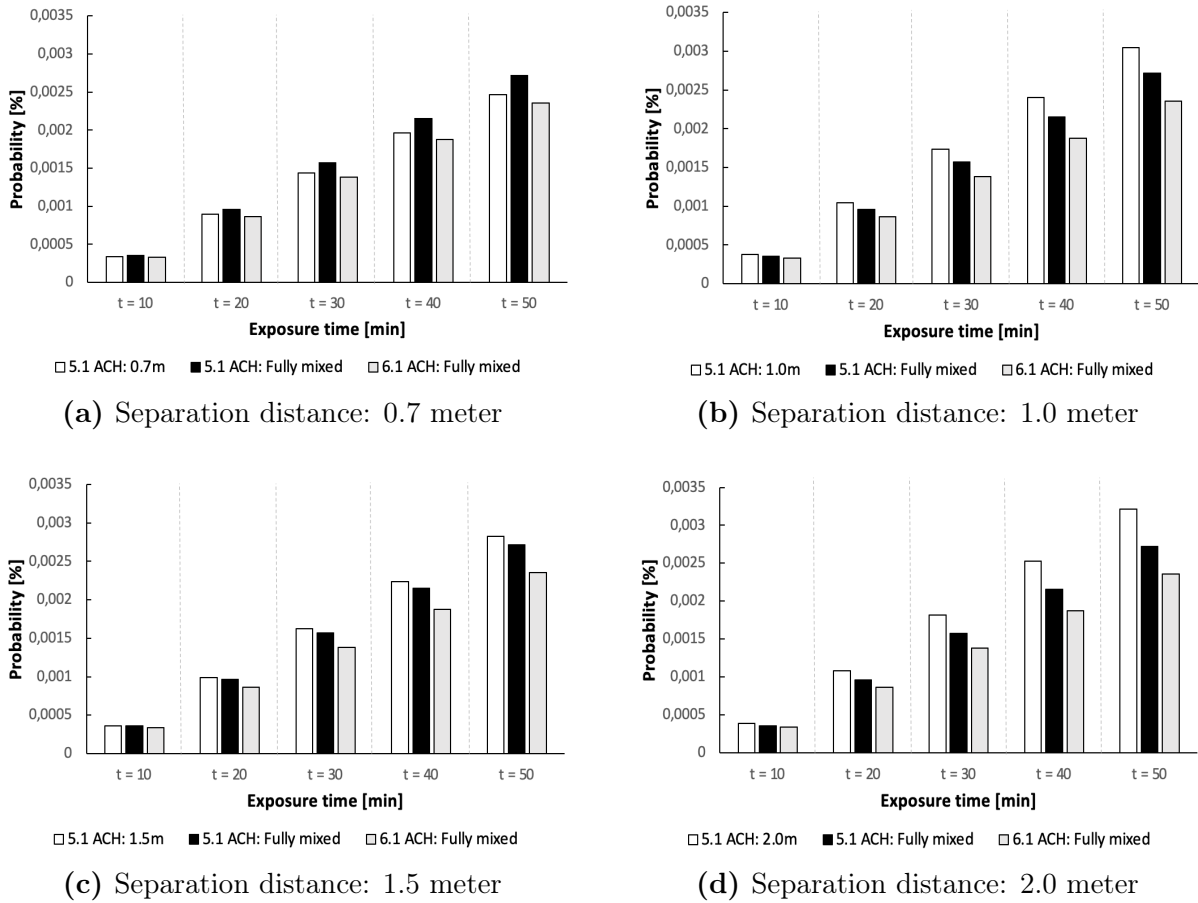


Figure 5.4: Comparison of the probability of infection for the measured ϵ_e at 5.1 ACH, fully-mixed conditions at 5.1 ACH and 6.1 ACH at fully mixed conditions.

Figure 5.5 shows the probability of infection for three cases: 9.6 ACH with measured local air quality index from the lab, 9.6 ACH with fully-mixed conditions and increasing the airflow rate to 10.6 ACH with fully-mixed conditions. It shows that both options i) and ii) are beneficial to reduce the probability of infection. The biggest decrease is obtained by increasing the airflow rate by 1 ACH. Even if increased airflow rate reduces the probability of infection the most, Figure 5.5 shows that the difference in applying either of the measures is small.

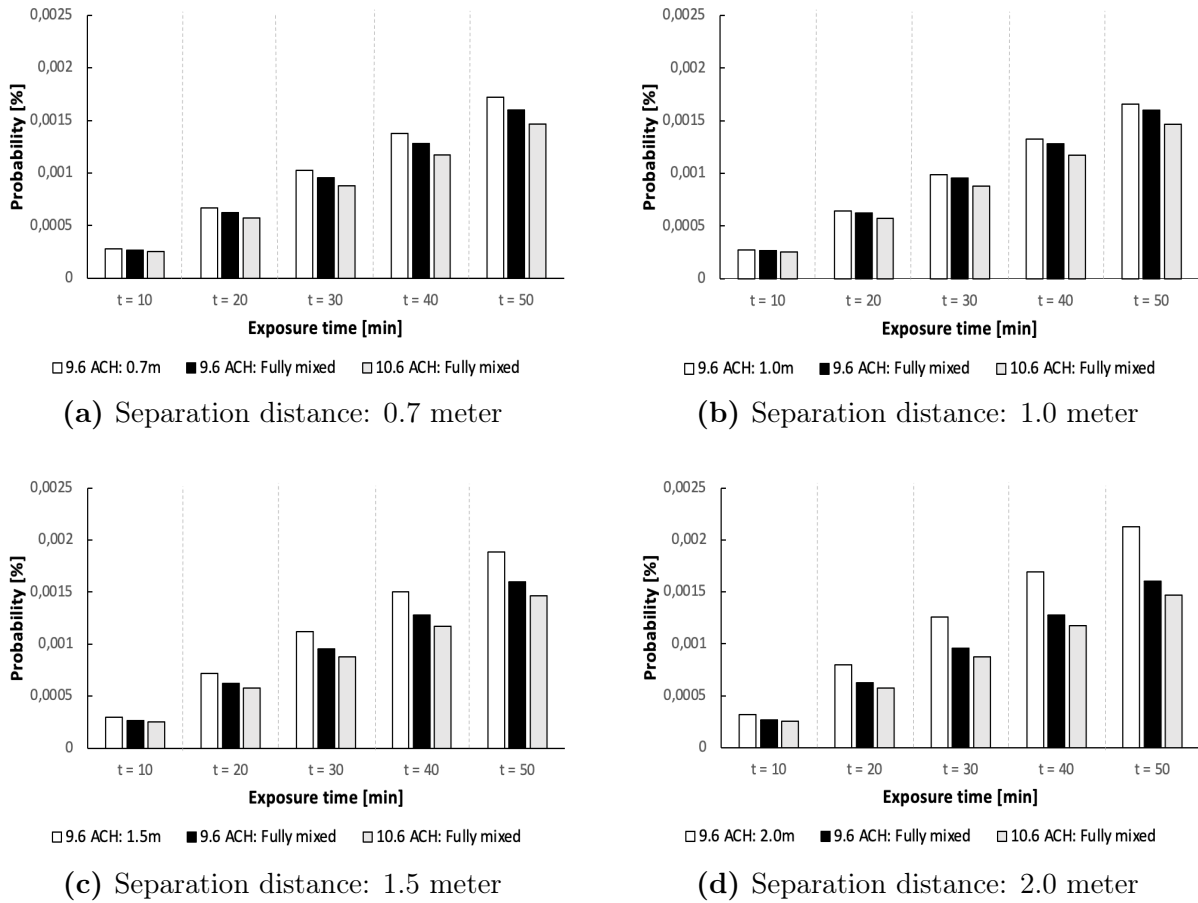


Figure 5.5: Comparison of the probability of infection for the measured ϵ_e at 9.6 ACH, fully-mixed conditions at 9.6 ACH and 10.6 ACH at fully mixed conditions.

Both Figure 5.4 and Figure 5.5 showed that increasing the airflow rate by 1 ACH reduced the risk of infection more than improving the local air quality index to $\epsilon = 1$. However, with increasing airflow rate from 5.1 to 9.6 ACH, it can be observed that the difference in probability of infection for infection-prevention measure i) and ii) becomes smaller and smaller. As a result, improving the local air quality index when the airflow rate is 9.6 ACH may be more advantageous. Increased energy expenses for increased fan power can thus be saved. If the local air quality index already is adequate, as demonstrated with 2.7 ACH, a 1 ACH increase in the ventilation airflow rate should be used as an infection-preventive measure.

The chosen measure to decrease the probability of infection become more important with increased exposure time. This is shown in Figure 5.3, Figure 5.4 and Figure 5.5 where the probability of infection is highest for exposure time $t = 50$ minutes.

Even though the results from this thesis shows low probability of infection, other experimental set-ups and real situations could cause higher probability and measures

should to be considered. Additionally, this thesis only investigated breathing mode from the infected manikin. If the manikin was simulated to sneeze, cough or talk, the probability of infection could most likely increase. Consequently, implemented measures of either improved local air quality index or increased ventilation airflow rate would be even more critical.

5.4 Modified Wells-Riley model: advantages and disadvantages

Aganovic *et al.* (2021) model for assessment of airborne exposure and probability of infection was used as a basis for the theoretical modelling in this thesis. Advantages and disadvantages about the model are discussed in this section.

To address non-fully mixed conditions, the model was enhanced with the personal exposure index/local air quality index. The new modification eliminates one of the most significant flaws in the original Wells-Riley equation, which assumes fully-mixed conditions at all times. However, Figure 4.22 showed that the probability of infection for fully-mixed conditions ($\epsilon = 1$) and the measured ϵ 's in the lab did not differ significantly. This indicates that the model proposed by Aganovic *et al.* (2021) works well and can be used as a prediction tool with the assumption of fully-mixed conditions without the need of experimental measurements. This is a strength, as predictions of the probability of infection can be made effectively for indoor environments with simple calculations.

The virus inactivation rate (k) was shown to be dependent on relative humidity in 3.3. For all scenarios, one k -value was used to simplify the calculations. This may have led to a small source of error, as the relative humidity fluctuated from scenario to scenario. Because the relative humidity varied from scenario to scenario, this could have been a modest source of error. Because the k -value proposed by Aganovic *et al.* (2021) did not vary significantly on relative humidity, the source of error may not be very significant.

The viral load in sputum, c_v , was estimated as a *mild-to-moderate* case of infection. This value is dependent on what type of coronavirus mutant there is, how severe the sickness is and if the infected person is symptomatic/asymptomatic. This value also influences the results.

The conversion factor, c_i , was estimated based on Aganovic *et al.* (2021). This value was

assumed based on the state-of-art literature when the article was published. This value may develop over time and may also influence the calculated probability of infection.

6 Conclusion

The probability of infection from airborne coronavirus was studied at three ventilation airflow rates (2.7, 5.1 and 9.6 ACH) and four separation distances between a sitting exposed and a standing infected person (0.7, 1.0, 1.5 and 2.0 meters). The personal exposure index/local air quality index was calculated based on tracer-gas measurements. The probability of infection was determined by a new modification of the Wells-Riley equation. The primary purpose was to recommend guidelines for reducing the risk of exposure to airborne coronavirus indoors.

The main findings can be summarized in the following points:

- The lowest exposure was measured for the highest airflow rate at 9.6 ACH, while the highest exposure was measured for the lowest airflow rate at 2.7 ACH. This highlights the importance of adequate ventilation in indoor spaces during a pandemic.
- The probability of infection was highest for 2.7 ACH, but overall low for all scenarios with a maximum value of 0.004%
- The highest exposure and the lowest personal exposure index/local air quality index were measured at 2.0 separation distance for all investigated ventilation airflow rates.
- Exposure to exhaled contamination from an infected person cannot be completely eliminated by ventilation alone.

From the experimental set-up in this thesis, improvement of the local air quality index should be implemented when the airflow rate is 9.6 ACH. This will give a lower probability of infection, as well as saved energy costs for fan power by not increasing the ventilation airflow rate. For 2.7 ACH, the local air quality index was superior to fully-mixed conditions and therefore a 1 ACH increase in the ventilation airflow rate should be applied as the infection-preventive measure. Additionally, two meters of separation distance may be insufficient if the exposed person is close to the exhaust or are located a place where the ventilation airflow pushes aerosols towards this location. This must be validated with a CFD simulation.

During the whole pandemic period, increased ventilation airflow rates have been highlighted as an infection-preventive measure. The thesis highlights that improvement of the local air quality index in the inhalation zone of an exposed person also can contribute to reduce

exposure. Research about exposure risk in ventilated spaces is very important, and an extended toolbox in how to fight viruses in ventilated spaces can be decisive in how the humanity face future pandemics.

7 Further work

Recommendations regarding further work is hereby recommended by the author:

- CFD simulation of the airflow pattern to validate the results. The experimental measurements can also be repeated to validate the results.
- Introduce a breathing function for the sitting breathing thermal manikin to obtain a even more realistic experimental set-up
- More orientations and positions between the infected and the exposed manikin should be analyzed. This can be both manikins standing, exposed standing & infected sitting, face-to-back, face-to-side and back-to-back.
- Run measurements for more airflow rates in the laboratory to clarify the benefit of increasing the airflow rate or improving the local air quality index to reduce the probability of infection
- The ventilation system should be checked by the operating personnel. Several issues was found during the measurements. One of them was that the BEMS-system shows a higher ventilation airflow rate than actually delivered to the laboratory room. This should be calibrated. Also, the ventilation system sometimes use a lot of time (1-2 hours) to respond to changes in the airflow rate made in the BEMS-system.
- It was discussed if it was better to improve the ventilation performance or to increase the ventilation airflow rate to decrease the probability of infection. It would be interesting to investigate further how "bad" the ventilation performance needs to be before the marginal decrease in probability of infection is significantly affected by one of the measures.

References

- Aganovic, A. and Cao, G. (2019), ‘Evaluation of airborne contaminant exposure in a single-bed isolation ward equipped with a protected occupied zone ventilation system’, *Indoor and built environment* **28**(8). doi: 10.1177/1420326X18823048.
- Aganovic *et al.* (2021), ‘Estimating the impact of indoor relative humidity on sars-cov-2 airborne transmission risk using a new modification of the wells-riley model’, *Building and Environment* **205**, 108278. doi: 10.1016/j.buildenv.2021.108278.
- Ahlawat, A., Mishra, S. and Wiedensohler, A. (2020), ‘An overview on the role of relative humidity in airborne transmission of sars-cov-2 in indoor environments’, *Aerosol Air Qual. Res.* **20**, pp. 1856–1861. doi: 10.4209/aaqr.2020.06.0302.
- Ai *et al.* (2020), ‘Tracer gas is a suitable surrogate of exhaled droplet nuclei for studying airborne transmission in the built environment’, *Building simulation* **13**, pp. 489–496. doi: 10.1007/s12273-020-0614-5.
- Ai, Z., Hashimoto, K. and Melikov, A. (2019), ‘Airborne transmission between room occupants during short term events: Measurement and evaluation’, *Indoor Air* **29**(4), pp. 563–576. doi: 10.1111/ina.12557.
- Beggs, C. and Avital, E. (2021), ‘A psychrometric model to predict the biological decay of the sars-cov-2 virus in aerosols’, *PeerJ Life and Environment* **9**, 11024. doi: 10.7717/peerj.11024.
- Berry *et al.* (2022), ‘A review of methods to reduce the probability of the airborne spread of covid-19 in ventilation systems and enclosed spaces’, *Environmental Research* **203**, 111765. doi: 10.1016/j.envres.2021.111765.
- Brohus, H. (1997), *Personal Exposure to Contaminant Sources in Ventilated Rooms*, PhD thesis, Aalborg University.
URL: https://www.cfd-benchmarks.com/digitalAssets/592/592388_brohus_h_1997.pdf
- Brouns, C. and Waters, B. (1991), *A guide to Contaminant Removal Effectiveness*, Technical Report 28.2, AIVC. Accessed: 12 April 2022.
URL: https://www.aivc.org/sites/default/files/members_area/medias/pdf/Technotes/

*TN28.2%20GUIDE%20TO%20CONTAMINANT%20REMOVAL%20EFFECTIVENESS.
PDF*

- Buonanno, G., Stabile, L. and Morawska, L. (2020), 'Estimation of airborne viral emission: Quanta emission rate of sars-cov-2 for infection risk assessment', *Environment International* **141**, 105794. doi: 10.1016/j.envint.2020.105794.
- Buonanno *et al.* (2020), 'Quantitative assessment of the risk of airborne transmission of sars-cov-2 infection: Prospective and retrospective applications', *Environment International* **145**, 106112. doi: 10.1016/j.envint.2020.106112.
- Cammarata, A. and Cammarata, G. (2021), 'Dynamic assessment of the risk of airborne viral infection', *Indoor Air* **31**(6), pp. 1759–1775. doi: 10.1111/ina.12862.
- CDC (2021), 'Science brief: Sars-cov-2 and surface (fomite) transmission for indoor community environments'. Accessed: 6 April 2022.
URL: <https://www.cdc.gov/coronavirus/2019-ncov/more/science-and-research/surface-transmission.html>
- Cheng *et al.* (2021), 'Experimental and simulated evaluations of airborne contaminant exposure in a room with a modified localized laminar airflow system', *Environmental Science and Pollution research* **28**(8), 1–22. doi: 10.1007/s11356-021-12685-4.
- Cheng *et al.* (2022), 'Predominant airborne transmission and insignificant fomite transmission of sars-cov-2 in a two-bus covid-19 outbreak originating from the same pre-symptomatic index case', *Journal of Hazardous Materials* **425**, 128051. doi: 10.1016/j.jhazmat.2021.128051.
- Cotman *et al.* (2021), 'Factors affecting aerosol sars-cov-2 transmission via hvac systems; a modeling study', *PLoS Comput Biol* **17**(10), e1009474. doi: 10.1371/journal.pcbi.1009474.
- Dai, H. and Zhao, B. (2020), 'Association of the infection probability of covid-19 with ventilation rates in confined spaces', *Building simulation* **13**(6), pp. 1321–1327. doi: 10.1007/s12273-020-0703-5.
- FHI (2020a), 'Fakta om koronaviruset SARS-CoV-2 og sykdommen covid-19'. Accessed: 20 February 2022.

URL: <https://www.fhi.no/nettpub/coronavirus/fakta/fakta-om-koronavirus-coronavirus-2019-ncov/?term=&h=1#smittemaate>

FHI (2020b), 'Inneklima og risiko for smitte av covid-19 - råd om ventilasjon'. Accessed: 15 February 2022.

URL: https://www.fhi.no/contentassets/1af4c6e655014a738055c79b72396de8/inneklima-og-risiko-for-smitte-av-covid-19---rad-om-ventilasjon_27102020.pdf

Greenhalgh *et al.* (2021), 'Ten scientific reasons in support of airborne transmission of sars-cov-2', *The Lancet* **397**(10285). doi: 10.1016/S0140-6736(21)00869-2.

Grieve, P. W. (1989), 'Measuring ventilation using tracer-gases'.

URL: https://www.aivc.org/sites/default/files/airbase_3884.pdf

Han, H. (2012), 'Ventilation effectiveness measurements using tracer gas technique', *Fluid Dynamics, Computational Modeling and Applications* . doi: 10.13140/2.1.2140.0000.

Harvard School of Public Health (2020), 'Op-ed: Humidity can aid in the fight against covid-19'. Accessed: 2 February 2022.

URL: <https://www.hsph.harvard.edu/news/hsph-in-the-news/op-ed-humidity-can-aid-in-the-fight-against-covid-19/>

Ivanov, M. (2019), 'Exhaled air speed measurements of respiratory air flow, generated by ten different human subjects, under uncontrolled conditions', *E3S Web of Conferences* **111**, 02074. doi: 10.1051/e3sconf/201911102074.

Jayaweera *et al.* (2020), 'Transmission of covid-19 virus by droplets and aerosols: A critical review on the unresolved dichotomy', *Environmental Research* **188**, 109819. doi: 10.1016/j.envres.2020.109819.

Johns Hopkins Medicine (n.d.), 'Vital signs (body temperature, pulse rate, respiration rate, blood pressure)'. Accessed: 10 March 2022.

URL: <https://www.hopkinsmedicine.org/health/conditions-and-diseases/vital-signs-body-temperature-pulse-rate-respiration-rate-blood-pressure>

Jurelionis *et al.* (2015), 'The impact of the air distribution method in ventilated rooms on the aerosol particle dispersion and removal: The experimental approach', *Energy and buildings* **86**, pp. 305–313. doi: 10.1016/j.enbuild.2014.10.014.

Lee, H. and Awbi, H. (2004), 'Effect of internal partitioning on indoor air quality of rooms

- with mixing ventilation—basic study’, *Building and Environment* **39**(2), pp. 127–141. doi: 10.1016/j.buildenv.2003.08.007.
- Li, C. and Tang, H. (2021), ‘Study on ventilation rates and assessment of infection risks of covid-19 in an outpatient building’, *Journal of Building Engineering* **42**, 103090. doi: 10.1016/j.jobbe.2021.103090.
- Li *et al.* (2021), ‘Transmission characteristics of respiratory droplets aerosol in indoor environment: an experimental study’, *International journal of of environmental health research* **1-12**. doi: 10.1080/09603123.2021.1910629.
- Li, Y., Cheng, P. and Jia, W. (2021), ‘Poor ventilation worsens short-range airborne transmission of respiratory infection’, *Indoor Air* **32**(1), e12946. doi: 10.1111/ina.12946.
- Liu *et al.* (2016), ‘Short-range airborne transmission of expiratory droplets between two people’, *Indoor Air* **27**(2), 452–462. doi: 10.1111/ina.12314.
- Marshall, J. D. and Nazaroff, W. W. (2006), ‘Intake fraction’. Accessed: 12 March 2022. URL: <https://depts.washington.edu/airqual/reports/Intake%20Fraction%20--%20proofs.pdf>
- Mittal, R., Meneveau, C. and Wu, W. (2020), ‘A mathematical framework for estimating risk of airborne transmission of covid-19 with application to face mask use and social distancing’, *Physics of Fluids* **32**(10), 101903. doi: 10.1063/5.0025476.
- Nilsson, P. (2003), *Achieving the Desired Indoor Climate*, Studentlitteratur AB.
- Noorimotlagh *et al.* (2021), ‘A systematic review of possible airborne transmission of the covid-19 virus (sars-cov-2) in the indoor air environment’, *Environmental Research* **193**, 110612. doi: 10.1016/j.envres.2020.110612.
- Norwegian Building Authority (2017), ‘§13-3 ventilasjon i byggverk for publikum og arbeidsbygning’. Accessed: 13 October 2021. URL: <https://dibk.no/regelverk/byggteknisk-forskrift-tek17/13/i/13-3/>
- Ojima, J. (2012), ‘Gaseous contaminant distribution in the breathing zone’, *Industrial Health* **50**(3). doi: 10.2486/indhealth.ms1314.
- Olmedo *et al.* (2011), ‘Study of the human breathing flow profile in a room with three different ventilation strategies’, *IAQ conference* .

URL: https://www.researchgate.net/publication/287678203_Study_of_the_human_breathing_flow_profile_in_a_room_with_three_different_ventilation_strategies

Olmedo *et al.* (2012), 'Distribution of exhaled contaminants and personal exposure in a room using three different air distribution strategies', *Indoor Air* **22**(1), pp. 64–76. doi: 10.1111/j.1600-0668.2011.00736.x.

Price engineering (2016), 'Engineering guide: Displacement ventilation'. Section J. Accessed: 2 February 2022.

URL: <https://www.priceindustries.com/content/uploads/assets/literature/engineering-guides/displacement-ventilation-engineering-guide.pdf>

Qian, H. and Li, Y. (2010), 'Removal of exhaled particles by ventilation and deposition in a multibed airborne infection isolation room', *Indoor Air* **20**(4), pp. 284–297. doi: 10.1111/j.1600-0668.2010.00653.x.

Qian *et al.* (2006), 'Dispersion of exhaled droplet nuclei in a two-bed hospital ward with three different ventilation systems', *Indoor Air* **16**(2), pp. 111–128. doi: 10.1111/j.1600-0668.2005.00407.x.

Rencken *et al.* (2021), 'Patterns of sars-cov-2 aerosol spread in typical classrooms', *Building and environment* **204**, 108167. doi: 10.1016/j.buildenv.2021.108167.

Riley, R. (1982), 'Indoor airborne infection', *Environment International* **8**(1-6), pp. 317–320. doi: 10.1016/0160-4120(82)90043-5.

Robertson, P. (2021), 'Ashrae recommended air changes per hour'. Accessed: 5 February 2022.

URL: <https://smartairfilters.com/en/blog/ashrae-air-changes-per-hour-office-residential/?rel=1>

Rocha-Melogno *et al.* (2021), 'Quantitative risk assessment of covid-19 aerosol transmission indoors: a mechanistic stochastic web application', *Environmental Technology* **1-12**. doi: 10.1080/09593330.2021.1998228.

Shang *et al.* (2022), 'An improved numerical model for epidemic transmission and infection risks assessment in indoor environment', *Journal of Aerosol Science* **162**, 105943. doi: 10.1016/j.jaerosci.2021.105943.

Shuter, B. and Aslani, B. (2000), 'Evaluating thermal environments by using a thermal

- manikin with controlled skin surface temperature', *Eur J Appl Physiol.* **82**(3). doi: 10.1007/s004210050679.
- Stego (n.d.), 'Ptc heater'. Accessed: 1 March 2022.
URL: <https://docs.rs-online.com/8348/0900766b8168040b.pdf>
- Su *et al.* (2022), 'Infection probability under different air distribution patterns', *Building and Environment* **207**(B), 108555. doi: 10.1016/j.buildenv.2021.108555.
- Sun, S., Li, J. and Han, J. (2020), 'The last inches: Human thermal plume as an overlooked factor in airborne transmission of covid-19 in the human microenvironment', *Social Science Research Network* . doi: 10.2139/ssrn.3754655.
- Sze, G. and Chao, C. (2010), 'Review and comparison between the wells-riley and dose-response approaches to risk assessment of infectious respiratory diseases', *Indoor Air* **20**(1).doi: 10.1111/j.1600-0668.2009.00621.x.
- TinyTag (2018), 'Tinytag plus 2 dual channel temperature/relative humidity (-25 to +85°C to 100% rh'. Accessed: 5 April 2022.
URL: <http://gemini2.assets.d3r.com/pdfs/original/3242-tgp-4500.pdf>
- van Doremalen *et al.* (2020), 'Aerosol and surface stability of sars-cov-2 as compared with sars-cov-1', *N Engl J Med* **382**(16), pp. 1564–1567. doi: 10.1056/NEJMc2004973.
- Villafruela, J., Olmedo, I. and San José, J. (2016), 'Influence of human breathing modes on airborne cross infection risk', *Building and environment* **106**, pp. 340–351.
URL: doi: 10.1016/j.buildenv.2016.07.005
- Wang *et al.* (2022), 'A coupled computational fluid dynamics and wells-riley model to predict covid-19 infection probability for passengers on long-distance trains', *Saf Sci* **147**, 105572. doi: 10.1016/j.ssci.2021.105572.
- WHO (2020), 'Transmission of sars-cov-2: implications for infection prevention precautions: scientific brief'. Accessed: 10 February 2022.
URL: <https://www.who.int/news-room/commentaries/detail/transmission-of-sars-cov-2-implications-for-infection-prevention-precautions>
- WHO (2021), 'Coronavirus disease (covid-19): How is it transmitted?'. Accessed: 10 February 2022.

URL: <https://www.who.int/news-room/questions-and-answers/item/coronavirus-disease-covid-19-how-is-it-transmitted>

Xu *et al.* (2021), ‘Airborne infection risks of sars-cov-2 in u.s. schools and impacts of different intervention strategies’, *Sustainable Cities and Society* **74**, 103188. doi: 10.1016/j.scs.2021.103188.

Xu *et al.* (2022), ‘Prediction and control of aerosol transmission of sars-cov-2 in ventilated context: from source to receptor’, *Sustainable Cities and Society* **76**, 103416. doi: 10.1016/j.scs.2021.103416.

Zhang, S. and Lin, Z. (2021), ‘Dilution-based evaluation of airborne infection risk - thorough expansion of wells-riley model’, *Building and Environment* **194**, 107674. doi: 10.1016/j.buildenv.2021.107674.

Zhang *et al.* (2020), ‘The impact of air change rate on the air quality of surgical microenvironment in an operating room with mixing ventilation’, *Journal of Building Engineering* **32**, 101770. doi: 10.1016/j.jobee.2020.101770.

Zhang *et al.* (2021), ‘Evidence for lack of transmission by close contact and surface touch in a restaurant outbreak of covid-19’, *Journal of Infection* **83**(2), pp. 207–216. doi: 10.1016/j.jinf.2021.05.030.

A Risk assessment

Risk Assessment Report

HVAC-laboratory

Project name	Experimental study on the effect of ventilation solutions on the risk of COVID-19 infection
Facility name	HVAC-laboratory
Building and room number	Varmetekniske laboratorier, HVAC-laboratory
Project leader	Guangyu Cao
Facility responsible	Guangyu Cao
HES coordinator	Morten Grønli
HES responsible	Terese Løvås
Risk assessment performed by	Mathilde Ruud

Approval:

Apparatur kort (UNIT CARD) valid for:	6 months
Forsøk pågår kort (EXPERIMENT IN PROGRESS) valid for:	6 months

Role	Name	Date	Signature
Project leader	Guangyu Cao		
HES coordinator	Morten Grønli		
HES responsible	Terese Løvås		

TABLE OF CONTENTS

1	INTRODUCTION	1
2	DESCRIPTIONS OF EXPERIMENTAL SETUP.....	1
3	EVACUATION FROM THE EXPERIMENTAL AREA	3
4	WARNING	4
4.1	Before experiments.....	4
4.2	Abnormal situation.....	4
5	ASSESSMENT OF TECHNICAL SAFETY	5
5.1	HAZOP.....	5
5.2	Flammable, reactive and pressurized substances and gas	5
5.3	Pressurized equipment.....	5
5.4	Effects on the environment (emissions, noise, temperature, vibration, smell)	5
5.5	Radiation	5
5.6	Chemicals.....	6
5.7	Electricity safety (deviations from the norms/standards)	6
6	ASSESSMENT OF OPERATIONAL SAFETY	6
6.1	Procedure HAZOP.....	6
6.2	Operation procedure and emergency shutdown procedure.....	6
6.3	Training of operators.....	7
6.4	Technical modifications.....	7
6.5	Personal protective equipment.....	7
6.6	General Safety	7
6.7	Safety equipment	7
6.8	Special predations	7
7	QUANTIFYING OF RISK - RISK MATRIX.....	8
	ATTACHMENT E: PROCEDURE FOR RUNNING EXPERIMENTS.....	IX
	ATTACHMENT F: TRAINING OF OPERATORS	XI
	APPARATURKORT / UNITCARD.....	XII
	FORSØK PÅGÅR /EXPERIMENT IN PROGRESS	XIII
	ATTACHMENT H GUIDANCE TO RISK ASSESSMENT	XV

1 INTRODUCTION

The purpose of the experiment is to investigate the risk of getting infected with different ventilation solutions in the HVAC-lab in Varmetekniske laboratorier. Do tracer gas measurements in the HVAC-lab with various ventilation setups. The gas will be released from one point in the room. Electrical equipment will be used to generate heat.

The experiment consists of the following steps:

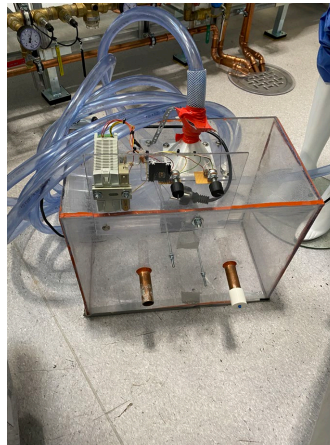
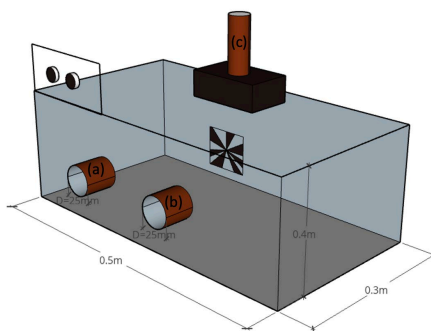
- Adjustment of ventilation (balancing the system, set-point temperature, air change rate and turn off the rotary heat exchanger to avoid tracer gas to re-transmit into the room)
- Turn on electrical equipment to generate heat
- Tracer gas N₂O will be released into the room
- Measurement of ventilation efficiency by tracer gas and further calculate the infection probability
- Measurement of relative humidity and temperature

2 DESCRIPTIONS OF EXPERIMENTAL SETUP

Manikin A is simulating an infected teacher, shown in **Figure 1**. Manikin A is heated up by electric wires inside. Manikin A will be standing still during all experiments. To generate a realistic exhaled jet, a tube is connected to the mouth of the manikin. This tube leads from the manikin and outside the room to a “breathing box”, as shown in **Figure 2**. The breathing box have two intakes and one exhaust. One intake takes in room air, while the other is dosed with N₂O tracer gas. To control how much tracer gas is dosed from the bottle, it is connected to a rotameter outside the room. Inside the breathing box, N₂O tracer gas and room air is mixed and then the exhaust tube is connected to the manikins’ mouth. The breathing box and the tracer gas bottle is placed outside the room. There is a valve on the bottle to shut the dosing completely off. Right before the manikins’ mouth, there is mounted heating elements to heat the exhaled air to 34 degrees celsius. The heating element is controlled by a varyac to obtain the correct temperature.



Figure 1: Manikin simulating an infected teacher. The tube close to the manikin's mouth will be put through the manikin's mouth (with a bored hole). Inside the tube there is a heating element to heat the exhaled air. Right-hand side picture shows this close-up.



Manikin B is simulating a healthy sitting student, shown in Figure 3. An electric vehicle is used to control the position of the manikin, and the controller is placed outside the room, so no personnel is inside the room while dosing tracer gas. The manikin is heated up by electric wires inside and controlled by the box shown in Figure 3, to generate a realistic thermal plume around the student. A sampling tube is placed on the manikin to measure the concentration of N_2O tracer gas.



A hole is bored into the exhaust duct to measure the exhaust concentration of N_2O . One sampling tube will be placed in the supply air. The 3 remaining sampling tubes (6 in total) will be placed in strategic places in the room to catch variation of N_2O concentration in the room.

The goal is to calculate the infection risk with different ventilation solutions and several distances between the student and the teacher. The ventilation scenarios are to vary the Air Changes per Hour (ACH) on four different levels: 0, 3, 6 and 9 ACH, the room temperature: 18, 20 and 22 degrees celsius, and four different distances between the infector and the susceptible: 0.5 meters, 1.0 meters, 1.5 meters and 2 meters. ACH and temperature will be regulated with the SD-system on the PC inside the HVAC-laboratory. The rotating heat exchanger in the air handling unit will be turned off to avoid that dosing of N_2O will re-enter the room.

No people will be presented in the room during the measurements.

3 EVACUATION FROM THE EXPERIMENTAL AREA

Evacuate at signal from the alarm system or local gas alarms with its own local alert with sound and light outside the room in question

Evacuation from the rigging area takes place through the marked emergency exits to the assembly point, (corner of Old Chemistry Kjelhuset or parking 1a-b.)

Action on rig before evacuation:

Turn off tracer-gas supply. Shut down air handling unit. Unplug electrical equipment and thermal manikin.

4 WARNING

4.1 Before experiments

Send an e-mail with information about the planned experiment to:

experiments@ept.ntnu.no

The e-mail must include the following information:

- Name of responsible person: Guangyu Cao
- Experimental setup/rig: HVAC-lab
- Start Experiments: (date and time) Medio March
- Stop Experiments: (date and time) June

You must get the approval back from the laboratory management before start up. All running experiments are notified in the activity calendar for the lab to be sure they are coordinated with other activity.

4.2 Abnormal situation

FIRE

If you are NOT able to extinguish the fire, activate the nearest fire alarm and evacuate area.

Be then available for fire brigade and building caretaker to detect fire place.

If possible, notify:

NTNU
Morten Grønli, Mob: 918 97 515
Terese Løvås: Mob: 918 97 007
NTNU – SINTEF Beredskapstelefon: 800 80 388

GAS ALARM

If a gas alarm occurs, close gas bottles immediately and ventilate the area. If the level of the gas concentration does not decrease within a reasonable time, activate the fire alarm and evacuate the lab. Designated personnel or fire department checks the leak to determine whether it is possible to seal the leak and ventilate the area in a responsible manner.

PERSONAL INJURY

- First aid kit in the fire / first aid stations
- Shout for help

- Start life-saving first aid
- **CALL 113** if there is any doubt whether there is a serious injury

OTHER ABNORMAL SITUATIONS

NTNU:

You will find the reporting form for non-conformance on:

<https://innsida.ntnu.no/wiki/-/wiki/Norsk/Melde+avvik>

5 ASSESSMENT OF TECHNICAL SAFETY

5.1 HAZOP

The experiment set up is divided into the following nodes:

Node 1	Test rig
--------	----------

ATTACHMENTS B: HAZOP

Conclusion: (Safety taken care of)

5.2 Flammable, reactive and pressurized substances and gas

Are any flammable, reactive and pressurized substances and gases in use?

NO	NO
----	----

Attachments: EX zones?

Conclusion:

5.3 Pressurized equipment

Is any pressurized equipment in use?

NO	NO
----	----

ATTACHMENTS D: TEST CERTIFICATE FOR LOCAL PRESSURE TESTING

Conclusion:

5.4 Effects on the environment (emissions, noise, temperature, vibration, smell)

Will the experiments generate emission of smoke, gas, odour or unusual waste?

Is there a need for a discharge permit, extraordinary measures?

NO	
----	--

Attachments:

Conclusion:

5.5 Radiation

YES	Radiation Sources need to have an own risk assessment
NO	NO

Attachments:

Conclusion:

5.6 Chemicals

Will any chemicals or other harmful substances be used in the experiments? Describe how the chemicals should be handled (stored, disposed, etc.) Evaluate the risk according to safety datasheets, MSDS. Is there a need for protective actions given in the operational procedure?

YES	<p>The tracer gas used is N₂O, which can give a narcotic effect in high concentrations. The amount of N₂O released during the experiments is 0.594 L/minute = 9.9 mL/s = 1.9602 mg/s.</p> <p>ACGIH TLV-TWA: 50ppm</p> <p>For each of the scenarios, the ventilation rate is: 252 m³/h (0.07 m³/s), 504 m³/h (0.14 m³/s) and 756 (0.21 m³/s). This gives a total amount of ppm respectively at: 28 mg/m³ = 17.5 ppm, 14 mg/m³ = 8.75 ppm and 9.33 mg/m³ = 5.8 ppm.</p>
-----	--

Attachments: MSDS for N₂O

Conclusion: There is no risk of human exposure to N₂O.

5.7 Electricity safety (deviations from the norms/standards)

NO	NO
----	----

Attachments:

Conclusion:

6 ASSESSMENT OF OPERATIONAL SAFETY

Ensure that the procedures cover all identified risk factors that must be taken care of. Ensure that the operators and technical performance have sufficient expertise.

6.1 Procedure HAZOP

The method is a procedure to identify causes and sources of danger to operational problems.

ATTACHMENT C: HAZOP PROCEDURE

6.2 Operation procedure and emergency shutdown procedure

The operating procedure is a checklist that must be filled out for each experiment. Emergency procedure should attempt to set the experiment set up in a harmless state by unforeseen events.

ATTACHMENT E: PROCEDURE FOR RUNNING EXPERIMENTS

Emergency shutdown procedure:

6.3 Training of operators

A Document showing training plan for operators

- *What are the requirements for the training of operators?*
- *What it takes to be an independent operator*
- *Job Description for operators*

Attachments: Training program for operators

6.4 Technical modifications

- *Technical modifications made by the operator (e.g.Replacement of components, equal to equal)*
- *Technical modifications that must be made by Technical staff (for example, modification of pressure equipment).*
- *What technical modifications give a need for a new risk assessment(by changing the risk picture)?*

Conclusion:

6.5 Personal protective equipment

- *It is mandatory use of eye protection in the rig zone*
- *It is mandatory use of protective shoes in the rig zone.*
- *Use gloves when there is opportunity for contact with hot/cold surfaces.*
- *Use of respiratory protection apparatus*

Conclusion: Mandatory to use eye protection in the rig zone

6.6 General Safety

- *The area around the staging attempts shielded.*
- *Gantry crane and truck driving should not take place close to the experiment.*
- *Gas cylinders shall be placed in an approved carrier with shut-off valve within easy reach.*
- *Monitoring, can experiment run unattended, how should monitoring be?*

6.7 Safety equipment

- *Have portable gas detectors to be used during test execution?*
- *Warning signs, see the Regulations on Safety signs and signaling in the workplace*

6.8 Special predations

For example:

- *Monitoring.*
- *Safety preparedness.*
- *Safe Job Analysis of modifications, (SJA)*

- Working at heights
- Flammable / toxic gases or chemicals

7 QUANTIFYING OF RISK - RISK MATRIX

The risk matrix will provide visualization and an overview of activity risks so that management and users get the most complete picture of risk factors.

IDnr	Activity	Consequence	Likelihood	RV
01	Moving of thermal manikin (electrical shock)	D	1	D1

Conclusion: If precautions are taken, the activity/process is acceptable.

RISK MATRIX

CONSEQUENCE	(E) Very critical	E1	E2	E3	E4	E5
	(D) Critical	D1	D2	D3	D4	D5
	(C) Dangerous	C1	C2	C3	C4	C5
	(B) Relatively safe	B1	B2	B3	B4	B5
	(A) Safe	A1	A2	A3	A4	A5
		(1) Minimal	(2) Low	(3) Medium	(4) High	(5) Very high
		LIKELIHOOD				

The principle of the acceptance criterion. Explanation of the colors used in the matrix

COLOUR	DESCRIPTION
Red	Unacceptable risk Action has to be taken to reduce risk
Yellow	Assessment area. Actions has to be considered
Green	Acceptable risk. Action can be taken based on other criteria

ATTACHMENT E: PROCEDURE FOR RUNNING EXPERIMENTS

Project Experimental study on the effect of ventilation solutions on the risk of COVID-19 infection	Date	Signature
Facility HVAC-lab		
Project leader Guangyu Cao		

	Conditions for the experiment:	Completed
	Experiments should be run in normal working hours, 08:00-16:00 during winter time and 08.00-15.00 during summer time. Experiments outside normal working hours shall be approved. Always use protection glasses while using thermal manikin	
	One person must always be present while running experiments and should be approved as an experimental leader.	
	An early warning is given according to the lab rules and accepted by authorized personnel.	
	Be sure that everyone taking part of the experiment is wearing the necessary protecting equipment and is aware of the shut down procedure and escape routes.	
	Preparations	Carried out
	Post the "Experiment in progress" sign.	
	Make sure electrical cables are properly routed and no pinching of cables	
	Distribute electrical equipment evenly on different electrical circuits in the HVAC-lab	
	Start up air handling unit with "student mode". Turn off rotary heat exchanger. Control that the system work properly	
	Open valve for tracer gas and control for leakage	
	Connect electrical equipment and control if they function properly	
	During the experiment	
	Observe electrical equipment from outside the room. No smoke shall be seen.	
	Listen for abnormal noises from ventilation system	
	End of experiment	
	Close the valve of the tracer bottle	
	Disconnect electrical equipment	
	Switch the AHU back to "Drift" mode and all settings back to normal so others can use the room normally.	
	Remove all obstructions/barriers/signs around the experiment.	
	Tidy up and return all tools and equipment.	
	Tidy and cleanup work areas.	
	Return equipment and systems back to their normal operation settings (fire alarm)	
	To reflect on before the next experiment and experience useful for others	

	Was the experiment completed as planned and on scheduled in professional terms?	
	Was the competence which was needed for security and completion of the experiment available to you?	
	Do you have any information/ knowledge from the experiment that you should document and share with fellow colleagues?	

Important notes:

Unplug all electrical equipment when leaving the room.

Make sure that the tracer gas bottle valve is shut down before leaving.

Operator(s):

Navn	Dato	Signatur
Mathilde Ruud		

ATTACHMENT F: TRAINING OF OPERATORS

Project Experimental study on the effect of ventilation solutions on the risk of COVID-19 infection	Date	Signature
Facility HVAC-room		
Project leader Guangyu Cao		

Knowledge about EPT LAB in general	
Lab <ul style="list-style-type: none"> • Access • routines and rules • working hour 	
Knowledge about the evacuation procedures.	
Activity calendar for the Lab	
Early warning, experiments@ept.ntnu.no	
Knowledge about the experiments	
Procedures for the experiments	
Emergency shutdown.	
Nearest fire and first aid station.	

I hereby declare that I have read and understood the regulatory requirements has received appropriate training to run this experiment and are aware of my personal responsibility by working in EPT laboratories.

Operator(s):

Navn	Dato	Signatur
Mathilde Ruud	09.03.22	

APPARATURKORT / UNITCARD

Dette kortet SKAL henges godt synlig på apparaturen!
This card MUST be posted on a visible place on the unit!

Apparatur (Unit) HVAC-room	
Prosjektleder (Project Leader) Guangyu Cao	Telefon mobil/privat (Phone no. Mobile/private) 91897689
Apparaturansvarlig (Unit Responsible) Guangyu Cao	Telefon mobil/privat (Phone no. Mobile/private) 91897689
Sikkerhetsrisikoer (Safety hazards) Do not touch the thermal manikins while it is plugged, always use glasses while using breathing thermal manikin. Hot electrical equipment. Tracer gas N2O.	
Sikkerhetsregler (Safety rules) Turn off the thermal manikin while it is plugged. Unplug all electrical equipment before leaving the room. Turn the AHU system back to "drift" mode before leaving. Make sure the tracer gas valve is completely shut before leaving.	
Nødstop prosedyre (Emergency shutdown) Switch off and unplug the thermal manikin Disconnect all electrical equipment Shut down tracer gas-supply	

Her finner du (Here you will find):

Prosedyrer (Procedures)	In the room
Bruksanvisning (Users manual)	In the room

Nærmeste (Nearest)

Brannslukningsapparat (fire extinguisher)	First floor VVS-lab (syd)
Førstehjelpsskap (first aid cabinet)	First floor VVS-lab (syd)

**NTNU, Institutt for energi og
prosesseteknikk**

Dato

Signert

FORSØK PÅGÅR /EXPERIMENT IN PROGRESS

Dette kortet SKAL henges opp før forsøk kan starte!
This card MUST be posted on the unit before the experiment startup!

Apparatur (Unit) HVAC-lab	
Prosjektleder (Project Leader) Guangyu Cao	Telefon mobil/privat (Phone no. mobile/private) 91897689
Apparaturansvarlig (Unit Responsible) Guangyu Cao	Telefon mobil/privat (Phone no. mobile/private) 91897689
Godkjente operatører (Approved Operators) Mathilde Ruud	Telefon mobil/privat (Phone no. mobile/private) 94828272
Prosjekt (Project) Experimental study on the effect of ventilation solutions on the risk of COVID-19 infection	
Forsøksstid / Experimental time (start - stop) 25.03.2022-01.06.2022	
Kort beskrivelse av forsøket og relaterte farer (Short description of the experiment and related hazards) <p>Temperature and relative humidity will be measured in the occupied zone (H=1.6m approx.). The N2O tracer gas will be used to simulate a breathing (corona)infected person sitting on a chair (tube inserted into the manikin). Concentration of N2O will be measured at several target points (i.e., 0.5 meter, 1 meter, 1.5 meters and 2 meters in front of the breathing manikin) and by the exhaust, whereas the ventilation efficiency can be calculated from different scenarios. The scenarios are built up with different variables that will vary from scenario to scenario: location of exhaust, supply set point temperature, target points (distance from infector) and ventilation rate. The measured ventilation efficiency, temperature and relative humidity will serve as a basis to calculate the risk of infection on different ventilation solutions.</p> <p>List of instruments: Instruments to measure, N2O temperature and relative humidity Breathing thermal manikin</p> <p>Tracer gas measurements in the HVAC-lab with various ventilation setups. The gas will be released outside the room into a breathing box, and the gas is released from a manikins' mouth inside the room. Various electrical equipment will be turned on to generate heat. Tracer gas is N2O</p> <p>Hazards: hot electric equipment, high N2O concentration in the air inside the HVAC-lab.</p>	

NTNU
Institutt for energi og prosesssteknikk

Dato

ATTACHMENT H GUIDANCE TO RISK ASSESSMENT

Chapter 5 Assessment of technical safety.

Ensure that the design of the experiment set up is optimized in terms of technical safety.

Identifying risk factors related to the selected design, and possibly to initiate re-design to ensure that risk is eliminated as much as possible through technical security.

This should describe what the experimental setup actually are able to manage and acceptance for emission.

5.1 HAZOP

The experimental set up is divided into nodes (eg motor unit, pump unit, cooling unit.). By using guidewords to identify causes, consequences and safeguards, recommendations and conclusions are made according to if necessary safety is obtained. When actions are performed the HAZOP is completed.

(e.g. "No flow", cause: the pipe is deformed, consequence: pump runs hot, precaution: measurement of flow with a link to the emergency or if the consequence is not critical used manual monitoring and are written into the operational procedure.)

5.2 Flammable, reactive and pressurized substances and gas.

According to the Regulations for handling of flammable, reactive and pressurized substances and equipment and facilities used for this:

Flammable material: Solid, liquid or gaseous substance, preparation, and substance with occurrence or combination of these conditions, by its flash point, contact with other substances, pressure, temperature or other chemical properties represent a danger of fire.

Reactive substances: Solid, liquid, or gaseous substances, preparations and substances that occur in combinations of these conditions, which on contact with water, by its pressure, temperature or chemical conditions, represents a potentially dangerous reaction, explosion or release of hazardous gas, steam, dust or fog.

Pressurized : Other solid, liquid or gaseous substance or mixes having fire or hazardous material response, when under pressure, and thus may represent a risk of uncontrolled emissions

Further criteria for the classification of flammable, reactive and pressurized substances are set out in Annex 1 of the Guide to the Regulations "Flammable, reactive and pressurized substances"

<http://www.dsb.no/Global/Publikasjoner/2009/Veiledning/Generell%20veiledning.pdf>

http://www.dsb.no/Global/Publikasjoner/2010/Tema/Temaveiledning_bruk_av_farlig_stoff_Del_1.pdf

Experiment setup area should be reviewed with respect to the assessment of Ex zone

- Zone 0: Always explosive atmosphere, such as inside the tank with gas, flammable liquid.
- Zone 1: Primary zone, sometimes explosive atmosphere such as a complete drain point
- Zone 2: secondary discharge could cause an explosive atmosphere by accident, such as flanges, valves and connection points

5.4 Effects on the environment

With pollution means: bringing solids, liquid or gas to air, water or ground, noise and vibrations, influence of temperature that may cause damage or inconvenience effect to the environment.

Regulations: <http://www.lovdato.no/all/hl-19810313-006.html#6>

NTNU guidance to handling of waste: <http://www.ntnu.no/hms/retningslinjer/HMSR18B.pdf>

5.5 Radiation

Definition of radiation

Ionizing radiation: Electromagnetic radiation (in radiation issues with wavelength <100 nm) or rapid atomic particles (e.g. alpha and beta particles) with the ability to stream ionized atoms or molecules.
Non ionizing radiation: Electromagnetic radiation (wavelength >100 nm), og ultrasound ₁ with small or no capability to ionize.
Radiation sources: All ionizing and powerful non-ionizing radiation sources.
Ionizing radiation sources: Sources giving ionizing radiation e.g. all types of radiation sources, x-ray, and electron microscopes.
Powerful non ionizing radiation sources: Sources giving powerful non ionizing radiation which can harm health and/or environment, e.g. class 3B and 4. MR ₂ systems, UVC ₃ sources, powerful IR sources ₄ .
₁ Ultrasound is an acoustic radiation ("sound") over the audible frequency range (> 20 kHz). In radiation protection regulations are referred to ultrasound with electromagnetic non-ionizing radiation.
₂ MR (e.g. NMR) - nuclear magnetic resonance method that is used to "depict" inner structures of different materials.
₃ UVC is electromagnetic radiation in the wavelength range 100-280 nm.
₄ IR is electromagnetic radiation in the wavelength range 700 nm - 1 mm.

For each laser there should be an information binder (HMSRV3404B) which shall include:

- General information
- Name of the instrument manager, deputy, and local radiation protection coordinator
- Key data on the apparatus
- Instrument-specific documentation
- References to (or copies of) data sheets, radiation protection regulations, etc.
- Assessments of risk factors
- Instructions for users
- Instructions for practical use, startup, operation, shutdown, safety precautions, logging, locking, or use of radiation sensor, etc.
- Emergency procedures
- See NTNU for laser: <http://www.ntnu.no/hms/retningslinjer/HMSR34B.pdf>

5.6 The use and handling of chemicals.

In the meaning chemicals, a element that can pose a danger to employee safety and health

See: <http://www.lovdato.no/cgi-wift/ldles?doc=/sf/sf/sf-20010430-0443.html>

Safety datasheet is to be kept in the HSE binder for the experiment set up and registered in the database for chemicals.

Chapter 6 Assessment of operational procedures.

Ensures that established procedures meet all identified risk factors that must be taken care of through operational barriers and that the operators and technical performance have sufficient expertise.

6.1 Procedure Hazop

Procedural HAZOP is a systematic review of the current procedure, using the fixed HAZOP methodology and defined guidewords. The procedure is broken into individual operations (nodes) and analyzed using guidewords to identify possible nonconformity, confusion or sources of inadequate performance and failure.

6.2 Procedure for running experiments and emergency shutdown.

Has to be prepared for all experimental setups.

The operating procedure has to describe stepwise preparation, startup, during and ending conditions of an experiment. The procedure should describe the assumptions and conditions for starting, operating parameters with the deviation allowed before aborting the experiment and the condition of the rig to be abandoned.

Emergency procedure describes how an emergency shutdown have to be done,

- *what happens when emergency shutdown, is activated. (electricity / gas supply) and*
- *which events will activate the emergency shutdown (fire, leakage).*

Chapter 7 Quantifying of RISK

Quantifying of the residue hazards, Risk matrix.

To illustrate the overall risk, compared to the risk assessment, each activity is plotted with values for the likelihood and consequence into the matrix. Use task IDnr.




Example: If activity IDnr. 1 has been given a probability 3 and D for consequence the risk value become D3, red. This is done for all activities giving them risk values.

In the matrix are different degrees of risk highlighted in red, yellow or green. When an activity ends up on a red risk (= unacceptable risk), risk reducing action has to be taken

RISK MATRIX

CONSEQUENCE	(E) Very critical	E1	E2	E3	E4	E5
	(D) Critical	D1	D2	D3	D4	D5
	(C) Dangerous	C1	C2	C3	C4	C5
	(B) Relatively safe	B1	B2	B3	B4	B5
	(A) Safe	A1	A2	A3	A4	A5
		(1) Minimal	(2) Low	(3) Medium	(4) High	(5) Very high
		LIKELIHOOD				

COLOUR	DESCRIPTION
--------	-------------

Red		Unacceptable risk Action has to be taken to reduce risk
Yellow		Assessment area. Actions has to be considered
Green		Acceptable risk. Action can be taken based on other criteria

The principle of the acceptance criterion. Explanation of the colors used in the matrix

Likelihood

Minimal 1	Low 2	Medium 3	High 4	Very high 5
Once every 50 years or less	Once every 10 years or less	Once a year or less	Once a month or less	Once a week

Consequence

Grading	Human	Environment	Financial/material
E Very critical	May produce fatality/ies	Very prolonged, non-reversible damage	Shutdown of work >1 year.
D Critical	Permanent injury, may produce serious health damage/sickness	Prolonged damage. Long recovery time.	Shutdown of work 0.5-1 year.
C Dangerous	Serious personal injury	Minor damage. Long recovery time	Shutdown of work < 1 month
B Relatively safe	Injury that requires medical treatment	Minor damage. Short recovery time	Shutdown of work < 1week
A Safe	Injury that requires first aid	Insignificant damage. Short recovery time	Shutdown of work < 1day

B Deposition and contact/fomites

Droplet transmission is defined by that bacteria or virus is contained in larger droplets that is emitted from a person that is coughing, singing and talking (Jayaweera *et al.*, 2020). These large particles are referred to as droplets and can only travel short distances before they evaporate. WHO defines “larger droplets” as particle sizes with diameter $> 5 \mu\text{m}$ (2014, as cited in Jayaweera *et al.*, 2020).

Droplet transmission can cause deposition transmission or contact/fomite transmission (Jayaweera *et al.*, 2020). Deposition happens when big droplets deposits directly on the eyes, nose or mouth (mucous membranes) of a susceptible person. This usually happens if the infector sneezes or coughs.

Contact transmission can happen if an infected exhales large droplets that lands on surfaces (fomites), thereby a susceptible touches the surface and then their mucous membranes (FHI, 2020a). CDC (2021) states that fomite transmission are dependent on several factors: environmental factors (relative humidity, temperature, evaporation), time from the droplet falls to a susceptible touch the surface, transmittance efficiency from hand to surface and from hand to mucous membrane, amount of virus-laden particles from infector, deposition on surfaces (airflow and ventilation dependent) and the virus dose that can cause infection from fomites. Measures as hand hygiene and surface sanitizing decrease the risk of infection.

Several studies have found that fomite transmission have a less significant role in transmission of the coronavirus compared to other routes. Cheng *et al.* (2022) found that fomite transmission was negligible in an infection outbreak on a bus in China, while airborne transmission was the biggest contributor to infection. Zhang *et al.* (2021) also found that fomite transmission was ruled out of an infection outbreak in a restaurant, and that the long-range airborne route was significant.

C Tracer-gas characteristics

In this thesis, N_2O was used as tracer gas. Important information about this tracer gas are described in Table C.1.

Table C.1: Key properties about N₂O as tracer gas. Modified from Grieve (1989).

Tracer gas	Formula	Density compared to air	Molecular weight [$\frac{g}{mol}$]	Additional
Nitrous oxide	N ₂ O	1.53	44.013	Anaesthetic and widely used as tracer

D Additional equipment

D.1 Smoke visualization tools

The Drager Air-Flow Tester Kit, as shown in Figure D.1, was used to observe the route for exhaled aerosols from the infected manikin. The smoke generator consisted of Air-Flow test tubes, a bulb and sealing caps.

**Figure D.1:** Drager Air-Flow Tester kit for smoke visualization of exhaled jet.

The Manual Easysmoker, as shown in Figure D.2, was used to visualize the airflow pattern.

**Figure D.2:** Manual EasySmoker to visualize the airflow pattern in the laboratory.

D.2 Heating element

A heating element was used to heat the exhaled air jet from the infected manikin that simulated an infected teacher. The required power to heat the exhaled air to 34 degrees celsius was calculated by Equation D.1.

$$Q = \rho \cdot V \cdot c \cdot \Delta T \quad (\text{D.1})$$

where

- ρ is the density of air = $1.28 \text{ [kg/m}^3\text{]}$
- V is the volume of exhaled air $\text{[m}^3\text{/min]}$
- c is the heating capacity of air = $1010 \text{ [}\frac{\text{J}}{\text{kg}\cdot\text{K}}\text{]}$
- ΔT is the temperature difference = $34-20 \text{ [K]}$.

The resulting required power to heat the air was 3.22 W . The heating elements used was a 5 W STEGO PTC Heater of type RCE 016 (Stego, n.d.). The heater body of the equipment was aluminum and is shown in Figure D.3.



Figure D.3: 5 W heating element to heat up exhaled air from the infected manikin.

E Deposition rate values

The needed values to calculate the deposition rate for particles between 0 and 8 μm is shown in Table E.1. The represented values are droplet diameter, mean mass diameter and droplet number concentration. Further details about the variables are shown in Aganovic *et al.* (2021).

Table E.1: Droplet diameter, mean mass diameter and droplet number concentration to calculate the deposition rate for size ranges from 0 to 8 μm (Aganovic *et al.*, 2021).

Size range [μm]	Droplet diameter, [μm]	D_{eq}	Mean diameter, [μm]	mass D_{ms}	Droplet number concentrations, N_i [$\frac{\text{part}}{\text{cm}^3}$]
0.3-0.8	0.55		0.239		0.118
0.8-2	1.4		0.515		0.152
2-4	3		1.056		0.00459
4-8	6		2.070		0.0662

